

# MEASUREMENT AND MODELING OF FLUID-FLUID MISCIBILITY IN MULTICOMPONENT HYDROCARBON SYSTEMS

A Dissertation

Submitted to the Graduate Faculty of the  
Louisiana State University and  
Agricultural and Mechanical College  
in partial fulfillment of the  
Requirements for the degree of  
Doctor of Philosophy

in

The Department of Petroleum Engineering

by

**Subhash C. Ayirala**

B.Tech in Chemical Engineering, Sri Venkateswara Univeristy, Tirupati, India, 1996  
M.Tech in Chemical Engineering, Indian Institute of Technology, Kharagpur, India, 1998  
M.S. in Petroleum Engineering, Louisiana State University, 2002  
August 2005

## **DEDICATION**

This work is dedicated to my wife, Kruthi; my parents; my brother, Dhanuj and my beloved sisters, Hema, Suma and Siri.

## ACKNOWLEDGEMENTS

I am deeply indebted to my mentor and advisor Dr. Dandina N. Rao for his able guidance, motivation and moral support throughout this work. It is very fortunate to work with Dr. Rao on an exciting project in Enhanced Oil Recovery. I am thankful to Dr. Anuj Gupta, Dr. Karsten E. Thompson, Dr. Edward B. Overton and Dr. Donald Dean Adrian for serving as members on the examination committee. I am also thankful to Dr. Brij B. Maini, professor, University of Calgary for his valuable suggestions and comments given to improve the quality of this dissertation.

The financial support of this project by the U.S Department of Energy under Award No. DE-FC26-02NT-15323 is greatly appreciated. I express my sincere thanks to Dr. Jerry Casteel of NPTO/DOE for his support and encouragement. I also thank Dr. Jong Lee of Petro-Canada and Dr. David Fong and Dr. Frank McIntyre of Husky Oil for helpful technical discussions.

I would like to express my sincere thanks to my friends Madhav Kulkarni, Daryl Sequiera and Wei Xu for providing technical help during this project whenever needed. I am also greatly indebted to all the faculty members, staff and graduate students in the Petroleum Engineering Department for their help and friendship offered during my stay at LSU. Finally I express my profound gratitude to my wife, parents, brother and sisters, who always served as the source of inspiration to finish this project.

# TABLE OF CONTENTS

<b>DEDICATION</b> .....	ii
<b>ACKNOWLEDGEMENTS</b> .....	iii
<b>LIST OF TABLES</b> .....	vii
<b>LIST OF FIGURES</b> .....	x
<b>ABSTRACT</b> .....	xiv
<b>1. INTRODUCTION</b> .....	1
1.1 Problem Statement.....	1
1.2 Objectives.....	4
1.3 Methodology.....	5
<b>2. LITERATURE REVIEW</b> .....	8
2.1. Current EOR Scenario in United States.....	8
2.2. Definition of Fluid-Fluid Miscibility.....	9
2.3. Need for Fluid-Fluid Miscibility in Gas Injection EOR.....	10
2.4. Experimental Techniques to Determine Gas-Oil Miscibility.....	11
2.4.1. Slim-Tube Displacement Test.....	12
2.4.2. Rising Bubble Apparatus.....	14
2.4.3. Pressure Composition (P-X) Diagrams.....	14
2.4.4. The New Vanishing Interfacial Tension (VIT) Technique.....	15
2.5. Mass Transfer Effects in Gas-Oil Miscibility Development.....	16
2.6. Computational Models to Determine Gas-Oil Miscibility.....	17
2.6.1. EOS Models.....	18
2.6.2. Analytical Models.....	20
2.7. Interfacial Tension.....	22
2.7.1. Role of Interfacial Tension in Fluid-Fluid Phase Equilibria.....	22
2.7.2. IFT Measurement Techniques.....	25
2.7.2.1. Capillary Rise Technique.....	26
2.7.2.2. Drop Weight Method.....	28
2.7.2.3. Ring Method.....	29
2.7.2.4. Wilhelmy Plate Apparatus.....	30
2.7.2.5. Pendent Drop Method.....	31
2.7.2.6. Sessile Drop Method.....	34
2.7.2.7. Spinning Drop Method.....	35
2.7.3. IFT Predictive Models.....	36
2.7.3.1. Parachor Model.....	36
2.7.3.2. Corresponding States Theory.....	43
2.7.3.3. Thermodynamic Correlations.....	45
2.7.3.4. Gradient Theory.....	47

<b>3. EXPERIMENTAL APPARATUS AND PROCEDURES</b> .....	52
3.1. Standard Ternary Liquid System.....	53
3.1.1. Reagents.....	53
3.1.2. Experimental Setup and Procedure.....	53
3.2. Standard Gas-Oil Systems.....	58
3.2.1. Reagents.....	58
3.2.2. Experimental Setup and Procedure.....	58
<b>4. RESULTS AND DISCUSSION</b> .....	63
4.1. IFT Measurements in a Standard Ternary Liquid System.....	64
4.1.1. Solubility and Miscibility.....	64
4.1.2. Solvent-Oil Ratio Effects on IFT.....	66
4.1.3. IFT Measurements Using Capillary Rise Technique.....	72
4.1.4. Correlation of Solubility and Miscibility with IFT.....	75
4.1.5. Determination of VIT Miscibility.....	77
4.2. IFT Measurements in Standard Gas-Oil Systems.....	78
4.2.1. Bubble Point Pressure Estimation of Synthetic Live Oil.....	78
4.2.2. Density Meter Calibration and Density Measurements of Pure Fluids.....	79
4.2.3. IFT Measurements in n-Decane-CO <sub>2</sub> System at 100° F.....	82
4.2.4. IFT Measurements in Synthetic Live Oil-CO <sub>2</sub> System at 160° F.....	86
4.2.5. Effect of Gas-Oil Ratio on Dynamic Interfacial Tension.....	90
4.3. Comparison of VIT Experiments of RKR and Terra Nova Reservoir Fluids with EOS Model Computations.....	94
4.3.1. EOS Tuning.....	94
4.3.2. Gas-Oil Miscibility Determination Using EOS Model.....	98
4.3.3. Reality Check.....	106
4.4. Application of Parachor IFT Model to Predict Fluid-Fluid Miscibility.....	109
4.4.1. Gas-Oil IFT Calculations.....	109
4.4.2. Gas-Oil Miscibility Calculations.....	112
4.4.3. Mass Transfer Effects on Fluid-Fluid Miscibility.....	114
4.5. Newly Proposed Mechanistic Parachor Model for Prediction of Dynamic IFT and Miscibility in Multicomponent Hydrocarbon Systems.....	115
4.5.1. Background on Development of Proposed Mechanistic Parachor Model.....	116
4.5.2. Application of the Proposed Mechanistic Model to Crude Oil-Gas Systems.....	120
4.5.3. Application of the Proposed Mechanistic Model to Crude Oil Systems.....	136
4.5.4. Sensitivity Studies on Proposed Mechanistic Parachor Model.....	140
4.5.5. Generalized Regression Models for Mechanistic Model Exponent Prediction.....	143
4.5.6. Validation of the Generalized Regression Models for Mechanistic Model Exponent Prediction.....	147
4.5.7. Prediction of Dynamic Gas-Oil Miscibility Using the Mechanistic Model.....	150
4.6. Modeling of Dynamic Gas-Oil Interfacial Tension and Miscibility in Standard Gas-Oil Systems at Elevated Pressures and Temperatures.....	152
4.6.1. n-Decane-CO <sub>2</sub> System at 100° F.....	152
4.6.2. Synthetic Live Oil-CO <sub>2</sub> System at 160° F.....	154
4.7. Relationship between Developed Miscibility in Gas Injection EOR Projects and Laboratory Gas-Oil Interfacial Tension Measurements.....	159

**5. CONCLUSIONS AND RECOMMENDATIONS**..... 168  
5.1. Summary of Conclusions.....168  
5.2. Recommendations for Future Work.....176

**REFERENCES CITED**..... 178

**VITA**..... 190

## LIST OF TABLES

1. Optimum Weight Factors for Proper EOS Tuning.....	19
2. Effect of Pressure on Parachors of Crude Cuts.....	42
3. Summary of Parachor Characteristics.....	43
4. Solubility of Benzene in Water at Various Ethanol Enrichments.....	65
5. Measured Benzene Interfacial Tensions in Non-Equilibrated Aqueous Ethanol at Various Ethanol Enrichments and Feed Compositions.....	67
6. Measured Benzene IFT's in Pre-Equilibrated Aqueous Ethanol at 30% and 40% Ethanol Enrichments and Various Feed Compositions.....	71
7. Benzene IFT's in Pre-Equilibrated Aqueous Ethanol at Ethanol Enrichments Above 40%.....	73
8. Measured Equilibrium Benzene Contact Angles at Various Ethanol Enrichments in Aqueous Phase.....	74
9. Summary of Equilibrated Fluid Densities and Capillary Rise Heights Measured in n-Decane-CO <sub>2</sub> System at 100° F.....	83
10. Summary of IFT's Measured in n-Decane-CO <sub>2</sub> System at Various Pressures and Gas-Oil Ratios in the Feed.....	84
11. Summary of Equilibrated Fluid Densities and Capillary Rise Heights Measured in Synthetic Live Oil-CO <sub>2</sub> System at 160° F.....	87
12. Summary of IFT's Measured in Synthetic Live Oil-CO <sub>2</sub> System at Various Pressures and Gas-Oil Ratios in the Feed.....	87
13. Composition of Rainbow Keg River Fluids Used.....	95
14. Composition of Terra Nova Fluids Used.....	95
15. Comparison of MMP's from VIT Technique and EOS Calculations Using Various Tuning Approaches for Rainbow Keg River Reservoir Fluids.....	97

16. Comparison of MMP's from VIT Technique and EOS Calculations Using Various Tuning Approaches for Terra Nova Reservoir Fluids.....	97
17. Composition (in Mole%) of Solvents Used in VIT Tests as well as in EOS Calculations for Rainbow Keg River Reservoir Fluids.....	99
18. Composition (in Mole%) of Solvents Used in VIT Tests as well as in EOS Calculations for Terra Nova Reservoir Fluids.....	99
19. Comparison of Measured IFT's with Parachor Model Predictions for RKR Reservoir Fluids.....	110
20. Comparison of IFT Measurements with Parachor Model for RKR Fluids at 87° C and 14.8 MPa...	120
21. Comparison of IFT Measurements with Parachor Model for RKR Fluids at 87° C and 14.0 MPa...	121
22. Diffusivities between Oil and Gas at Various C <sub>2+</sub> Enrichments for RKR Reservoir Fluids at 87° C.....	124
23. Comparison of IFT Measurements with Mechanistic Parachor Model for RKR Fluids at 87° C and 14.8 MPa.....	125
24. Comparison of IFT Measurements with Mechanistic Parachor Model for RKR Fluids at 87° C and 14.0 MPa.....	125
25. Comparison of IFT Measurements with Parachor Model for Terra Nova Fluids at 96° C and 30.0 MPa .....	127
26. Diffusivities between Oil and Gas at Various C <sub>2+</sub> Enrichments for Terra Nova Reservoir Fluids at 96° C and 30.0 MPa.....	129
27. Comparison of IFT Measurements with Mechanistic Parachor Model for Terra Nova Fluids at 96° C and 30.0 MPa.....	131
28. Parachor and Mechanistic Parachor Model IFT Predictions for Schrader Bluff Reservoir Fluids at 82° F and 1300 psi.....	132
29. Diffusivities between Oil and Solvent at Various NGL Enrichments in Solvent for Schrader Bluff Reservoir Fluids at 82° F and 1300 psi.....	134

30. Physical Properties of Crude Oils Used.....	136
31. Comparison of IFT Measurements with Parachor and Mechanistic Parachor Model Predictions for Crude Oil A.....	137
32. Comparison of IFT Measurements with Parachor and Mechanistic Parachor Model Predictions for Crude Oil C.....	137
33. Comparison of IFT Measurements with Parachor and Mechanistic Parachor Model Predictions for Crude Oil D.....	138
34. Model Exponents for Different Single Experimental IFT Measurement Points in the Mechanistic Parachor Model for RKR Fluids at 14.8 MPa.....	141
35. Model Exponents for Different Single Experimental IFT Measurement Points in the Mechanistic Parachor Model for Terra Nova Fluids at 30.0 MPa.....	141
36. Summary of Similarities Observed between the Exponent in the Mechanistic Model and the Parachor.....	147
37. Comparison of IFT Measurements with Parachor Model in n-Decane-CO <sub>2</sub> System at 100° F.....	153
38. Comparison of IFT Measurements with Parachor Model in Synthetic Live Oil-CO <sub>2</sub> System at 160° F.....	154
39. Diffusivities between Oil and Gas at Various Pressures in Synthetic Live Oil-CO <sub>2</sub> System at 160° F.....	156
40. Comparison between IFT Measurements and Mechanistic Parachor Model Predictions in Synthetic Live Oil-CO <sub>2</sub> System at 160° F.....	157

## LIST OF FIGURES

1. Gas Injection EOR in US.....	8
2. Miscible CO <sub>2</sub> Gas Injection EOR in US .....	8
3. Effect of Temperature on Parachor.....	40
4. Parachor vs. Molecular Weight for Crude Cuts and n-Paraffins.....	41
5. Effect of Solute Composition on Parachor.....	43
6. Schematic of the Experimental Setup Used for Pendent Drop IFT Measurements.....	54
7. Schematic of the Capillary Rise Technique Used.....	55
8. Photograph of the Equipment Used for Contact Angle Measurements.....	57
9. Photograph of the Equipment Used for IFT Measurements at Elevated Pressures and Temperatures.....	59
10. Phase Diagram of Benzene, Ethanol and Water Ternary System.....	64
11. Solubility of Benzene in Water at Various Ethanol Enrichments.....	66
12. Effect of Solvent-Oil Ratio on IFT in Feed Mixtures of Non-Equilibrated Benzene (Oil) and Aqueous Ethanol (Solvent).....	68
13. Photographs Showing the Effect of Benzene Dissolution in Non-Equilibrated Aqueous Ethanol Solvent at 30% Ethanol Enrichment.....	70
14. Photographs Showing the Absence of Benzene Dissolution in Pre-Equilibrated Aqueous Ethanol Solvent at 30% Ethanol Enrichment.....	70
15. Effect of Feed Solvent-Oil Ratio on IFT in Pre-Equilibrated Aqueous Ethanol Solvent.....	71
16. Benzene Equilibrium Contact Angles Against Ethanol Enrichment in Aqueous Phase.....	74
17. Correlation of Solubility and Miscibility with IFT.....	75
18. Correlation between IFT and Solubility.....	76

19. Plot of IFT vs. Ethanol Enrichment to Determine Miscibility.....	77
20. Bubble Point Pressure Determination of Live Synthetic Oil at 160° F.....	79
21. Comparison between Measured and PR-EOS Calculated CO <sub>2</sub> Densities at 100° F.....	80
22. Comparison between Measured and PR-EOS Calculated CO <sub>2</sub> Densities at 160° F.....	80
23. Measured Densities of Pure n-decane at 100° F.....	81
24. Measured Densities of Pure Synthetic Live Oil at 160° F.....	82
25. Effect of Gas-Oil Ratio on IFT in n-Decane-CO <sub>2</sub> System at 100° F.....	84
26. Determination of VIT Miscibility in n-Decane-CO <sub>2</sub> System at 100° F.....	85
27. Effect of Gas-Oil Ratio on IFT in Synthetic Live Oil-CO <sub>2</sub> System at 160° F.....	88
28. Determination of VIT Miscibility in Synthetic Live Oil-CO <sub>2</sub> System at 160° F.....	89
29. Effect of Gas-Oil Ratio on Dynamic Interfacial Behavior.....	90
30. Concentration Profiles of a Diffusing Component in Gas-Liquid Systems.....	93
31. Representation of Condensing Drive Mechanism on a Pseudo-Ternary Diagram for RKR Fluids at a C <sub>2+</sub> Concentration of 52.5% in Solvent.....	102
32. Comparison of Miscibility Conditions of RKR Fluids Obtained from VIT Experiments and EOS Calculations.....	103
33. Comparison of Miscibility Conditions of Terra Nova Fluids Obtained from VIT Experiments and EOS Calculations.....	104
34. Effect of Tuning on EOS MMP Predictions for Terra Nova Fluids.....	105
35. Comparison of Tuned PR-EOS Predictions with Experimental PVT Data of RKR Reservoir Crude Oil.....	107
36. Comparison of Tuned PR-EOS Predictions with Experimental PVT Data of Terra Nova Reservoir Crude Oil.....	108

37. Comparison of Experimental IFT's with Parachor Model for RKR Fluids at a Pressure of 14.8 MPa.....	111
38. Comparison of Experimental IFT's with Parachor Model for RKR Fluids at a Pressure of 14.0 MPa.....	111
39. Comparison of VIT Miscibility of RKR Fluids with EOS Calculations and Parachor Model.....	113
40. MMP Determination using Parachor Computational Model for RKR Fluids.....	113
41. Comparison between IFT Measurements and Parachor Model for RKR Fluids at 87° C and 14.8 MPa .....	121
42. Comparison between IFT Measurements and Parachor Model for RKR Fluids at 87° C and 14.0 MPa.....	122
43. Determination of Mass Transfer Enhancement Parameters for RKR Reservoir Fluids.....	123
44. Comparison between IFT Measurements and Mechanistic Parachor Model for RKR Fluids at 87° C and 14.8 MPa.....	126
45. Comparison between IFT Measurements and Mechanistic Parachor Model for RKR Fluids at 87° C and 14.0 MPa .....	126
46. Comparison between IFT Measurements and Parachor Model for Terra Nova Fluids at 96° C and 30.0 MPa.....	128
47. Determination of Mass Transfer Enhancement Parameter for Terra Nova Reservoir.....	129
48. Comparison between IFT Measurements and Mechanistic Parachor Model for Terra Nova Fluids at 96° C and 30.0 MPa.....	131
49. Comparison of IFT Measurements with Parachor and Mechanistic Parachor Models for Schrader Bluff Crude Oil with (PBG+NGL) Solvents at 82° F and 1300 psi.....	133
50. Comparison of IFT Measurements with Parachor and Mechanistic Parachor Models for Schrader Bluff Crude Oil with (CO <sub>2</sub> +NGL) Solvents at 82° F and 1300 psi.....	135
51. Comparison of IFT Measurements with Parachor and Mechanistic Parachor Model Predictions for Crude Oil A.....	138

52. Comparison of IFT Measurements with Parachor and Mechanistic Parachor Model Predictions for Crude Oil C.....	139
53. Comparison of IFT Measurements with Parachor and Mechanistic Parachor Model Predictions for Crude Oil D.....	139
54. Sensitivity Studies for the Effect of Number of Experimental Data Points on Mechanistic Model Results for RKR Fluids at 87° C and 14.8 MPa.....	142
55. Sensitivity Studies for the Effect of Number of Experimental Data Points on Mechanistic Model Results for Terra Nova Fluids at 96° C and 30.0 MPa. ....	142
56. Multiple Linear Regression Model for the Mechanistic Model Exponent Prediction in Crude Oil-Solvent Systems.....	145
57. Simple Linear Regression Model for the Mechanistic Model Exponent Prediction in Crude Oil Systems.....	147
58. Validation of the Generalized Regression Model for Exponent Prediction in Prudhoe Bay Crude Oil-Solvent System.....	149
59. Validation of the Generalized Regression Model for Exponent Prediction in Prudhoe Bay Crude Oil System.....	150
60. Comparison of IFT Measurements with Parachor Model in n-Decane-CO <sub>2</sub> System at 100° F.....	153
61. Comparison of IFT Measurements with Parachor Model in Synthetic Live Oil-CO <sub>2</sub> System at 160° F.....	155
62. Comparison of IFT Measurements with Mechanistic Parachor Model in Synthetic Live Oil-CO <sub>2</sub> System at 160° F.....	157
63. Comparison between Mechanistic Parachor Model Results using the Exponents from both Compositional as well as IFT Data.....	159
64. Demonstration of Multi-Stages of Gas-Oil Contact in VIT Technique.....	166

## ABSTRACT

Carbon dioxide injection has currently become a major gas injection process for improved oil recovery. Laboratory evaluations of gas-oil miscibility conditions play an important role in process design and economic success of field miscible gas injection projects. Hence, this study involves the measurement and modeling of fluid-fluid miscibility in multicomponent hydrocarbon systems. A promising new vanishing interfacial tension (VIT) experimental technique has been further explored to determine fluid-fluid miscibility. Interfacial tension measurements have been carried out in three different fluid systems of known phase behavior characteristics using pendent drop shape analysis and capillary rise techniques. The quantities of fluids in the feed mixture have been varied during the experiments to investigate the compositional dependence of fluid-fluid miscibility.

The miscibility conditions determined from the VIT technique agreed well with the reported miscibilities for all the three standard fluid systems used. This confirmed the sound conceptual basis of VIT technique for accurate, quick and cost-effective determination of fluid-fluid miscibility. As the fluid phases approached equilibrium, interfacial tension was unaffected by gas-oil ratio in the feed, indicating the compositional path independence of miscibility. Interfacial tension was found to correlate well with solubility in multicomponent hydrocarbon systems. The experiments as well as the use of existing computational models (equations of state and Parachor) indicated the importance of counter-directional mass transfer effects (combined vaporizing and condensing mass transfer mechanisms) in fluid-fluid miscibility determination.

A new mechanistic Parachor model has been developed to model dynamic gas-oil miscibility and to determine the governing mass transfer mechanism responsible for miscibility development in multicomponent hydrocarbon systems. The proposed model has been validated to predict dynamic gas-oil miscibility in several crude oil-gas systems. This study has related various types of developed miscibility in gas injection field projects with gas-oil interfacial tension and identified the multitude of roles played by interfacial tension in fluid-fluid phase equilibria. Thus, the significant contributions of this study are further validation of a new measurement technique and development of a new computational model for gas-oil interfacial tension and miscibility determination, both of which will have an impact in the optimization of field miscible gas injection projects.

# 1. INTRODUCTION

## 1.1 Problem Statement

Nearly about two thirds of original oil in place remains unrecovered in the crude oil reservoirs after the application of primary (pressure depletion) and secondary (waterflooding) oil recovery technologies. This remaining oil amounts to a staggering 377 billion barrels in the known oil fields of the United States. Hence, more attention is being paid to Enhanced Oil Recovery (EOR) processes to recover this huge amount of trapped oil.

Currently miscible CO<sub>2</sub> gas injection has become the most popular EOR process in the United States for light oil reservoirs. In addition to recovering the trapped oil, this EOR process has the added advantage of CO<sub>2</sub> sequestration for the reduction of greenhouse gas emissions into the atmosphere. The trapping of crude oil in oil reservoirs after primary and secondary oil recovery processes is mainly due to rock-fluids interactions including capillary forces, which prevent the oil from flowing within the pores of reservoir rock, thereby leaving huge amounts of residual oil in reservoirs. These capillary forces can be reduced to a minimum if the interfacial tension between the injected fluid and the trapped crude oil is reduced to zero. Zero interfacial tension is nothing but miscibility between the injected gas and crude oil. Thus there is a need for miscibility development between injected gas and the crude oil in a gas injection EOR process to remobilize the huge amounts of trapped oil and improve the oil recovery. Oil recovery in a miscible gas injection process can be maximized by choosing the operating conditions such that the injected gas becomes miscible with the crude oil. Hence an accurate prior laboratory evaluation of gas-oil miscibility conditions is essential for

process design and economic success of miscible gas injection field projects. The primarily available experimental methods to evaluate gas-oil miscibility under reservoir conditions are the Slim-Tube Test (STT), the Rising Bubble Apparatus (RBA) and the method of constructing Pressure-Composition Diagrams (PXD). Apart from these experimental techniques, several computational models are also available to determine gas-oil miscibility. The most important and popular among these models are the equation of state (EOS) model and the analytical model.

In its very definition, fluid-fluid miscibility means the absence of an interface between the fluid phases, that is, the value of interfacial tension between the two phases is zero. However, none of the presently used conventional experimental techniques mentioned above for gas-oil miscibility evaluation satisfy this fundamental definition of miscibility. They do not provide direct and quantitative information on interfacial tension. Instead, they rely on indirect interpretation of miscibility from the amount of oil-recovered in a slim-tube test or qualitatively from the appearance of gas bubbles rising in a column of oil in the rising-bubble apparatus. Furthermore, some of these techniques are time consuming (eg. 4-5 weeks for a slim-tube test measurement) and also there exist neither a standard design nor a standard set of criteria to determine miscibility in slim-tube and rising bubble experimental techniques resulting in uncertainty and lack of confidence in the results obtained.

To overcome the disadvantages of the above-mentioned conventional approaches to determine gas-oil miscibility, recently a new technique of Vanishing Interfacial Tension (VIT) has been developed based on the fundamental definition of zero interfacial tension at miscibility [1 - 3]. In this method, the gas-oil interfacial tension is measured at

reservoir temperature and at varying pressures or enrichment levels of gas phase. The gas-oil miscibility condition is then determined by extrapolating the plot between interfacial tension and pressure or enrichment to zero interfacial tension. In addition to being quantitative in nature, this method is quite rapid (1-2 days) as well as cost effective. This new technique so far has been successfully implemented for optimization of two miscible gas injection field projects, namely Rainbow Keg River (RKR) in Alberta and the Canadian Terra Nova offshore field. However, this technique remains to be further verified for model fluid systems with known phase behavior characteristics and also needs to be compared with computational models of miscibility prediction. These concerns need to be addressed in further developing this promising new technique for gas-oil miscibility evaluation that has already demonstrated its usefulness and cost-effectiveness in two different field applications. Further development of the VIT technique is also required to enable its wide acceptance by industry and to answer the questions regarding the compositional dependence of this technique on mass transfer interactions between the fluids due to varying gas-oil ratios in the gas-oil mixture.

The terms miscibility and solubility are widely used in phase behavior studies of ternary fluid systems. The distinction between these two terms still appears to be somewhat hazy, leading to their synonymous use in some quarters. This needs to be explored further to determine the relationship between these two properties to clear the long existing confusion. As noted earlier, miscibility of two fluids is related to interfacial tension between them by the fundamental definition and hence the computational models used to predict interfacial tension can also be used to model fluid-fluid miscibility.

However, to the best of our knowledge, no attempts have been made so far in this direction to model fluid-fluid miscibility from interfacial tension.

While most of the thermodynamic properties refer to individual fluid phases, interfacial tension is unique in the sense that it is a property of the interface between the fluid phases. The IFT, being a property of the interface, is strongly dependent on mass transfer interactions between the fluid phases and hence can be used as a good indicator of mass transfer effects between the fluid phases. These multiple roles of interfacial tension in phase behavior characterization and fluid phase equilibria have not been duly recognized. This is further compounded with the difficulty that, still there exists no computational model to accurately predict interfacial tension in hydrocarbon systems involving multicomponents in both liquid and vapor phases such as crude oil-gas systems. Furthermore, the utility of dynamic interfacial tension to infer information on governing mass transfer mechanism (vaporizing / condensing) responsible for thermodynamic equilibrium has been largely ignored. These important aspects in the study of interfacial interactions during fluid-fluid miscibility that have been long ignored have defined the scope of the present study.

## **1.2 Objectives**

The objectives of this study are:

- (1) To conduct interfacial tension measurements in a standard ternary liquid system of known phase behavior characteristics at ambient conditions to relate solubility, miscibility and interfacial tension

- (2) To carry out interfacial tension measurements in standard gas-oil systems of known phase behavior characteristics at elevated pressures and temperatures to further validate the new VIT technique
- (3) To study the compositional dependence of VIT technique by varying the solvent-oil ratio in the feed mixture during the IFT measurements in standard fluid systems at ambient conditions as well as at elevated pressures and temperatures
- (4) To compare the VIT experimental results of Rainbow Keg River (RKR) and Terra Nova reservoirs with the miscibility predictions of EOS model
- (5) To investigate the utility of the conventional Parachor IFT model to predict fluid-fluid miscibility in multicomponent hydrocarbon systems
- (6) To develop a new computational model to predict dynamic IFT and to model fluid-fluid miscibility in multicomponent hydrocarbon systems
- (7) To model fluid-fluid miscibility measured in standard gas-oil systems at elevated pressures and temperatures

### **1.3 Methodology**

One standard ternary liquid system and two standard gas-oil systems of known phase behavior characteristics have been chosen for IFT measurements in this study. The standard ternary liquid system used consisted of benzene, ethanol and water. This system has been studied in the literature and its phase diagram and solubility data at ambient conditions have been well established. IFT measurements have been carried out in this standard ternary liquid system at ambient conditions using the pendent drop and capillary rise techniques. The measured IFT data have then been used to correlate solubility and miscibility with IFT and to determine miscibility conditions using the VIT technique. The

VIT miscibility has then been compared with the miscibility conditions reported from the phase diagram and the solubility data to evaluate the validity of the VIT technique for the standard ternary liquid system.

The first standard gas-oil system used consisted of n-decane against CO<sub>2</sub> gas. This standard gas-oil system has known miscibility conditions from rising bubble and slim-tube measurement techniques at 100° F. The synthetic oil mixture consisting of 25 mole% n-C<sub>1</sub>, 30 mole% n-C<sub>4</sub> and 45 mole% n-C<sub>10</sub> against CO<sub>2</sub> gas has been selected as the second standard gas-oil system for VIT experimentation. This system has reported miscibility values from slim-tube, phase diagram measurements and analytical model predictions at 160° F. The well-known capillary rise technique has been adapted and initially calibrated with pendent drop technique for IFT measurements in n-decane-CO<sub>2</sub> system at 100°F. Then, IFT measurements have been conducted at elevated pressures using the capillary rise technique in the two standard gas-oil systems of n-decane-CO<sub>2</sub> and synthetic oil mixture-CO<sub>2</sub> at 100°F and 160°F, respectively. The measured IFT data have then been used to determine miscibility using the VIT technique as well as for comparison with the reported miscibilities from the other techniques to validate the VIT technique in standard gas-oil systems.

Different solvent-oil ratios in the feed mixture have been used during the IFT measurements in all the three standard fluid systems at ambient conditions as well as at elevated pressures and temperatures to investigate the compositional dependence of the miscibility conditions determined from the VIT technique.

Miscibility conditions have been computed for Rainbow Keg River (RKR) and Terra Nova reservoir fluids using equation of state (EOS) computational model. The effects of

tuned and untuned equations of state on EOS miscibility predictions have been examined. Both tuned and un-tuned equations of state miscibility predictions have then been compared with the miscibilities reported from the VIT experiments for both the reservoir fluids to validate the VIT technique. The conventional Parachor IFT model has been used to determine miscibility for Rainbow Keg River (RKR) reservoir fluids to evaluate the performance of Parachor model to determine fluid-fluid miscibility.

Due to the poor performance of Parachor model to determine IFT and fluid-fluid miscibility in multicomponent hydrocarbon systems, a new mechanistic Parachor model has been developed in this study to model gas-oil IFT, miscibility and to determine the governing mass transfer mechanism responsible for miscibility development in gas-oil systems. The newly proposed mechanistic Parachor model has been validated by modeling the IFT's reported in literature for several crude oil and crude oil-gas systems. Finally, the interfacial tensions and miscibilities measured in the two standard gas-oil systems of n-decane-CO<sub>2</sub> and synthetic oil mixture-CO<sub>2</sub> at elevated pressures and temperatures have been modeled using the proposed mechanistic Parachor model.

## 2. LITERATURE REVIEW

### 2.1 Current EOR Scenario in United States

Nearly about 377 million barrels of crude oil remains trapped in reservoirs after primary recovery and secondary water floods in United States alone. This enormous known to exist oil resource in depleted oil fields shows the potential prospect for improved oil recovery processes in the U.S.

Currently in U.S, 48% of EOR production comes from gas injection and the remaining 52% of EOR production is from steam injection projects [4]. Stosur et al. [5] have studied EOR developments and their future potential in the U.S and concluded that miscible CO<sub>2</sub> gas injection is slowly taking the lead and will continue to grow faster than other EOR methods. This changing EOR scenario in U.S is clearly depicted in Figures 1-2. In Figure 1, the total EOR production and the percent of total EOR production from gas injection are plotted for the past two decades. Similarly, the gas injection EOR production and the percent of gas injection EOR production from miscible CO<sub>2</sub> gas injection are plotted for the last two decades in Figure 2.

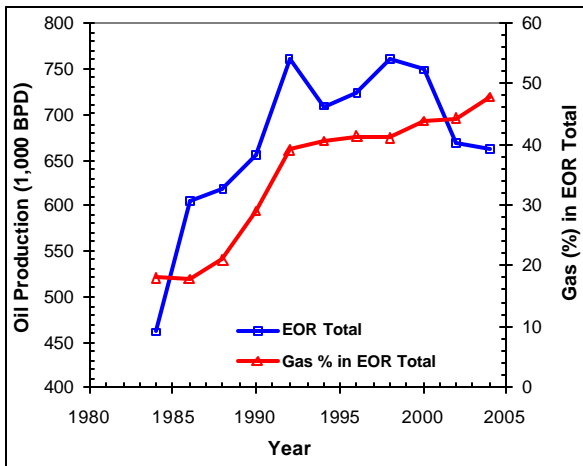


Figure 1: Gas Injection EOR in US

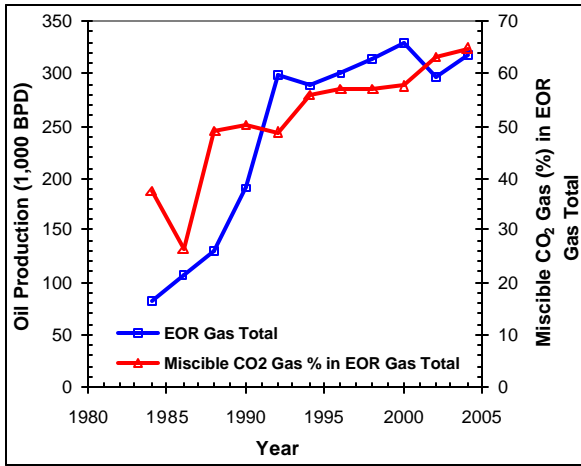


Figure 2: Miscible CO<sub>2</sub> Gas Injection EOR in US

From Figure 1, it can be seen that the percent of gas injection share in total EOR production has steadily increased from 18% in 1984 to about 48% in 2004. This clearly shows the increasing popularity of gas injection processes for improved light oil recovery applications in the United States.

In Figure 2, the wide utility of miscible CO<sub>2</sub> gas injection can be seen among the other gas injection EOR processes. The CO<sub>2</sub> miscible gas injection is contributing the major portion of gas injection EOR production and its share in gas injection EOR has steadily increased from 38% in 1984 to about 65% in 2004.

Thus, from the above discussion on EOR statistics in the United States, it can be said that currently miscible CO<sub>2</sub> gas injection process has become the most popular EOR process for light oil reservoirs in the U.S. Similar conclusion can be made even on the World EOR scenario [4]. The economics of these miscible gas injection projects in the field can be improved by operating the reservoir pressures close to minimum miscibility pressures (MMP) or using the hydrocarbon injection gas enrichments close to minimum miscibility enrichments (MME). However, this requires accurate laboratory measurements of gas-oil miscibility conditions. Hence the laboratory measurements of minimum miscibility pressures and compositions have become an integral part in the design of field miscible gas injection projects.

## **2.2 Definition of Fluid-Fluid Miscibility**

Rao [1], Rao and Lee [2] and Rao and Lee [3] have reviewed the literature and reported the following definitions of fluid-fluid miscibility.

The term, “Miscible Displacement”, may be defined as any oil recovery displacement process where there is an absence of a phase boundary or interface between the displaced and displacing fluids [6].

Two fluids are miscible when they can be mixed together in all proportions and all mixtures remain in a single phase. Because only one phase results from mixtures of miscible fluids, there are no interfaces and consequently no interfacial tension between the fluid phases [7].

Miscibility is defined as that physical condition between two or more fluids that permits them to mix in all proportions without the existence of an interface [8].

Two fluids that mix together in all proportions within a single fluid phase are “miscible” [9].

Thus, from the above cited literature on definitions of fluid-fluid miscibility, it is clearly evident that, the very definition of fluid-fluid miscibility is the absence of interface between the fluids, that is, zero interfacial tension between the two fluid phases.

### **2.3 Need for Fluid-Fluid Miscibility in Gas Injection EOR**

Nearly about two thirds of original oil in place found in oil reservoirs is left behind at the end of primary depletion and secondary waterfloods. This is mainly due to capillary forces that prevent oil from flowing within the pores of reservoir rock, trapping large amounts of residual oil in reservoirs. The capillary force (capillary pressure) can be defined as the force per unit area resulting from the interaction of the fluid-solid surface forces and the fluid-fluid interfacial forces and the geometry of the porous medium in which they exist and is given by:

$$P_c = \frac{2s \cos q}{r} \dots\dots\dots (1)$$

Where  $P_c$  is the capillary pressure,  $\sigma$  is the oil-water interfacial tension and  $\theta$  is the contact angle and  $r$  is the capillary pore radius.

These capillary forces can be reduced to a minimum if the interfacial tension between the injected fluid and the trapped crude oil is reduced to zero. Zero interfacial tension is nothing but miscibility between the injected fluid and reservoir crude oil [6 - 9]. Thus there is a need for miscibility development between the gas injected (hydrocarbon gas or  $\text{CO}_2$ ) and the crude oil in order to remobilize these huge amounts of trapped oil and improve the overall oil recovery efficiency.

#### **2.4 Experimental Techniques to Determine Gas-Oil Miscibility**

Minimum miscibility pressures (MMP) and minimum miscibility enrichments (MME) are the two important parameters used for assessing miscibility conditions for displacements of oil by gas. The minimum miscibility pressure as the name implies is the lowest possible pressure at which the injected gas ( $\text{CO}_2$  or hydrocarbon) can achieve miscibility with reservoir oil at reservoir temperature. The minimum miscibility enrichment is the minimum possible enrichment of the injection gas with  $\text{C}_2\text{-C}_4$  components at which miscibility can be attained with reservoir oil at reservoir temperature. Operating pressures below MMP or injection gas enrichments below MME result in immiscible displacements of oil by gas and, consequently, lower oil recoveries. Hence, prior laboratory evaluation of gas-oil miscibility conditions is essential for economic success of field miscible gas injection projects.

The primary experimental methods to evaluate miscibility under reservoir conditions are the slim-tube displacement, the rising bubble apparatus and the technique of constructing pressure composition (P-X) diagrams.

### **2.4.1 Slim-Tube Displacement Test**

This test is the most common and has been widely accepted as the “petroleum industry standard” to determine gas-oil miscibility. Slim-tube is a narrow tube packed with sand or glass beads. The tube is saturated with live oil at reservoir temperature above the saturation pressure. The oil is then displaced from the tube by injecting the gas at constant pressure. Several displacements are conducted at different pressures (or enrichments), some above MMP (or MME) and the others below MMP (or MME) and the oil recovery is monitored during the displacements. The miscibility conditions are then determined by plotting the oil recovery versus pressure (or enrichment). The point on the plot at which the recovery changes slope is considered to be the MMP (or MME).

Although the slim-tube is widely accepted, there is neither a standard design, nor a standard operating procedure, nor a standard set of criteria for determining miscibility conditions using this technique [10]. Elsharkawy et al. [10] thoroughly reviewed the literature and discussed several non-uniformities observed in the design and operation of this experimental technique. Some of the important observations from the study of Elsharkawy et al. [10] are quoted below.

“Slim tube length, diameter, type of packing, and the permeability and porosity of the packing have varied greatly in the design used in industry. There are more than 30 studies in the literature that show the effects of these design variables on MMP determination. Unfortunately, some of the conclusions of these studies are contradictory”.

“There is considerable difference of opinion among researchers on the effect of packing material on miscibility conditions determined using slim-tube. Some say that

packing material has no effect, while the others maintain that oil recovery depends on the dispersion level caused by the packing material”.

“There is a considerable difference of opinion reported in literature on the effect of flooding rate on oil recovery and miscibility”.

Furthermore, there exists no fixed criteria for determining miscibility with a slim-tube and hence individual researchers have defined their own criteria to identify slim-tube miscibility. Klins [11] described the different available slim-tube miscibility definitions in the literature in detail and are cited below.

“80% of the in place oil is recovered at CO<sub>2</sub> breakthrough and 94% at a GOR of 40,000 SCF/bbl [12].”

“90% oil recovery at 1.2 hydrocarbon pore volumes of CO<sub>2</sub> injected [13].”

“Smooth transition from zero to full light transmittance over a production interval of several percent of a pore volume” in a 5-ft long vertical sand pack run below the critical velocity as defined by Dumore [14].

“Breakpoint in the [oil] recovery [versus pressure] curve is clearly identifiable ..... a slim tube miscibility can be defined there [15].”

Normally, one displacement test within a slim-tube requires one day, with another day or two in between for cleaning and resaturation of the slim-tube. Thus, this test is costly, very time consuming and it may take several weeks (normally 4 to 5) to complete one miscibility measurement. Therefore, the main disadvantages associated with this technique are:

- The lack of fixed design, operating procedure and miscibility defining criteria
- The indirect interpretation of miscibility from oil recovery

- It requires very long times and hence is expensive

### **2.4.2 Rising Bubble Apparatus**

In this method, the miscibility is determined directly from the visual observations of changes in shape and appearance of bubbles of injected gas rising in a visual high pressure cell filled with the reservoir crude oil. A series of tests are conducted at different pressures or enrichment levels of the injected gas and the bubble shape is monitored to determine miscibility. Bubble shapes gradually vary from “spherical,” to “ellipsoidal,” to “ellipsoidal cap,” and finally to “skirted ellipsoidal cap” as miscibility is approached.

This test is completely qualitative in nature and the miscibility is simply inferred from visual observations. Hence, some subjectivity is associated with the miscibility interpretation of this technique, as it lacks quantitative information. Therefore, the results obtained from this test are somewhat arbitrary, but however this test is quite rapid and requires less than 2 hours to determine miscibility [10]. This method is also cheaper and requires smaller quantities of fluids, compared to slim-tube. The main disadvantages associated with this technique are:

- The subjective interpretation of miscibility from visual observations
- Lack of any quantitative information to support the results
- Some arbitrariness associated with miscibility determination

### **2.4.3 Pressure Composition (P-X) Diagrams**

The pressure composition diagrams are constructed by conducting phase behavior measurements in high-pressure visual cells at reservoir temperature. On the diagram, the composition is expressed as a mole fraction of injection gas. Different amounts of

injection gas are added to reservoir crude oil and the loci of bubble point and dew point pressures are determined to generate the phase boundaries.

A single phase exists above the phase boundary lines, while the two phases coexist below the phase boundaries. In other words, miscibility develops outside the two-phase envelope, while immiscibility exists inside the two-phase envelope. The conditions needed for miscibility development between any composition of injection gas and reservoir crude oil at reservoir temperature can be determined from the diagram. However, this test is also time consuming, quite expensive, cumbersome, requires large amounts of fluids and subject to experimental errors.

#### **2.4.4 The New Vanishing Interfacial Tension (VIT) Technique**

To overcome most of the disadvantages of the above-mentioned conventional experimental approaches to determine miscibility, recently a new technique of vanishing interfacial tension (VIT) has been reported for gas-oil miscibility evaluation [1 - 3]. This method is based on the fundamental definition of zero interfacial tension at miscibility.

In this method, the gas-oil interfacial tension is measured at reservoir temperature as a function of pressure or gas enrichment. The gas-oil miscibility is then determined by extrapolating the plot between interfacial tension and pressure or enrichment to zero interfacial tension. In addition to being quantitative in nature, this technique is quite rapid (1-2 days) as well as cost effective. This technique has been so far successfully utilized in optimizing the injection gas compositions for two miscible gas injection projects, one in Rainbow Keg River (RKR) reservoir, Alberta and the other in Canadian Terra Nova offshore field. However, this technique remains to be further validated for fluid systems of known phase behavior characteristics and also needs to be compared with

computational models of miscibility prediction. Furthermore, the compositional dependence of miscibility conditions determined using this technique still remain to be explored. All these concerns need to be addressed in order to further develop this promising new technique for gas-oil miscibility evaluation that has already demonstrated its usefulness and cost-effectiveness in two different field applications. This is one of the main objectives of the present study.

## **2.5 Mass Transfer Effects in Gas-Oil Miscibility Development**

The compositional changes resulting from the mass transfer between reservoir oil and injected gas during the gas injection displacement processes are mainly responsible for gas-oil miscibility development. During displacements of oil by gas, miscibility develops mainly due to three types of mass transfer mechanisms between the fluids in reservoir, namely vaporizing mechanism, condensing mechanism and combined condensing/vaporizing mechanism.

In the vaporizing process, the injected gas is relatively a lean gas consisting of mostly methane and other low molecular weight hydrocarbons. As the injected fluid moves through the reservoir, it contacts the reservoir oil several times and becomes enriched in composition by vaporizing the intermediate components ( $C_2$  to  $C_4$ ) from the crude oil. This process continues till the injected gas attains miscibility with reservoir oil.

In the condensing process, the injected gas contains significant amounts of intermediates ( $C_2$  to  $C_4$ ). During the multiple contacts of the injected gas with crude oil in the reservoir, the intermediates condense from gas phase into the oil phase. The continuation of this process modifies the reservoir oil composition to become miscible with injected gas, resulting in miscible displacement.

In the combined condensing/vaporizing process, the light intermediate compounds in the injected gas ( $C_2$  to  $C_4$ ) condense into the reservoir oil, while the middle intermediate compounds ( $C_5$ - $C_{10}$  to  $C_{30}$ ) in the crude oil vaporize into the injected gas. This prevents miscibility between fluids near the injection point as the oil becomes heavier. As the injection of gas continues, there will be no further condensation of light intermediates from the injected gas into this saturated oil. However, the vaporization of middle intermediates continues from the oil enriching the injected gas further. As this condensation/vaporization process continues farther into the reservoir, the gas becomes enriched to greater and greater extents as it contacts more and more oil and eventually becomes miscible with reservoir oil. This mechanism involving simultaneous counter-directional mass transfer of components between the phases is shown to be the one that most frequently occurs during the displacements of oil by gas [16].

Thus, from the above discussion on gas-oil miscibility development in crude oil reservoirs, it is evident that miscibility develops dynamically by multiple contacts of the crude oil with injected gas due to simultaneous counter-directional mass transfer interactions between crude oil and gas. Therefore, this implies the possible relationship of dynamic gas-oil miscibility with dynamic gas-oil interfacial tension and hence the use dynamic gas-oil interfacial tension to predict the dynamic gas-oil miscibility in gas injection EOR projects needs to be explored.

## **2.6 Computational Models to Determine Gas-Oil Miscibility**

Several computational models are available in the literature to determine fluid-fluid miscibility. The most important among these models are equation of state (EOS)

calculations and analytical models based on tie-line length calculations. The brief description of these two computational models is provided below.

### **2.6.1 EOS Models**

Phase behavior calculations of reservoir fluids are routinely carried out using equations of state in petroleum industry today. Among all the equations of state available, Peng-Robinson (PR) [17] equation of state is perhaps the most popular and is widely used. It is a common practice to tune equations of state prior to use for accurate phase behavior prediction of reservoir fluids. However, there still exists uncertainty in the current literature whether to tune or not to tune equations of state for reliable phase behavior calculations.

Before using any EOS for phase-behavior calculations, it is necessary to calibrate the EOS against the experimental data by adjusting the input values of some uncertain parameters in the EOS so as to minimize the difference between the predicted and measured values. This adjustment which usually takes place via a regression routine is known as EOS tuning. The effectiveness of each experimental property is introduced into the EOS model through its weight factor. Weight factors are assigned to each property based on its accuracy and reliability of measurement. The weakness of EOS towards calculation of some specific properties, the reliability of data and the target for the fluid properties study affect the values of different weight factors. This triggered the need for a fixed set of weight factors to compensate for the EOS weakness. As a result, Coats and Smart [18], Coats [19] and Behbahaninia [20] recommended a universal set of weight factors for proper tuning of EOS, which are shown in Table 1.

**Table 1: Optimum Weight Factors for Proper EOS Tuning (Coats and Smart, 1986; Coats, 1988; Behbahaninia, 2001)**

Property	Weight Factor
Saturation Pressure	50
Oil Specific Gravity	5 – 10
Gas Compressibility Factor	2 – 3
All Other Properties	1

The higher the weight factor, more accurate is the measurement of that data and hence more importance must be given to match that property. However, if the input parameters of EOS were adjusted widely by assigning weight factors other than those suggested above to match the experimental data, it would lead to unrealistic results. This is known as over tuning of EOS. Pederson et al. [21] discussed the dangers of over tuning of EOS and provided many examples of reliable predictions without any tuning, but only by a proper analysis and characterization of real reservoir fluids. Danesh [22] suggested that, in general, any leading EOS, which predicts the phase behavior data reasonably well without tuning, would be the most appropriate choice for phase behavior calculations.

With the use of equations of state (EOS) model, the predictions of phase behavior have become more reliable due to advances in computer-implementation of iterative vapor-liquid equilibrium flash calculations. However, this approach requires large amounts of compositional data of the reservoir fluids for computations, which have to be obtained from laboratory PVT measurements.

The gas-oil miscibility computations made using EOS models and their comparison with the experimental measurements reported in literature are discussed below.

Lee and Reitzel [23] determined the miscibility conditions of Pool A crude oil from the Brazeau River Nisku field with an injection gas containing 90 mole% of methane by conducting laboratory slim-tube tests. They compared the experimental results with PR-EOS calculations and found that the EOS predictions were higher by about 4.0 MPa than the experimental slim-tube measurement. They attributed this deviation to inaccuracies in estimating the critical points as well as to lack of suitable experimental PVT data to fine tune the PR-EOS. Firoozabadi and Aziz [24] compared the slim-tube miscibility conditions with PR-EOS calculations for four different reservoir fluids. They found that PR-EOS predictions were consistently higher by about 0.7-9.0 MPa for all the four systems studied. Hagen and Kossack [25] measured the MMP of methane-propane-n-decane system using a high-pressure sapphire cell and compared their experimental result with slim-tube displacements and modified three-parameter PR-EOS calculations. They were able to perfectly match the sapphire cell measurement of MMP with three parameter PR-EOS, using binary interaction coefficients as regression variables. Ahmed [26] proposed a new “miscibility function” using the analogy of miscibility with critical point at which the K-values for all the components converge to unity. He used this miscibility function in PR-EOS and matched the slim-tube experimental results of several reservoir fluid systems reported in literature with an absolute average deviation of about 3.4%.

### **2.6.2 Analytical Models**

The analytical solution for a ternary oil-gas system consisting of crude oil and natural gas was first proposed by Welge et al. [27]. Helfferich [28] later developed an elegant mathematical theory for two-phase three-component flow in porous media. Dumore et al.

[29] extended the Helfferich's mathematical theory to complex ternary gas injection displacement processes.

Monroe et al. [30] successfully applied the theory of Helffrich to quaternary systems. They made an important contribution by introducing an additional tie-line called, crossover tie-line to the already existing initial and injection tie lines that are known to influence the analytical solution behavior. These analytical theory solutions were later used by Johns, Dindoruk and Orr [31 - 35] to develop the so-called analytical model to compute gas-oil miscibility.

The analytical model [36 - 38] has been widely used in recent years to calculate MMP's and MME's for real systems. The main principle involved in this analytical approach is that all key tie-lines intersect each other in a multicomponent system and hence these tie- line intersections can be used to determine the MMP's. The key tie-lines are first determined for various increasing pressures. MMP is then defined as the pressure at which one of the key tie-lines becomes a critical tie-line, that is, a tangential tie-line of zero length to the critical locus. Besides speed and accuracy, the main advantage of this method is that the computed MME's and MMP's are dispersion-free. Oil and gas mixing due to dispersion affects the displacement efficiency and hence the oil recovery. Dispersional effects are much likely to be greater in the field than observed in the laboratory. The main disadvantage of this analytical technique is that a good equation of state fluid characterization is required.

Jessen et al. [39] developed an algorithm based on analytical solution for calculation of minimum miscibility pressure for the displacement of oil by multicomponent gas injection. They introduced a new global approach using the key tie-line identification

approach initially proposed by Wang and Orr [40]. They predicted the MMP's of several gas-oil systems using their analytical model and the model predictions are shown to be in good agreement with slim-tube measurements.

Wang and Orr [41] used a model based on analytical theory to calculate the MMP's for displacements involving multiple components in both the oil and gas phases. They matched the analytical model MMP predictions with numerical simulation and slim-tube displacement tests.

The fact that all miscibility evaluations are being compared against slim-tube results clearly indicates that the status of slim-tube as the industry standard. However, it needs to be noted that the slim-tube has limitations and uncertainties as discussed earlier in Section 2.4.1.

## **2.7 Interfacial Tension**

Since this study mainly deals with gas-oil miscibility determination using interfacial tension, various aspects related to interfacial tension such as the role of interfacial tension in fluid phase equilibria, IFT measurement techniques and available IFT predictive models reported in literature are thoroughly reviewed and presented in the following sections.

### **2.7.1 Role of Interfacial Tension in Fluid-Fluid Phase Equilibria**

Interfacial tension (IFT) is the surface tension that exists at the interface between the two immiscible fluid phases. In the bulk fluid phase, each molecule is surrounded by the molecules of same kind and hence the net force on the molecule is zero. However, a molecule at the interface is surrounded by the different molecules of both the bulk fluid

phases lying on each side of the interface. The very origin of interfacial tension lies in this asymmetrical force field experienced by the molecules at the interface.

Unlike all the physical properties of the bulk fluid phases, interfacial tension is unique in the sense that it relates to the interface between the two immiscible fluids. This interface consists of a thin region of finite thickness that includes all the characteristics of the respective bulk fluid phases in contact. Being a sensitive property, the interfacial tension is much more strongly affected by the thermodynamic variables such as pressure, temperature and the compositions of the bulk fluids than does the individual bulk phase properties. Since interfacial tension is a very resultant of the dissimilarity of the force field across the interface, it poses to be a good indicator of the dissimilarity of the two bulk fluid phases in contact. Higher the value of interfacial tension, the greater is the dissimilarity between the bulk fluid phases. If the properties of the two phases in contact approach each other, the interfacial tension must decrease. The interfacial tension approaches zero when the two bulk fluid phases become similar [42].

The time-dependent variations in the interfacial tension when the two immiscible fluid phases each containing multiple number of components are brought into contact are as a result of various mass transfer interactions taking place between the fluid phases to reach the thermodynamic equilibrium. These interactions include simultaneous vaporization and condensation of the components between the two fluid phases and take place mostly by diffusion due to the concentration gradients and by dispersion. Thus, interfacial tension, being a property of interface, could indeed reflect these dynamic interactions occurring between the two fluid phases due to the variations in thermodynamic conditions. Hence, the dynamic behavior of interfacial tension reflects all

the mass transfer effects in its instantaneous value and hence can be used to characterize the mass transfer mechanisms (vaporizing or condensing) responsible for attaining that thermodynamic state.

The terms, miscibility, solubility and interfacial tension, are commonly used in fluid phase equilibria studies. Review of literature shows that zero interfacial tension is a necessary and sufficient condition to attain miscibility [6 - 9]. Blanco et al. [43] measured vapor-liquid equilibrium data at 141.3 KPa for the mixtures of methanol with n-pentane and n-hexane and then determined upper critical solubility for methanol, n-hexane mixtures from the measured miscibility data. This indicates the relationship of miscibility with upper critical solubility of a solute in solvent for ternary fluid systems. Lee [44] modified the adsorption model proposed by van Oss, Chaudhury and Good [45] by the inclusion of equilibrium spreading pressure to calculate the liquid-liquid interfacial tension. This study related equilibrium interfacial film pressure and the interfacial tension for prediction of miscibility of liquids and reported that all the theory of miscibility of liquids can also be applicable to the solubility of a solute in a solvent. Thus, the thermodynamic properties of miscibility, solubility and interfacial tension appear to be somehow correlated in ternary fluid systems.

Interfacial tension, being a property of the interface between two fluids, is assumed to be dependent on molar ratio of the two fluids (solvent-oil ratio) in the feed mixture. Simon et al. [46] measured the IFT of a reservoir crude oil at various solvent-oil ratios in the feed using high-pressure interfacial tensiometer. The results from this experimental study indicated dependence of IFT on solvent-oil ratio in the feed, in which an increase of IFT was observed with an increase in concentration of CO<sub>2</sub> gas in the feed. Such a

dependence of IFT on solvent-oil ratio in the feed indicates the influence of mass transfer effects on IFT.

Thus, the tension at the interface separating the three phases of matter is a unique property in that it can reveal to us a great deal of information about the phases in contact such as the solubility characteristics of one phase into the other, miscibility between the two fluid phases and the direction and extent of mass transfer of components taking place between the fluid phases. However, all these multitudes of roles played by interfacial tension in fluid-fluid phase equilibria have yet to be thoroughly understood and utilized as an easy and effective tool for multicomponent phase equilibria characterizations. This necessitates further study in this area to explore and understand these multiple roles of interfacial tension in fluid-fluid phase equilibria.

### **2.7.2 IFT Measurement Techniques**

A wide variety of interfacial tension measurement techniques have been reported in literature during the last century for the measurement of interfacial tension between two immiscible fluid phases. Rusanov and Prokhorov [47] thoroughly discussed in their recent monograph various available interfacial tension measurement techniques along with their theoretical bases and instrumentation. Drelich et al. [48] summarized the most commonly used interfacial tension measurement methods, both classical and modern.

The most widely used IFT measurement methods can be generally classified into two groups. The first group includes the capillary rise, drop weight, ring and Wilhelmy plate methods. These methods have been summarized by Adamson [49] in detail. The second group consists of the so-called shape methods, which include the pendent drop, sessile drop and the spinning drop methods. These have been summarized and compared by

Manning [50]. The choice of a particular method for interfacial tension measurement largely depends on the purpose and the adaptability of the technique to suit the experimental environment. The widely used interfacial tension measurement techniques and the principles and procedures involved in these techniques are briefly discussed below.

### 2.7.2.1 Capillary Rise Technique

This is one of the oldest and most commonly used methods for determining the interfacial tension between the fluids. The basis for this technique is very simple and it involves measuring the height of the meniscus in a circular glass tube of a known inner radius. Moderately reliable measurements of IFT can be made using this technique in a much lesser time. This technique can be also easily modified as a method of measurement of high precision and good accuracy.

The equations governing the capillary rise in a circular glass tube are well known. The force acting along a vertical capillary due to the upward pull of interfacial tension must be balanced by the oppositely directed force of gravity acting on the mass of liquid in the capillary above the outside level of the liquid. Thus, the force balance in a capillary is given by:

$$2pr\sigma \cos \theta = pr^2 h \Delta \rho \frac{g}{g_c} \dots\dots\dots (2)$$

Solving for interfacial tension ( $\sigma$ ) gives,

$$\sigma = \frac{rh\Delta\rho g}{2 \cos\theta g_c} \dots\dots\dots (3)$$

Where,  $\sigma$  = interfacial tension in  $mN / m$   
 r = pore throat radius in  $cm$

$h$  = capillary rise in *cm*  
 $\Delta\rho$  = density difference between the fluids in *g/cc*  
 $\theta$  = equilibrium contact angle in degrees  
 $g$  = acceleration due to gravity ( $980 \text{ cm/sec}^2$ )  
 $g_c$  = conversion ( $1 \frac{\text{g}\cdot\text{cm}/\text{sec}^2}{\text{dyne}}$ )

The capillary rise technique is the most accurate and hence can be used for precise measurements of interfacial tension. This is further substantiated by the following comments of other researchers.

“The capillary rise method is generally regarded as the most accurate of all the methods, partly because the theory has been worked out with considerable exactitude and partly because the experimental variables can be closely controlled [49].”

“The capillary rise method can be one of the most accurate techniques used to make surface tension measurements [48].”

“The capillary rise method is considered to be one of the best and most accurate absolute methods, good to a few hundredths of a percent in precision [49].”

Richards and Carver [51] and Harkins and Brown [52] provided the best discussions on the experimental aspects of capillary rise method. For most accurate results in this technique, the glass tube used must be clean and the liquid should wet the wall of the capillary completely. The capillary must be absolutely vertical with accurate uniform radius and should not deviate from the circularity in cross section. This technique can be easily adapted to high pressures and temperatures and is well suited to measure low interfacial tensions. Park and Lim [53] recently reported interfacial measurements in Nickel plating solution-CO<sub>2</sub>-surfactant systems using this technique at high pressures and

temperatures. They measured the interfacial tensions in the range of 70 mN/m to about 3 mN/m up to the temperatures of 71° C and the pressures of about 19 MPa.

**2.7.2.2 Drop Weight Method**

This is approximately a reasonable accurate method and is commonly used for measuring surface tension of a liquid-air or liquid-liquid interface. In this method, the weight of a drop falling from the end of a capillary tube of known radius is measured for sufficient time to determine the weight per drop accurately.

The weight (W) of the drop falling off from the capillary of radius (r) is then correlated to interfacial tension (σ) using the equation,

$$W = 2\pi r \sigma f \dots\dots\dots (4)$$

Where, f is the correction factor for drop weight to account for the unreleased portion of the drop volume from the end of capillary during the drop detachment.

Harkins and Brown [52] reported that the correction factor ‘f’ is a function of  $r/V^{1/3}$ , where V is the drop volume. They have experimentally determined and tabulated ‘f’ for different values of  $r/V^{1/3}$ .

Sonntag [54] proposed a cubic polynomial empirical correlation to determine the correction factor f as a function of  $r/V^{1/3}$  and is given by:

$$f = 0.167 + 0.193\left(\frac{r}{V^{1/3}}\right) - 0.0489\left(\frac{r}{V^{1/3}}\right)^2 - 0.0496\left(\frac{r}{V^{1/3}}\right)^3 \dots\dots\dots (5)$$

The measurement of interfacial tension with this technique is very simple, but however this technique is much sensitive to vibration. Even a small vibration during the experiment may result in drop detachment from capillary before the drop reaches its critical size. This technique is dynamic and not well suited to measure interfacial tension

in the systems that need longer time to establish their equilibrium interfacial tension. This technique is not very accurate and commercial application of this technique at high pressures and temperatures has not been reported.

**2.7.2.3 Ring Method**

This method is generally attributed to du Nouy [55]. In this method, the interfacial tension is determined from the force required to detach a ring from the interface. The ring is usually made up of platinum or platinum-iridium alloy with a radius (R) of about 2-3 cm. The radius of the wire (r) varies from 1/30 to 1/60 of that of the ring.

The detachment force is given by the interfacial tension ( $\sigma$ ) multiplied by the product of perimeter (p) of the three-phase contact line, which is equal to twice the circumference of the ring ( $4\pi R$ ), and the cosine of contact angle measured for the liquid meniscus in contact with the ring surface ( $\cos \theta$ ). Thus, the force balance for the ring is given by:

$$F = (s 4\pi R \cos \theta) \cdot f \dots\dots\dots (6)$$

Where, f is the correction factor to account for the additional amount of liquid removed during the detachment of ring from interface. The correction factor f varies from 0.75 to 1.05 and is a function of dimensions of the ring (R, r), its surface wettability ( $\theta$ ) and the difference in densities between the fluids ( $\Delta\rho$ ).

Harkins and Jordan [56] tabulated the correction factor ‘f’ for different values of R/r at  $\theta = 0^\circ$ . Zuidema and Waters [57] proposed the following empirical correlation to calculate the correction factor ‘f’.

$$f = 0.725 + \left( \frac{9.075 \times 10^{-4} F}{\rho^3 \Delta r g R^3} - \frac{1.679 r}{R} + 0.04534 \right)^{1/2} \dots\dots\dots (7)$$

The Eq. 7 is applicable only when  $0.045 \leq \Delta r g R^3 / F \leq 7.5$ .

Thus, the interfacial tension in a ring method can be computed using Eq. 6, the experimentally measured value of ‘F’ and the correction factor ‘f ‘ calculated using the Eq. 7.

The major disadvantage of this technique is the error caused by the deformation of the ring, which happens frequently during handling and cleaning. Care must be taken to have perfect wetting of ring surface by the denser fluid ( $\theta = 0^\circ$ ). Otherwise, additional correction of the instrument reading is required. This technique is not suited for low IFT measurements and it is also difficult to adapt this technique for IFT measurements at high pressures and temperatures.

**2.7.2.4 Wilhelmy Plate Apparatus**

This method is another detachment method, where the force required to detach an object from the interface of a fluid is used to determine the interfacial tension. In this method, a thin platinum plate is suspended from one arm of the balance with the plate immersed in liquid. The interfacial tension is then determined by measuring the pull during the detachment of the plate from the interface. The detachment of the plate can be accomplished either by lowering the liquid surface or raising the balance.

The force (F) measured during the detachment of plate by the micro-balance is used to calculate interfacial tension ( $\sigma$ ) using the equation,

$$\sigma = \frac{F}{p \cos \theta} \dots\dots\dots (8)$$

Where, p is the perimeter of the three phase contact line, which is calculated from the dimensions of the plate as; 2 (length + thickness) of the plate and  $\theta$  is the contact angle between the liquid meniscus and the plate surface. The results from this technique are

extremely sensitive to adsorption of organic compounds from the laboratory environment or test solutions.

### 2.7.2.5 Pendent Drop Method

When a drop is hanging from a tip, it elongates and forms the pendent drop due to significant variations in hydrostatic pressure. The two parameters of the so-formed pendent drop, namely the equatorial diameter ‘D’ and the diameter ‘d’ at a distance ‘D’ from the top of the drop are experimentally measured. The interfacial tension ( $\sigma$ ) is then calculated using the equation,

$$s = \Delta \rho g D^2 / H \dots\dots\dots (9)$$

Where,  $\Delta\rho$  is the density difference between the fluids and the parameter ‘H’ is a function of the shape factor ‘S’= d/D.

The value of the shape dependent parameter ‘H’ can be obtained from the tabulated data of 1/H vs. S values reported by Neiderhauser and Bartell [58] and Stauffer [59].

The disadvantage with this technique is that only four points in the drop profile were chosen to calculate the interfacial tension. Therefore, this technique does not truly represent the actual drop profile. Furthermore, even small errors in the measurements of diameters may result in large errors in interfacial tension value calculated.

However, with the advances in mathematical algorithms to solve complex equations, computer iterative calculations and high quality image analysis capabilities, the drop shape analysis techniques have been developed recently for IFT calculations by fitting the actual drop shape profiles of the pendent drops [60 - 63]. The basic principle of these drop shape analysis techniques is explained below.

The shape of a drop is determined by the combined effect of interfacial and gravity forces. Surface forces tend to make the drop spherical, where as the gravity forces try to elongate the pendent drop. When gravitational and surface tensional effects are comparable, then the interfacial tension can be determined from the drop shape analysis.

Mathematically, the force balance between the interfacial tension and gravity is well reflected in Laplace equation of capillarity. Hence, this equation has been used to fit the experimental drop profiles in drop shape analysis techniques. This equation represents the mechanical equilibrium between the two immiscible fluids. It relates the pressure difference across the interface to the interfacial tension and the curvature of the interface and is given by:

$$\sigma \left( \frac{1}{R_1} + \frac{1}{R_2} \right) = \Delta P \dots\dots\dots (10)$$

Where,  $\sigma$  is the interfacial tension,  $R_1$  and  $R_2$  are the two principal radii of curvature and  $\Delta P$  is the pressure difference across the interface.

Rotenberg et al. [64] developed a technique called Axisymmetric Drop Shape Analysis-Profile (ADSA-P), which is the most superior technique of all the available drop shape analysis techniques. This technique considers several points numbering about 50-100 on the actual measured drop profile of the pendent drop and fits a Laplacian curve to the measured profile. Then, an objective function is defined as the sum of the squares of the normal distances between the experimental points and the calculated curve to describe the deviation of the experimental profile from the theoretical profile. The objective function is finally minimized using a non-linear regression procedure to yield the interfacial tension. This is the most powerful method widely used to measure to

interfacial tension in a variety of systems for several years [65]. In this technique, a four parameter nonlinear least squares fit with a Newton optimization procedure and incremental loading has been used to approach the exact solution. However, this method has resulted in convergence problems for very flat drop shapes due to the limitations associated with Newton's algorithm. The Newton's method fails when the initial value is distant from the solution.

To overcome the disadvantages of ADSA-P technique developed by Rotenberg et al. [64], Jennings and Pallas [66] proposed a similar method using a modified Gauss-Newton scheme with restricted step to find the exact solution. However, they have used a linear interpolation to compute the residuals in an attempt to reduce the computational time. This simplification affects the accuracy of this method for highly curved surfaces.

As a result, del Rio and Neumann [67] recently proposed a more advanced version of ADSA-P, in which a combination of the Newton and Levenberg-Marquardt methods have been used to solve the equation. In this method, the computations first start with Newton optimization procedure due to its fast convergence capability and is then aborted as soon as divergence is detected. Then, the technique automatically switches to Levenburg-Marquardt method to approach the solution. The Levenburg-Marquardt method is computationally expensive, when compared to Newton method, but is known to be globally convergent. Del Rio and Neumann [67] used their ADSA-P technique for more accurate surface tension measurements and reported accuracies better than 0.5%.

Thus, with recent superior drop shape analysis techniques, this method has become the most reliable and accurate method to measure interfacial tension between fluids. This technique has been successfully used in recent literature for interfacial tension

measurements at elevated pressures and temperatures in crude oil-gas systems. Gasem et al. [68], Firozabadi et al. [69], Rao [1] and Rao and Lee [2] have reported interfacial tension measurements in crude oil-gas systems using this technique at reservoir conditions of temperature and pressure.

However, the major disadvantage of this technique is that it requires a drop shape to compute IFT. In situations of low interfacial tension between the fluids such as in gas-oil systems, it is difficult to form pendent drops. Hence, this technique fails in such situations. Therefore, this technique may not be applicable at conditions close to critical point, where the interfacial tension is close to zero. As all other techniques, this technique also requires extremely clean environment for reliable and reproducible results.

**2.7.2.6 Sessile Drop Method**

This method uses the analysis of the stationary drop profile resting on a solid substrate for interfacial tension calculations. In this method, the equator of the drop first needs to be identified and then the height from the top of the drop to the equator ( $z_c$ ) is measured. For a very large sessile drop, the following expression proposed by Sonntag [54] is used to compute the interfacial tension ( $\sigma$ ).

$$s = \Delta r g z_c^2 / 2 \dots\dots\dots (11)$$

However, it is experimentally difficult to precisely locate the equator of the drop and measure  $z_c$ . Although in some occasions this method may be the only one feasible, but it does not yield precise and accurate measurements.

Even the recently developed drop shape analysis techniques [60 - 64, 66, 67] may not be adequate for sessile drops, whose shapes are strongly influenced by gravity. The gravity forces normally tend to flatten a sessile drop. Therefore, these flattened data

points in a sessile drop may cause a large error even if they lie very close to the best fitting curve, and hence lead to considerable bias in solution. For very flat sessile drops, the effect of gravity dominates and hence the interfacial forces have negligible effect on the drop shape. Therefore, the use of drop shape to determine interfacial tension is not preferred for flattened sessile drops.

### 2.7.2.7 Spinning Drop Method

This method is particularly developed for measuring ultra low interfacial tensions. The principle of this method is based on rotating a drop for IFT measurement and was first proposed by Vonnegut [70]. Princen et al. [71] later developed this method into a workable method by solving the equations explicitly for IFT. However, the disadvantage of their method is that it requires drop volume to be accurately known, which is difficult to measure.

The method proposed by Princen et al. [71] was later modified by Cayias et al. [72] for IFT measurements without using the drop volume. They developed the University of Texas spinning drop interfacial tensiometer (UTSDIT) for low IFT measurements and is widely used in many laboratory and commercial applications today.

Gravitational effects on drop shape are minimized in this technique by rotating the suspended drop and liquid contained in a tube horizontally about its longitudinal axis. The radius ( $r$ ) of the cylindrical drop obtained at high rotational velocities ( $\omega$ ) and the density difference between the fluid phases ( $\Delta\rho$ ) are then used to determine the interfacial tension. Couper et al. [73] proposed the following equation to calculate the interfacial tension ( $\sigma$ ) using the spinning drop method, given by:

$$s = 0.25r^3\Delta\rho\omega^2 \dots\dots\dots (11)$$

This technique has been very successful for measuring ultra low interfacial tensions up to  $10^{-6}$  mN/m in immiscible oil-water systems [74]. Particularly for ultra low IFT systems, sufficient time should be allowed in this technique for the drop shape to reach the equilibrium. The major disadvantage of this technique is that it cannot be used at high pressures; however the modification of equipment for commercial application of this technique at high pressures is still evolving [75].

### **2.7.3 IFT Predictive Models**

Interfacial tension is an important property for many processes such as enhanced oil recovery by gas and chemical injection and flow through porous media, and in mass and heat transfer phenomena. However, the experimental data on interfacial tension for complex fluid systems involving multicomponents in both the fluid phases is scarce. Therefore, there has long been a need for a simple and accurate computational model for prediction of interfacial tension in multicomponent hydrocarbon systems. Several models have been proposed for the calculation of interfacial tensions of simple fluids and their mixtures in the past few decades. The most important among these models are the Parachor model [76, 77], the corresponding states theory [78], thermodynamic correlations [79] and the gradient theory [80]. Although all these models are based on some theoretical background, they require experimentally determined parameters to predict interfacial tension. The background, basis and the procedures involved in these models are discussed briefly below.

#### **2.7.3.1 Parachor Model**

This model is the oldest among all the IFT prediction models and because of simplicity is still most widely used in petroleum industry to estimate the interfacial

tension between fluids. Empirical density correlations are used in this model to predict the interfacial tension.

Macleod-Sudgen [76, 77] related surface tension of a pure compound to the density difference between the phases, as:

$$\mathbf{s}^{1/4} = P(\mathbf{r}_M^L - \mathbf{r}_M^V) \dots\dots\dots (13)$$

Where  $\mathbf{s}$  is the surface tension in mN/m,  $\mathbf{r}_M^L$  and  $\mathbf{r}_M^V$  are the molar density of the liquid and vapor phases, respectively, in gmole/cm<sup>3</sup> and the proportionality constant between IFT and  $\Delta\rho$ , P is known as the Parachor. The Parachor values of various pure compounds have been determined from measured surface tension data using Eq. 13. The Parachor values of different pure compounds are reported in the literature by several investigators [81- 84].

The equation proposed by Macleod-Sudgen [76, 77] was later extended to multicomponent hydrocarbon mixtures using the simple molar averaging technique of Weinaug and Katz's [85] for the mixture Parachor,

$$\mathbf{s}^{1/4} = \mathbf{r}_M^L \sum x_i P_i - \mathbf{r}_M^V \sum y_i P_i \dots\dots\dots (14)$$

Where  $x_i$  and  $y_i$  are the equilibrium mole fractions of component  $i$  in the liquid and vapor phases, respectively, and  $P_i$  is the Parachor of the component  $i$ . Parachor values of pure compounds are used in Eq. 14 to calculate the interfacial tension of the mixtures, considering the Parachor value of a component in a mixture is the same as that when pure [22].

This model has been extensively used for prediction of surface tensions of pure compounds and binary mixtures. However, the model gives poor IFT predictions in complex multicomponent hydrocarbon mixtures [86]. Several attempts have been already

made in the past to improve the Parachor model predictions for multicomponent systems. Fawcett [87] has reviewed these reported studies in detail. These attempts are mostly directed at improving the Weinaug and Katz's [85] molar averaging technique for the mixture Parachor determination. The Hough-Stegemeier [88] correlation is almost the same as Weinaug-Katz correlation, but with a slight change in the values of empirical parameters. Other investigators have revised the Weinaug-Katz correlation by using complex mixing rules in multicomponent mixtures [89], or incorporating a parameter, that depends on the density difference between the fluid phases [86]. The Lee-Chien's modification [90] is based on critical scaling theory and still retains the same functional form of Weinaug-Katz correlation. All these modifications are intended to match the experimental data based on empirical correlations and there appears to be no strong theoretical background associated with them.

In the application of the Parachor model to multicomponent mixtures, Parachor values of pure components are used in IFT predictions, considering each component of the mixture as if all the others were absent. It appears that significant interactions take place between the various components in a multicomponent mixture and hence the inability of pure component Parachor values to account for these interactions of each component with the others in a mixture appears to be the main reason for poor IFT predictions from the Parachor model in multicomponent hydrocarbon systems. Therefore, a thorough literature review was conducted to understand the physics and the thermodynamics behind the Parachor. The important findings from this review are discussed below.

- **Parachor Physics and Thermodynamics**

Exner [91] defined Parachor as the molar volume at such a temperature at which surface tension has the unit value as long as this temperature does not approach the critical temperature, as described by the following Eqs.15 and 16.

$$P = \frac{M}{r_l - r_v} \sigma^{1/4} \dots\dots\dots (15)$$

Where, P is the Parachor,  $\rho_l$  and  $\rho_v$  denote densities in liquid and vapor phase, respectively,  $\sigma$  is the surface tension and M is the molecular weight.

At temperatures lower than critical temperature,  $\rho_v$  can be neglected when compared to  $\rho_l$  and hence Eq. 15 simplifies to

$$P = Mr_l^{-1} \sigma^{1/4} \dots\dots\dots (16)$$

Parachor is compound specific. Parachor is temperature independent at temperatures below critical temperature for all non-polar and slightly polar compounds [91], as described below.

Eq. 16 can be written in more general form as,

$$P = Mr_l^{-1} \sigma^a \dots\dots\dots (17)$$

Differentiation of Eq. 17 with respect to temperature yields,

$$\frac{\partial P}{\partial T} P^{-1} = a \sigma^{-1} \frac{\partial \sigma}{\partial T} - r_l^{-1} \frac{\partial r_l}{\partial T} \dots\dots\dots (18)$$

With the assumption of temperature independence of Parachor  $\left( \frac{\partial P}{\partial T} = 0 \right)$ , Eq. 18 reduces to,

$$\frac{\partial \sigma}{\partial T} \left( \frac{\partial r_l}{\partial T} \right)^{-1} = a^{-1} \sigma r_l^{-1} \dots\dots\dots (19)$$

Exner [91] tested the temperature dependence of Parachor for polar and non-polar compounds by plotting the left hand  $\left(\frac{\partial s}{\partial T}\left(\frac{\partial r_l}{\partial T}\right)^{-1}\right)$  and the right hand sides  $(sr_l^{-1})$  of Eq.

19. This plot is included as Figure 3, below.

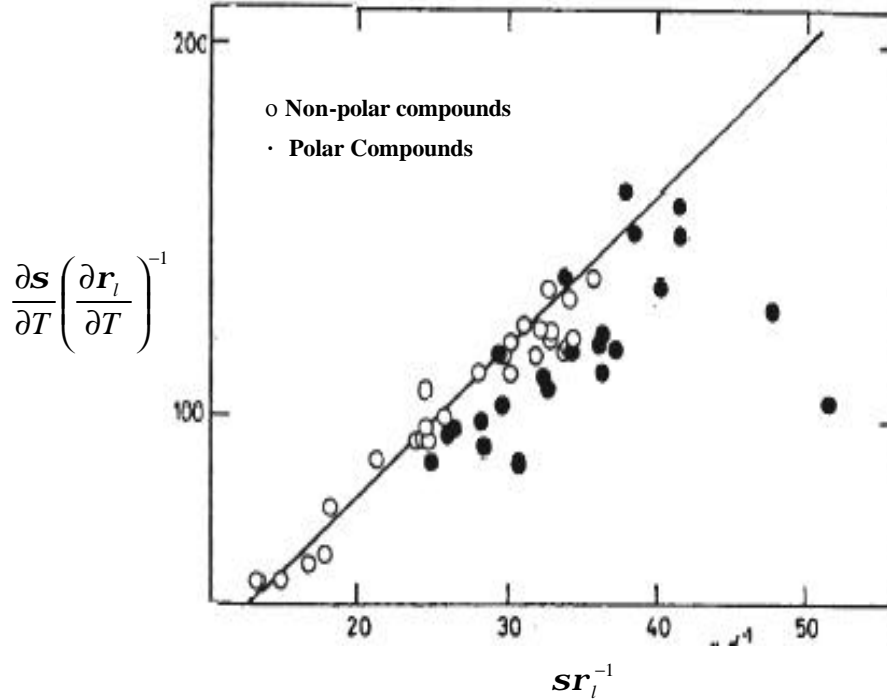


**Figure 3: Effect of Temperature on Parachor (After Exner, 1967; Ref. 91)**

From this plot, it can be seen that, the straight-line slope for all non-polar or slightly polar compounds such as hydrocarbons is almost 4.0, which satisfies the exponent of  $\alpha = \frac{1}{4}$  in the Eq. 16. Therefore, for these compounds a temperature independent Parachor can be assumed. However, for polar compounds, the slope of straight-line lower than 4.0 obtained indicates a higher value of exponent in Eq. 16 suggesting moderate increase of Parachor with temperature. Hence, temperature independence cannot be assumed for the Parachors of strongly associated compounds.

Parachor value of a compound is related to its molecular weight. Firoozibadi et al. [69] used the data from Katz et al. [92] and Rossini [93] to show a linear straight-line relationship between Parachor and molecular weight for n-alkanes. They also computed the Parachors of several distillation cuts of various crude oils from surface tension measurements and showed a quadratic relationship between Parachor and molecular weight for all the crude cuts, except for the residues. They attributed this discontinuity for the last heavy residue fractions largely to the presence of asphaltene materials. The plot of Firoozabadi et al. [69] showing the effect of molecular weight on Parachor for crude cuts and n-paraffins is included as Figure 4.

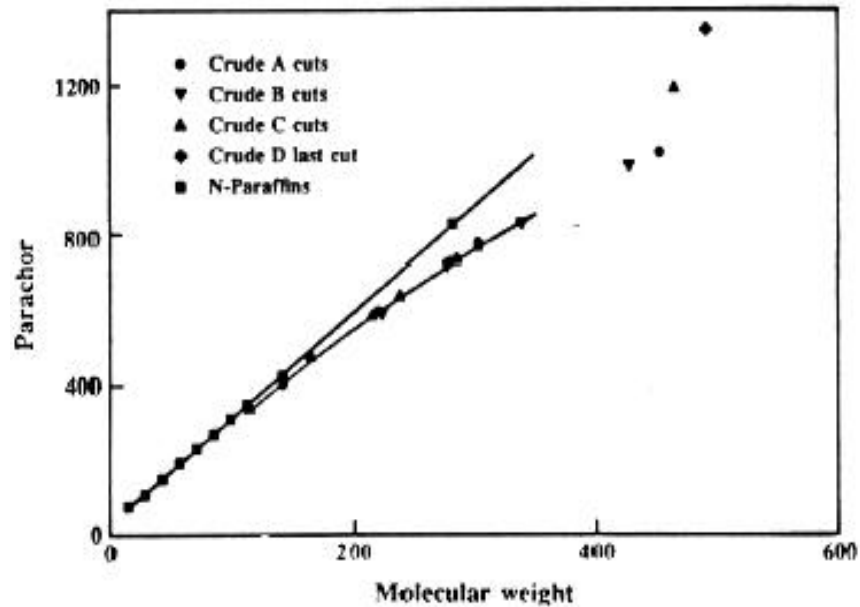


**Figure 4: Parachor vs. Molecular Weight for Crude Cuts and n-Paraffins**  
(After Firoozabadi et al., 1988; Ref. 69)

Parachor value of a compound does not depend on pressure [69]. Firoozabadi et al. [69] determined the Parachors of different crude cuts of various crude oils at different pressures and reported similar Parachor values for individual crude cuts at all the

pressures tested. The data showing the Parachor independence with pressure from the study of Firoozabadi et al. [69] is summarized in Table 2.

**Table 2: Effect of Pressure on Parachors of Crude Cuts (Firoozabadi et al., 1988)**

Crude	Cut M.wt	Pressure (psia)	Surface Tension (mN/m)	Parachor
A	303.0	2013	$13.9 \pm 0.3$	772
		1013	$15.7 \pm 0.6$	777
		13	27.6	780
B	338.5	1013	$16.2 \pm 0.5$	826
		513	$19.2 \pm 0.4$	828
C	285.0	1013	$19.1 \pm 0.4$	738
		513	$20.4 \pm 0.4$	729
		13	30.2	750

Parachor value of a mixture is related to solute concentration [94, 95]. Hammick and Andrew [95] computed Parachor values of mixtures of benzene (non-associated solvent) with various non-associated solutes such as carbon tetrachloride, m-xylene, cyclohexane and chloroform, using surface tension measurements. They found that the Parachor values of the solution are linearly related to solute concentration and either increase or decrease as the solute concentration in the solution is increased. The data from the study of Hammick and Andrew [95] are plotted in Figure 5.

Thus, the important characteristics of Parachor observed in the literature study are summarized in Table 3.

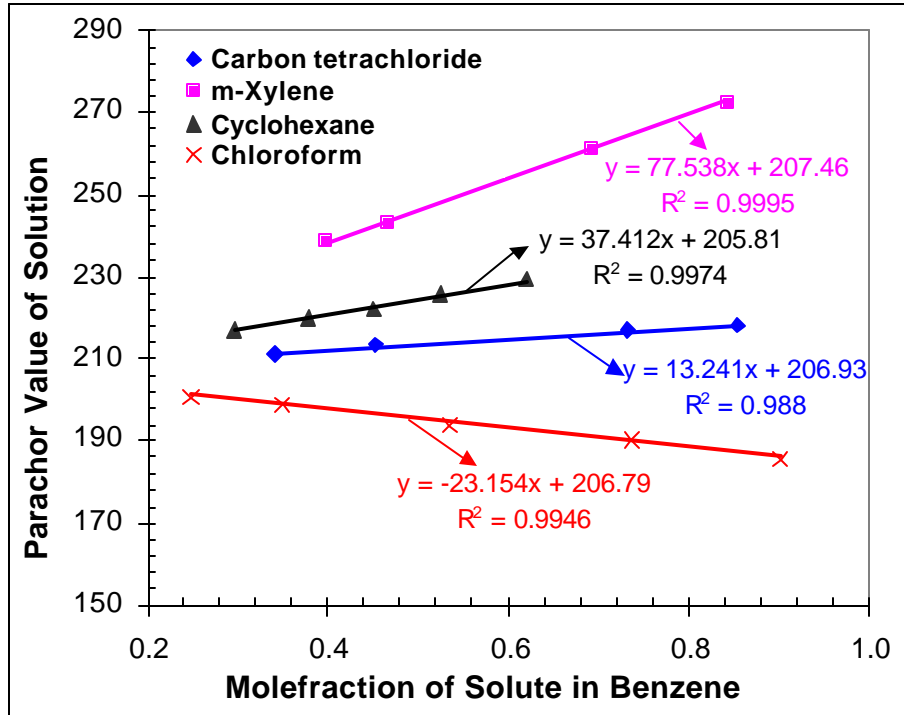


**Figure 5: Effect of Solute Composition on Parachor**  
(Using the Data from Hammick and Andrew, 1929; Ref. 95)

**Table 3: Summary of Parachor Characteristics**

S.No	Parachor Characteristics	Ref #
1	Specific for a compound	91
2	Independent of temperature	91
3	Related to molecular weight of the compound	69
4	Independent of pressure	69
5	Linearly related to solute composition	95

### 2.7.3.2 Corresponding States Theory

The corresponding state theory for IFT calculations is based on the principle that for a pure fluid, the vapor-liquid interfacial tension gradually reduces with temperature and vanishes at critical point. Van der Waals [96] first proposed the following equation to correlate surface tension ( $\sigma$ ) using the corresponding states law.

$$\mathbf{s} = \mathbf{s}_o (1 - T_r)^{\beta} \dots\dots\dots (20)$$

Where,  $T_r$  is the reduced temperature and  $\sigma_o$  and  $\beta$  are the arbitrary parameters. Van der Waals suggested that the parameter  $\beta$  was a universal constant.

Ferguson [97] later showed that surface tensions can be better represented, considering  $\beta$  as a specific parameter. He suggested a value of 1.21 for the exponent ‘ $\beta$ ’ for the cases where only limited data is available. Guggenheim [98] recommended a value of 1.22 for  $\beta$  based on his theoretical studies. Wright [99] experimentally determined  $\beta$  for 14 different compounds and reported variations in  $\beta$  from 0.994 to 1.230.

Brock and Bird [78] calculated the parameter  $\sigma_o$  based on critical properties and used the empirical exponent value of  $\beta = 11/9$  reported by Guggenheim [98] to propose the following equation for interfacial tension.

$$\mathbf{s} = A_c (1 - T_r)^{11/9} \dots\dots\dots (21)$$

Where,

$$A_c = (0.132\mathbf{b}_c - 0.279)(P_c^{2/3}T_c^{1/3}) \dots\dots\dots (22)$$

$\beta_c$  is the slope of the reduced vapor pressure vs. reduced temperature plot at critical point and is determined using the equation,

$$\mathbf{b}_c = 0.9076 \left( \frac{1 + (T_b / T_c) \ln(P_c / P_a)}{(1 - T_b / T_c)} \right) \dots\dots\dots (23)$$

Where,  $T_b$  is the normal boiling point of the substance and  $P_a$  is the atmospheric pressure.

However, the main disadvantage of this model is that all the correlations developed based on corresponding state theory are applicable only to pure fluids. They are not applicable to multicomponent mixtures as the compositions of liquid and vapor change with pressure and temperature.

### 2.7.3.3 Thermodynamic Correlations

For pure liquids, Eckert and Prausnitz [100] considered the system as surface and bulk phases of a pure species consisting of  $N'$  and  $N$  molecules, respectively. The surface free energy  $\sigma$  of the system is defined as the difference between the actual free energy  $G$  for the system of surface area  $\Omega$  and the free energy of the same system with zero surface area.

$$\sigma\Omega = G - (N + N')\mu^o \dots\dots\dots (24)$$

Where,  $\mu^o$  is the chemical potential of the bulk pure liquid.

Partition functions of the cell model were then applied to arrive at the following expression for configurational Helmholtz free energy (F) of the system.

$$F = -NkT \ln[ q \exp(u_c / RT)] - N'kT \ln[ q' \exp(u'_c / RT)] \dots\dots\dots (25)$$

Where,  $k$  is the Boltzmann constant,  $T$  is the absolute temperature,  $q$  is the cell partition function for the bulk liquid,  $u_c$  is the configurational molar energy for the bulk liquid,  $R$  is the gas constant,  $q'$  is the cell partition function of the surface and  $u'_c$  is the configurational molar energy of the surface.

At low to moderate pressures, the  $PV$  term for liquids can be neglected and hence it is reasonable to assume the Helmholtz and Gibbs free energies to be equal. Then, the chemical potential of the bulk pure liquid can be determined using the equation,

$$\mu^o = -kT \ln[ q \exp(u_c / RT)] \dots\dots\dots (26)$$

Now, using the assumption of equivalence of F and G, the Eqs. 24, 25 and 26 are combined and rearranged to yield the following expression for surface tension of the pure liquid.

$$-\frac{\mathbf{s}w}{kT} = \ln q' + \frac{u_c'}{RT} + \frac{\mathbf{m}^o}{kT} \dots\dots\dots (27)$$

Where, w is the surface area per molecule and is given by  $\Omega / N'$

Eq. 27 is the basic thermodynamic equation that can be used to determine the surface tension of a pure liquid from the thermodynamic properties of molecules. The thermodynamic reference state used in this equation is the ideal gas at the same temperature.

Eckert and Prausnitz [100] later extended the thermodynamic correlation of pure liquids to compute the interfacial tension ( $\sigma$ ) of binary liquid mixtures as:

$$\mathbf{s} = x_1\mathbf{s}_1 + x_2\mathbf{s}_2 + x_1x_2\mathbf{h} + \frac{kT}{x_1'w_1 + x_2'w_2} \left[ x_1' \ln \left( \frac{x_1'}{x_1g_1} \right) + x_2' \ln \left( \frac{x_2'}{x_2g_2} \right) \right] \dots\dots\dots (28)$$

Where,  $\xi_1$  is surface area fraction of component 1,  $\sigma_1$  is the surface tension of component 1,  $\xi_2$  is the surface area fraction of component 2,  $\sigma_2$  is the surface tension of the component 2,  $\eta$  is the surface configurational energy density difference,  $x_1'$  is the mole fraction of component 1 in surface,  $x_2'$  is the mole fraction of component 2 in surface,  $x_1$  is the mole fraction of component 1 in bulk liquid,  $x_2$  is the mole fraction of component 2 in bulk liquid,  $\gamma_1$  is the activity coefficient of component 1 in bulk liquid and  $\gamma_2$  is the activity coefficient of component 2 in bulk liquid.

Eckert and Prausnitz [100] used their thermodynamic model of Eq. 28 to predict the interfacial tension of several binary organic mixtures. The model predictions were shown

to be in good agreement with the experimental data with only small deviations in the order of about 0.1 to 0.2 mN/m. They attributed these deviations in the calculation procedure to experimental errors in measuring the bulk activity coefficients and the pure component surface tensions.

Clever and Chase [79] proposed the following thermodynamic model to estimate the interfacial tension in binary mixtures from the pure component surface tension values.

$$\exp(41.74\sigma / T) = x_1 \exp(41.74\sigma_1 / T) + x_2 \exp(-41.74\sigma_2 / T) \dots\dots\dots (29)$$

Where,  $\sigma$  is the mixture surface tension,  $\sigma_1$  and  $\sigma_2$  are the surface tensions of pure components 1 and 2,  $x_1$  and  $x_2$  are the respective mole fractions and T is the absolute temperature.

Clever and Chase [79] reproduced the measured surface tensions of n-hexane-cyclohexane mixtures with an average absolute deviation of about 0.05 mN/m at three different temperatures of 25°, 30° and 35° C with their thermodynamic model.

### 2.7.3.4 Gradient Theory

The gradient theory requires mainly two parameters, the free-energy density of the bulk fluid and the influence parameter of the interface to calculate the interfacial tension between the fluid phases. The free-energy density of the bulk homogeneous fluid is determined using suitable equation of state. The influence parameter carries the information on the molecular structure of the interface and it essentially determines the density gradient with response to the local deviation of chemical potential from its corresponding bulk phase value. The influence parameter is determined using the gradient theory and this parameter together with a homogeneous fluid equation of state is used to characterize the non homogenous vapor-liquid interface.

Cahn and Hilliard [101] first rediscovered and extended the square gradient theory initially proposed by van der Waals [102] for interfacial tension calculations. Urlic et al. [103] later derived an expression for interfacial tension using the gradient theory in the following manner.

The equilibrium densities of a pure fluid were first found using the widely known concept of ‘double tangent construction’. The density ( $\rho$ ) at any position ‘z’ was then retrieved from the same construction of double tangent. The distance between the two tangents was determined using the following function,  $\Delta w(\mathbf{r}(z), T)$ , given by:

$$\Delta w(\mathbf{r}(z), T) = f(\mathbf{r}(z), T) - \mu \mathbf{r}(z) + p \dots\dots\dots (30)$$

Where, f is the Helmholtz energy density, T is the temperature,  $\mu$  is the equilibrium chemical potential and p is the equilibrium pressure.

The square gradient term of Van der Waals was then added to the function given in Eq. 30 to account for gradients in density. Using this additional term, Urlic et al. [103] derived the following complete expression for interfacial tension ( $\sigma$ ).

$$s = \int_{-\infty}^{+\infty} \left[ \Delta w(\mathbf{r}(z), T) + c(\mathbf{r}(z), T) \left( \frac{d\mathbf{r}(z)}{dz} \right)^2 \right] dz \dots\dots\dots (31)$$

The parameter c in Eq. 31 is called as the influence parameter. Yang et al. [104, 105] and Bongiorno et al. [106] related this parameter to the direct correlation function of the homogeneous bulk fluid with the following expression,

$$c = -\frac{1}{12} \int_{r>a} r^2 u(r) dr \dots\dots\dots (32)$$

Where, the distance  $\alpha$  is the distance of minimum approach and  $u(r)$  is the intermolecular potential. The simplest equation for the influence parameter was obtained using the van der Waals theory and is given by,

$$a = -\frac{1}{2} \int_{r>\alpha} u(r) dr^3 \dots\dots\dots (33)$$

$$b = \frac{2}{3} \rho a^3 \dots\dots\dots (34)$$

$$\frac{c}{ab^{2/3}} = 0.305 \dots\dots\dots (35)$$

Carey et al. [107, 108] found that for real fluids, the ratio  $c / ab^{2/3}$  will not be usually equal to 0.305, the value obtained using the van der Waals theory and hence proposed the following alternate expression for the influence parameter.

$$c = 0.27(ab^{2/3}) + 2 \times 10^{-67} \dots\dots\dots (36)$$

The Eq. 36 was obtained by fitting the experimental surface tensions of several n-alkanes from n-C<sub>6</sub> to n-C<sub>16</sub>.

Cornelisse [109], Zuo and Stenby [110] and Miqueu et al. [111] later presented various mathematical equations to estimate the influence parameter by fitting the experimental surface tension data of several pure fluids.

However, all these expressions proposed for the influence parameter in the literature are not fully satisfactory. Miqueu et al. [111] thoroughly discussed the deficiencies of various influence parameter equations. Carey et al. [107, 108] derived the expression for influence parameter using limited number of components and for narrow temperature ranges with high surface tension values ( $\sigma > 14$  mN/m). Therefore, the application of this equation is doubtful in low IFT regions. Cornelisse [109] obtained the coefficients in the

influence parameter equation for each pure fluid, but unable to determine a universal trend for these coefficients. Zuo and Stenby [110] used the equation of state without volume corrections, while deriving the influence parameter equation. Hence, the inaccuracies in liquid volume predictions from the equations of state may result in erroneous values of the influence parameter.

The Helmholtz free energy density and the vapor liquid equilibrium data needed in the interfacial tension calculations of the gradient theory are determined using a suitable equation of state. Such a combination of gradient theory with equation of state for interfacial tension calculations was first proposed by Carey et al. [112]. The literature update on calculations of interfacial tension using the combination of gradient theory and equations of state is provided below.

Carey et al. [112] used Peng-Robinson (PR) Equation of state [17] and determined the influence parameter from the bulk phase properties to predict the surface tensions of 11 pure hydrocarbons, five pure alcohols and 16 binary mixtures. Sahimi et al. [113], Gupta and Robinson [114], Sahimi and Taylor [115] and Cornelisse et al. [116] used gradient theory and PR-EOS to estimate the interfacial properties of several binary systems containing carbon dioxide at high pressures. Perez-Lopez et al. [117] used the combination of gradient theory and a complex equation of state proposed by Mohanty and Davis [118] to predict the surface tension of pure fluids. Relatively good agreement of calculated surface tensions with experimental data was obtained with the Mohanty and Davis (MD) equation of state when compared to the use of PR-EOS in gradient theory calculations.

The gradient theory has been successfully used in the recent literature to determine interfacial tension of pure fluids and binary mixtures. However, it requires several experimentally determined coefficients for the influence parameter calculations. Because of its elaborative calculation procedure and lack of improved results relative to the other IFT predictive models, this method has not received much attention in petroleum industry. Furthermore, the application of gradient theory to test the measured IFT data in hydrocarbon systems containing multiple number of components in both the liquid and vapor phases has not been well reported.

Thus, from the above-cited detailed literature on IFT prediction models, it is clearly evident that there still exists no computational model to accurately predict IFT in hydrocarbon systems involving multiple number of components in both the fluid phases. Therefore, there exists a large void in this area of interfacial engineering that needs to be further investigated.

### 3. EXPERIMENTAL APPARATUS AND PROCEDURES

The experiments to measure interfacial tension were conducted in this study using two different types of fluid systems. The first system used is the standard ternary liquid system of benzene, ethanol and water at ambient conditions. The second system used consisted of two standard gas-oil systems, namely n-decane-CO<sub>2</sub> at 100° F and a synthetic oil mixture consisting of 25 mole% n-C<sub>1</sub>, 30 mole% n-C<sub>4</sub> and 45 mole% n-C<sub>10</sub> against CO<sub>2</sub> gas at 160° F. These systems have been considered as standard as the phase behavior characteristics of these systems are well-known. The IFT measurements were conducted in these two fluid systems using pendent drop shape analysis and capillary rise techniques depending on the adaptability of the technique to suit the experimental environment during the measurements.

Due to variations in the operating conditions of temperature and pressure, IFT measurements were conducted in the two fluid systems using two different sets of equipment incorporated with necessary accessories and instruments. The pendent drop IFT measurements in the standard ternary liquid system at ambient conditions were carried out using an already existing ambient experimental IFT setup. However, for IFT measurements in standard gas-oil systems at elevated pressures and temperatures, a high pressure and high temperature experimental system has been specially designed and assembled for use in this study. This system has the unique capability to operate up to 20,000 psi and 400° F. Therefore, all the details of the experimental apparatus and procedures used in the two fluid systems are discussed separately in the following two sections.

### **3.1 Standard Ternary Liquid System**

#### **3.1.1 Reagents**

Analytic grade reagents were used in the experiments. Benzene used in the experiments was from Fisher Scientific, having a purity of greater than 99%. Ethyl alcohol was from Aaper Alcohol and Chemical Company with a purity of 95%. Deionized water, from Water Quality Laboratory at Louisiana State University, was used. Acetone of purity 99.7%, from Fisher Scientific was used for cleaning the experimental apparatus.

#### **3.1.2 Experimental Setup and Procedure**

The schematic of the experimental setup used for pendent drop interfacial tension measurements is shown in Figure 6. It consisted of an optical cell, solvent reservoir, injection system to inject oil, light source and a camera system connected to a computer for the drop image capture and analysis. The IFT calculations were carried out by fitting the actual pendent drop profiles to the calculated theoretical profile using the Laplace equation of capillarity. The detailed discussion on this calculation procedure is provided in Section 2.7.2.5. The drop shape image analysis software [119] provided by the Kruss Company was used in this study for pendent drop IFT calculations.

Different molar solutions of ethanol and water were prepared using the desired volumetric percentages. These solutions were used as the solvents non-equilibrated with benzene in the experiments. For preparation of solvent solutions pre-equilibrated with benzene, 1000 ml of the non-equilibrated solvent was taken in a glass flask and measured volume of benzene, slightly above the solubility limit corresponding to that solvent composition, was poured into the flask. The flask was tightly closed and rigorously mixed

for 12 hours. After mixing, the solution was filtered to remove the formed oil-solvent emulsion drop-lets, using hardened ashless Whatman filter paper. Then, the filtered solution was allowed to settle for another 12 hours.

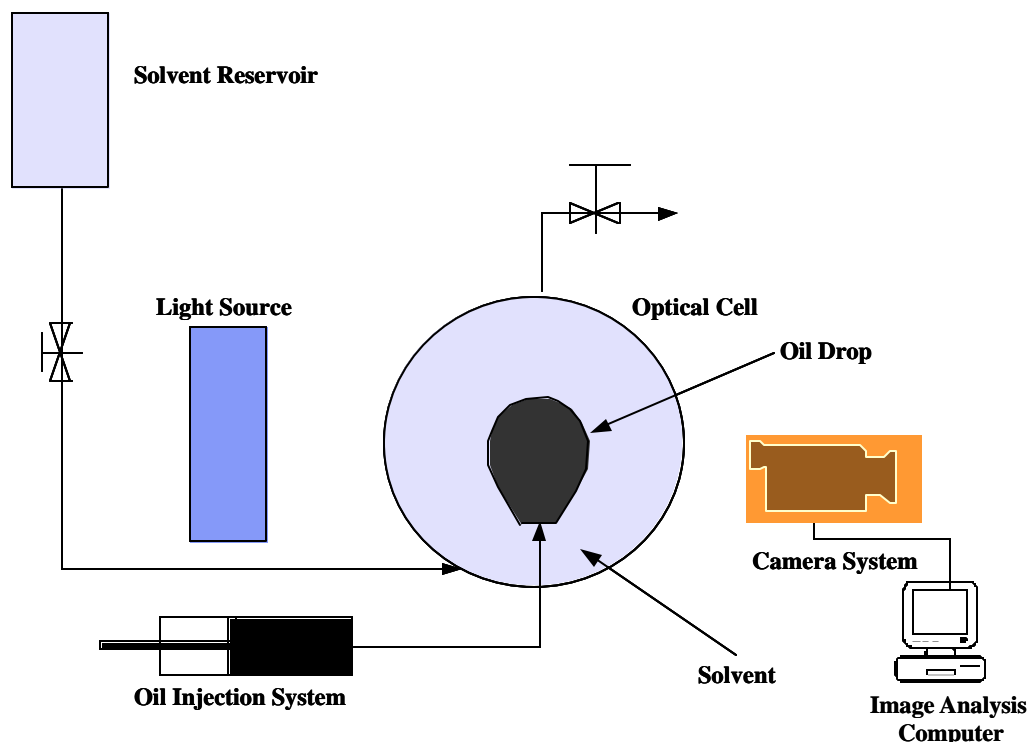


**Figure 6: Schematic of the Experimental Setup Used for Pendent Drop IFT Measurements**

Afterwards, the equilibrated benzene and solvent phases of the solution were carefully collected and stored for use in experiments. The optical cell was first cleaned with deionized water and then with acetone. The solvent (pre-equilibrated or non-equilibrated) is taken in a container (solvent reservoir), which was kept at a sufficient height to allow flow by gravity. The cell was gradually filled up and some solvent was allowed to drain from the top to ensure that there were no trapped air bubbles in the cell. The benzene was then injected into the cell, using the injection system, drop by drop. A

few benzene drops (normally 10-20) were allowed to rise through the solvent and rest at the top of the cell to allow for fluid saturation. Then, a benzene drop was allowed to hang from the capillary tip and the drop image was captured on the computer using the camera system. The captured pendent drop image was then analyzed for IFT using the drop shape image analysis software [119]. The volumes of benzene and the solvent in the cell were varied during the experiments to study the solvent-oil ratio effects on interfacial tension measurements.

At molar concentrations above certain ethanol enrichment in the aqueous phase, benzene pendent drops could not be formed as the benzene quickly escaped in streaks through the solvent. Therefore, the capillary rise technique was adapted and used to measure the interfacial tension at these concentrations. The schematic diagram of the capillary rise technique used is shown in Figure 7.

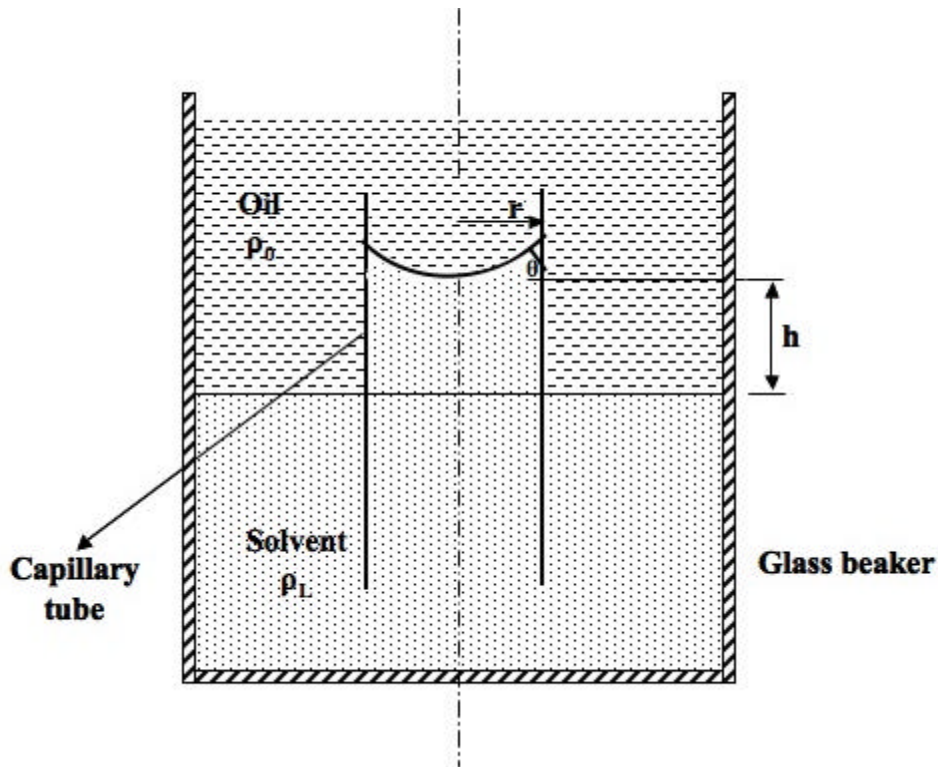


**Figure 7: Schematic of Capillary Rise Technique Used**

In the above schematic,  $r$  is the inner radius of the capillary tube,  $\rho_o$  and  $\rho_l$  are the densities of oil and solvent phases, respectively,  $\theta$  is the equilibrium contact angle and  $h$  is the capillary rise. The detailed discussion on the principle and the equations involved for IFT calculations in this technique are provided in Section 2.7.2.1.

At first, certain volume of aqueous ethanol at particular ethanol enrichment was taken in a glass beaker. Measured volume of benzene about one and one-half times above the solubility limit, was added to the aqueous ethanol. The two fluid phases were thoroughly mixed by shaking and allowed to settle for about one hour. Then, the solution clearly separated into two phases with less denser fluid phase at the top, while the denser fluid phase resting at the bottom. A glass capillary tube (radius  $r = 0.09$  cm) was then carefully inserted into the beaker using an adjustable stand so that it was completely immersed in the two fluid phases. Care was taken to avoid the contact of bottom end of the capillary tube with glass beaker. The interface between the fluid phases slowly raised through the capillary and stabilized at a definite height within a time of about 20 minutes. The capillary rise was then measured using a vernier-equipped cathetometer that reads in units of one-tenth of a millimeter.

The densities of the pre-equilibrated solvent and oil phases were measured using a PAAR DMA512 density meter. The equilibrium contact angles were measured using an ambient optical cell, pre-equilibrated fluid phases and glass substrates with which the capillary tubes were made. The photograph of the equipment used for equilibrium contact angle measurements is shown in Figure 8 and is described elsewhere [120].

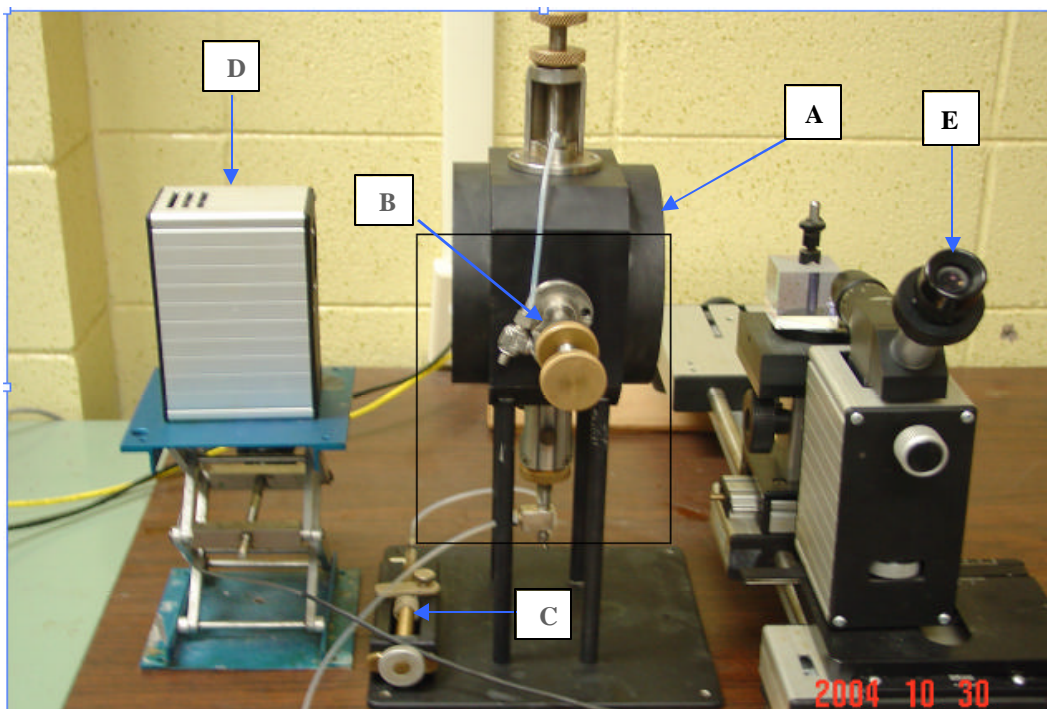


**Figure 8: Photograph of the Equipment Used for Contact Angle Measurements** (A: Optical cell; B: Crystal holder; C: Injection system, D: Light source; E: Goniometer)

The procedure used for benzene equilibrium contact angle measurements was as followed. The glass substrate was first aged in pre-equilibrated aqueous ethanol solvent for about 24 hours. The aged glass substrate was then placed in a crystal holder and assembled carefully into the thoroughly cleaned optical cell. The pre-equilibrated aqueous ethanol solvent was taken in a large container kept at a sufficient height and allowed to flow into the cell by gravity. After the cell was filled, some solvent was allowed to drain from the top to ensure the removal of trapped air bubbles in the cell. Then, the pre-equilibrated benzene drop was placed on the glass crystal using an injection syringe from the bottom of the cell. The cell was then set-aside with all the valves closed to age for 24 hours for the solvent-oil-crystal interactions to reach equilibrium. After 24 hours of aging, the equilibrium contact angle was measured using an eye-piece

goniometer and light source. The measured capillary rise, fluid phase densities and the equilibrium contact angles were then used in Eq. 3 to compute the interfacial tension in capillary rise technique.

## **3.2 Standard Gas-Oil Systems**

### **3.2.1 Reagents**

Analytical grade reagents were used in the experiments. The cleaning solvents (toluene and acetone) and the oil (n-decane) used in the experiments were from Fisher Scientific, all having a purity of 99.9%. The pure gases methane and butane used in the synthetic live oil preparation, the CO<sub>2</sub> gas used in the experiments and the N<sub>2</sub> gas used for drying and purging the flow lines were from Accurate Gas Products and have a purity of 99.7%, 99.5%, 99.9% and 99.9%, respectively. The synthetic live oil was prepared by adding appropriate amounts of light ends, methane and butane into n-decane to match the live oil composition.

### **3.2.2 Experimental Setup and Procedure**

Figure 9 shows the photograph of the apparatus used in this study for IFT measurements in the standard gas-oil systems at elevated pressures and temperatures. Part A in the picture is the high-pressure high-temperature optical cell (has a design rating of 400°F and 20,000 psi), in which the glass capillary tube is stationed. Part B is the transfer vessel wound with heating tapes, used to hold the oil at test conditions of temperature and pressures. Part C is the centrifugal positive displacement pump used to pump oil into the optical cell. Part D is the Ruska pump, which can store and inject the CO<sub>2</sub> gas into the optical cell. Part E is the heating oven used to maintain the temperature of the optical cell and the fluids at the desired value. Part F is the PAAR DMA-512 density meter wrapped

with heating tapes, used to measure the densities of equilibrated oil and gas phases during the experiments. Part G is the light source and part H is the digital video camera used to record the capillary rise observed in the capillary tube, inside the optical cell as well as to capture the pendent drops for drop shape analysis [119]. The detailed discussion on the principles and the equations used in pendent drop shape analysis and capillary rise techniques are provided in Sections 2.7.2.1 and 2.7.2.5, respectively. We believe that after Park and Lim [53], we were the next to successfully use this glass tube based capillary rise technique for IFT measurements with complex hydrocarbon fluids at elevated pressures and temperatures.

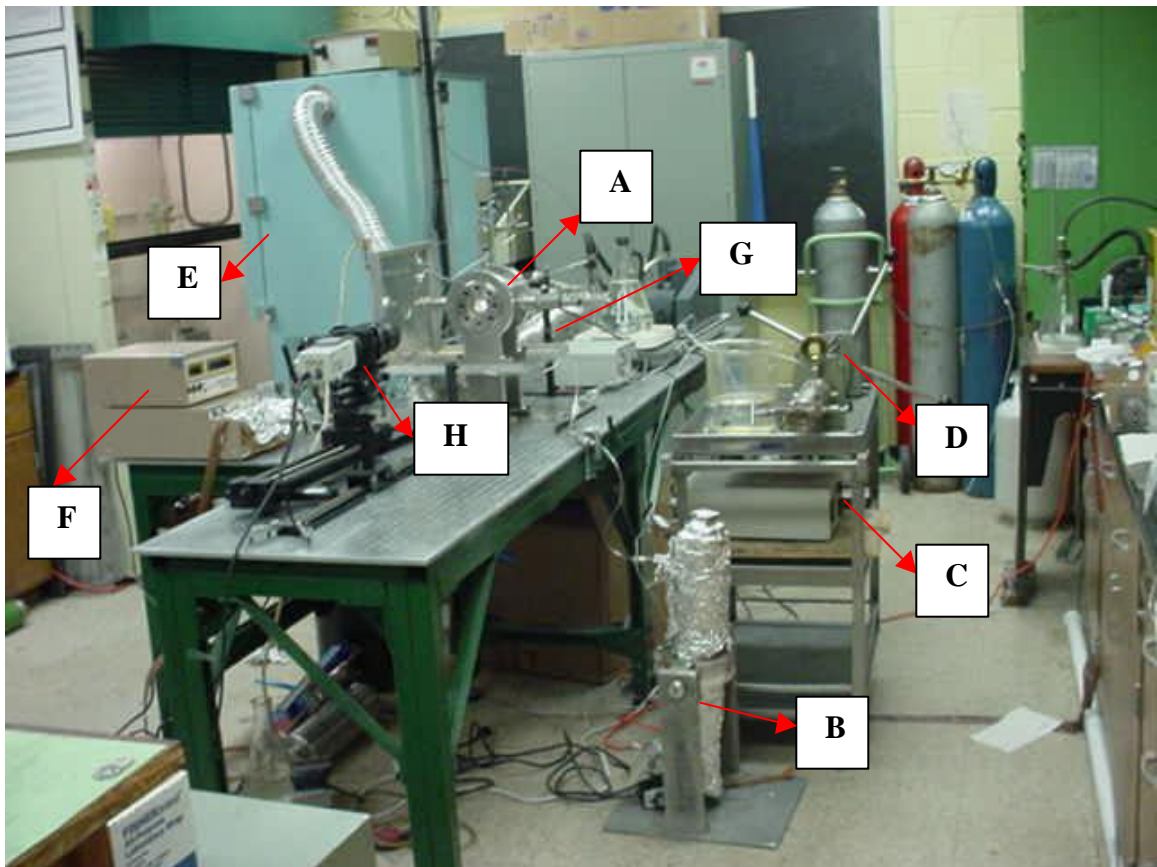


**Figure 9: Photograph of the Equipment Used for IFT Measurements at Elevated Pressures and Temperatures**

At first, the bubble point pressure (the minimum possible pressure at which the fluid will be in single phase) of the synthetic live oil mixture was determined at 160° F. All the interfacial tension measurements must be conducted at the pressures above the bubble point pressure to avoid severe compositional effects during the experiments. Hence, it is necessary to have prior estimation of bubble point pressure of the live oil before interfacial tension measurements. The procedure followed for the bubble point pressure determination of live oil was as followed.

The recombined live oil containing transfer vessel was heated to the test temperature of 160° F using heating tapes and then pressurized to working pressure using the centrifugal pump. Approximately 1 to 2 cc of water was drained through the valve connected to the water-side of the vessel. The vessel was then agitated using the rocking mechanism till the pump displays a constant pressure reading. The collected water was then weighed. The weight of the water collected as well as the pressure reading were recorded. The procedure was then repeated for at least four pressure volume readings until the live oil sample goes into the two-phase region (These measurements represent the region above the bubble point pressure). Similarly, at least four pressure volume readings were taken in the two-phase region, below the bubble point pressure. Now a plot of volume versus pressure was prepared and the bubble point pressure is indicated by the intersection of two distinct linear portions of the plot.

The density meter was initially calibrated for density measurements by measuring the densities of pure CO<sub>2</sub> gas as a function of pressure at 100° and 160° F. The densities of pure fluids, n-decane and synthetic live oil were then measured at various pressures (pressures above the bubble point pressure for the synthetic live oil) at 100° and 160°F,

respectively. A capillary tube of inside diameter 1.0 mm was carefully fitted into one of the crystal holders of the optical cell and is placed inside the cell. The cell was first filled with pure CO<sub>2</sub> gas using the Ruska pump and was heated to desired temperature using the temperature control of the heating oven. Then, the oil (n-decane / synthetic live oil) maintained at the desired temperature (100° / 160° F) in the transfer vessel was injected into the cell using the pump so that the cell was filled with fluids at a fixed initial gas-oil ratio. Nearly about an hour was then allowed for the fluid phases to equilibrate in the cell. The capillary rise observed in the glass tube was then recorded using the light source, digital camera, which was measured precisely using the magnification system of the camera and a computer. The equilibrated liquid and gas phases were allowed to flow through the density meter maintained at desired temperature for density measurements. These measurements were then repeated for different pressures. The pressure in the system was altered either by injecting or withdrawing small amounts of liquid or gas phases, while maintaining the initial gas-oil ratio in the cell as constant as possible.

The measured capillary rise and the densities of equilibrated fluid phases were then used in Eq. 2 to calculate the interfacial tension. A contact angle of  $\theta = 0^\circ$  was used during the IFT calculations as it is reasonable to assume that the liquids wet the glass completely. The whole procedure was then repeated by varying the initial gas-oil ratio of the fluids in the cell to study the effect of gas-oil ratio on IFT.

At certain pressures of specific gas-oil ratios in decane-CO<sub>2</sub> system at 100° F, the pendent drop images of CO<sub>2</sub> gas in n-decane were captured and analyzed for IFT using the drop shape analysis technique [119]. This was done to validate the newly used capillary rise technique for IFT measurements at elevated pressures and temperatures by

comparing the results of capillary rise technique with those obtained using the pendent drop technique. The dynamic variations in capillary rise with time were also measured in synthetic live oil-CO<sub>2</sub> system at 160° F at different gas-oil ratios to study the effect of gas-oil ratio on the dynamic interfacial behavior.

## 4. RESULTS AND DISCUSSION

The results of the research work conducted in this study have been divided and discussed thoroughly in the following seven sections. The first section deals with interfacial tension measurements in a standard ternary liquid system of benzene, ethanol and water at ambient conditions to correlate solubility, miscibility with IFT and to examine the validity of the VIT technique. The solvent-oil ratio in the feed mixture was varied during the experiments to study the effect, if any, of initial composition on IFT and hence on miscibility. The second section involves the interfacial tension measurements in standard gas oil-systems of known phase behavior characteristics at elevated pressures and temperatures to further examine the validity of the VIT technique as well as to study its compositional dependence. The two standard gas-oil systems used are n-decane-CO<sub>2</sub> at 100° F and synthetic oil mixture (25 mole% n-C<sub>1</sub>, 30 mole% n-C<sub>4</sub> and 45 mole% n-C<sub>10</sub>)-CO<sub>2</sub> at 160° F. The IFT measurements in these two sections were carried out using the pendent drop technique for high interfacial tensions and the capillary rise technique for low interfacial tensions.

The third section discusses the comparison of VIT experimental results of Rainbow Keg River and Terra Nova reservoir fluids with the miscibility predictions of EOS computational model. The effects of tuned and untuned equations of state on miscibility predictions from the EOS model are also discussed. Section 4 comprises the results of the investigation on applicability of the conventional Parachor IFT model to predict fluid-fluid miscibility using Rainbow Keg River reservoir fluids. Section 5 discusses the background and the results of the newly developed mechanistic Parachor model to predict IFT and model fluid-fluid miscibility in both crude oil and crude oil-gas systems. Section

6 discusses the modeling results of IFT and fluid-fluid miscibility using the mechanistic Parachor model in standard gas-oil systems at elevated temperatures and pressures. In Section 7, an effort is made to bring together all the aspects of experimental and practical considerations of gas-oil miscibility and its relation to gas-oil interfacial tension.

#### 4.1 IFT Measurements in a Standard Ternary Liquid System

##### 4.1.1 Solubility and Miscibility

The ternary phase diagram of the standard system of ethanol, water and benzene [121] is shown in Figure 10.

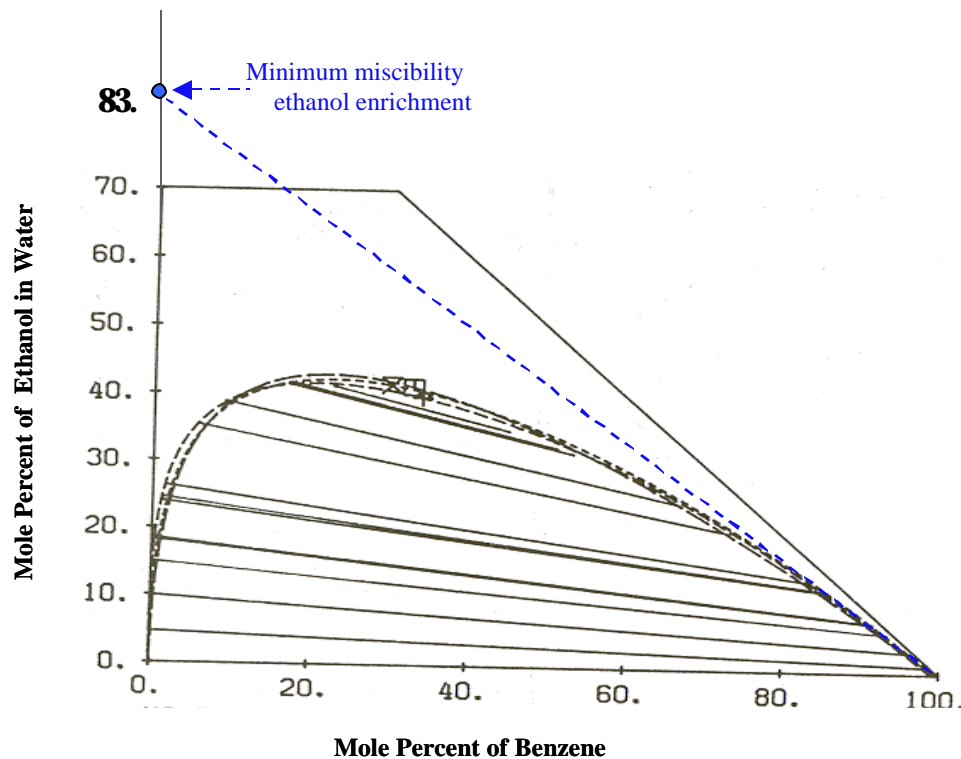


**Figure 10: Phase Diagram of Benzene, Ethanol and Water Ternary System (After Chang and Moulton, 1953; Ref. 121)**

From the ternary phase diagram (Figure 10), it can be seen that the limiting tie line passing through the oil (benzene) intersects the solvent (aqueous ethanol) at an ethanol

enrichment of 83%. Hence, this becomes the minimum miscibility ethanol enrichment for the system to attain miscibility, since at any enrichment lower than this, the tie line would pass through the two phase envelope indicating the presence of two phases in equilibrium.

The solubility of benzene in aqueous ethanol at various ethanol enrichments [122] is given in Table 4 and shown in Figure 11. From the Table 4 and Figure 11, the following important observations can be made.

**Table 4: Solubility of Benzene in Water at Various Ethanol Enrichments (Data from Sidgwick and Spurrel, 1920; Ref. 122)**

Solvent (Mole%)		Benzene Solubility (gms/liter)
Ethanol	Water	
34.8	65.2	134.3
46.6	53.4	343.2
53.3	46.7	629.1
61.2	38.8	1284.6
70.6	29.4	2351.6
78.0	22.0	5760.1

The solubility of benzene in aqueous ethanol begins at an ethanol enrichment of 35% and then gradually increases to become completely soluble at about 78% ethanol enrichment, exhibiting an exponential relationship between solubility and enrichment. As shown in Figure 11, the solubility characteristics can be divided into three regions: (1) Region 1 exists at ethanol enrichments below 35%, where benzene is completely insoluble; (2) Region 2 exists at ethanol enrichments between 35% and 78%, where benzene is partially soluble. In this region, below the solubility curve, benzene is completely soluble, whereas above the solubility curve, benzene is insoluble and (3) Region 3 exists at ethanol

enrichments above 78%, where benzene is soluble in all proportions and hence this can be called as the miscible region.

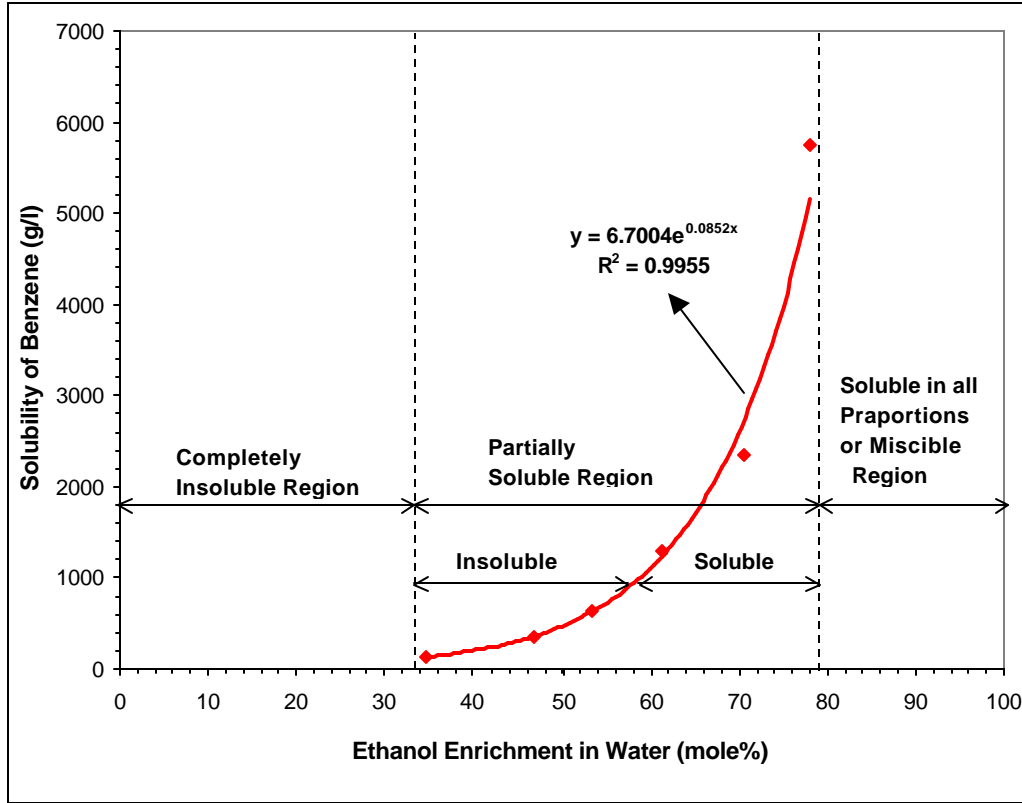


**Figure 11: Solubility of Benzene in Water at Various Ethanol Enrichments (Using the Data from Sidwick and Spurrel, 1920; Ref. 122)**

Thus the minimum miscibility ethanol enrichments for this standard ternary fluid system by both the phase diagram (83%) and the solubility data (>78%) appear to be in good agreement.

#### 4.1.2 Solvent-Oil Ratio Effects on IFT

At first, a calibration IFT experiment was conducted using pendent drop shape analysis technique [119] for a known standard fluid pair of n-decane and water. An IFT value of  $49.0 \pm 0.15$  mN/m was obtained, which is in good agreement with the published value of 50.5 mN/m reported by Jennings [123]. Then, different molar feed compositions

corresponding to 0, 10 and 40 volume % oil in the solvent were used to study the solvent-oil ratio effects on IFT measurements. The IFT's between the non-equilibrated fluids could not be measured above 40% ethanol enrichment, using the drop shape analysis technique. At these higher ethanol enrichments, pendent drops could not be formed as the oil quickly escaped in streaks through the solvent. The measured IFT experimental values for non-equilibrated fluids at different ethanol enrichments below 40% in aqueous phase and at different solvent-oil ratios in the feed mixtures of aqueous ethanol and benzene are summarized in Table 5 and shown in Figure 12. The standard deviations (from number of measurements at each ratio) in the range of 0.03 to 0.11 obtained in measured IFT values indicate extremely low variation in the measurements. The important observations from Table 5 and Figure 12 are the following.

**Table 5: Measured Benzene Interfacial Tensions in Non-Equilibrated Aqueous Ethanol at Various Ethanol Enrichments and Feed Compositions**

Solvent (Mole%)		Feed Composition (Mole%)		Benzene IFT (mN/m)
Ethanol	Water	Solvent	Benzene	
0	100	100.0	0.0	$32.58 \pm 0.110$
		97.8	2.2	$32.59 \pm 0.030$
		88.0	12.0	$32.62 \pm 0.030$
10	90	100.0	0.0	$12.11 \pm 0.110$
		97.4	2.6	$12.11 \pm 0.060$
		86.2	13.8	$12.16 \pm 0.045$
20	80	100.0	0.0	$4.85 \pm 0.064$
		97.0	3.0	$4.84 \pm 0.080$
		84.4	15.6	$5.00 \pm 0.050$
30	70	100.0	0.0	$2.30 \pm 0.035$
		96.6	3.4	$2.31 \pm 0.040$
		82.5	17.5	$2.62 \pm 0.030$
40	60	100.0	0.0	$1.23 \pm 0.052$
		96.2	3.8	$1.41 \pm 0.050$
		80.7	19.3	$1.99 \pm 0.048$

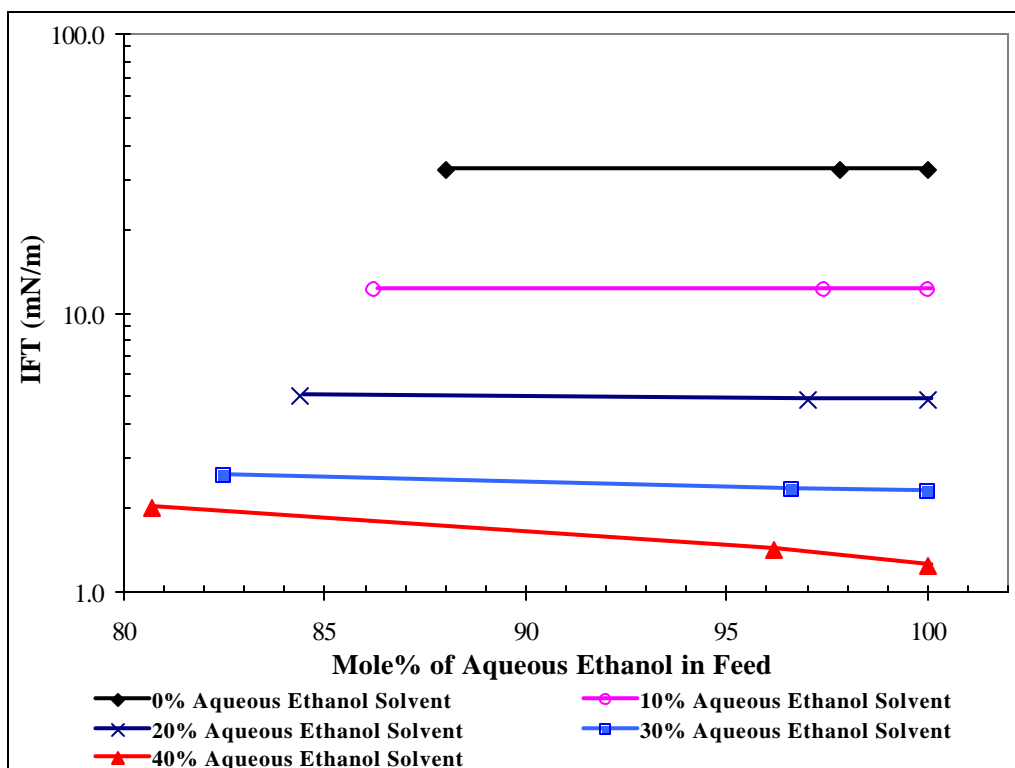


**Figure 12: Effect of Solvent-Oil Ratio on IFT in Feed Mixtures of Non-Equilibrated Benzene (Oil) and Aqueous Ethanol (Solvent)**

The IFT decreases steadily as the ethanol enrichment increases in aqueous phase. At ethanol enrichments of up to 20% in aqueous phase, IFT is found to be independent of solvent-oil ratio in the feed. However, for the ethanol enrichments of 30% and above, a slight increase in IFT is observed as the solvent-oil ratio in feed decreases. The increase of IFT with decrease in solvent-oil ratio is low at 30% ethanol enrichment and then becomes noticeable at 40% ethanol enrichment in aqueous phase. The possible reasons for the observed solvent-oil ratio effects on IFT at ethanol enrichments above 30% appear to be the following.

As can be seen in Table 4 and Figure 11, benzene solubility in aqueous ethanol begins at an ethanol enrichment of 35% and then gradually increases to become completely

soluble at an ethanol enrichment of 78%. Therefore, solubility of benzene in aqueous ethanol does not come into picture during the IFT measurements in insoluble regions of ethanol enrichments below 35%. Hence, absence of solvent-oil ratio effects on IFT is observed at ethanol enrichments below 30%. However, at ethanol enrichments above 35% in aqueous phase, the dissolution of benzene in aqueous ethanol interferes with IFT measurements due to varying amounts of benzene at different solvent-oil ratios in the feed. Hence, adding 10-20 drops of benzene in aqueous ethanol solvent during IFT measurements is not sufficient to accommodate complete saturation between the fluids. This appears to be the main reason for the dependence of IFT on feed solvent-oil ratios in partially soluble regions of above 30% ethanol enrichments in aqueous phase.

The solubility effects of benzene observed in aqueous ethanol in partially soluble regions at ethanol enrichments above 30% can be excluded by using the aqueous ethanol fully saturated with benzene (pre-equilibrated) as the solvent in IFT measurements. Figures 13 and 14 demonstrate the effects of benzene solubility on benzene drop size in non-equilibrated and pre-equilibrated 30% aqueous ethanol solvent, respectively. As can be seen in Figure 13, benzene drop gradually reduces in size with time and completely vanishes within 4 hours in non-equilibrated aqueous ethanol solvent. This can be attributed to continued solubility of benzene in non-equilibrated aqueous ethanol. However, contrarily, absence of benzene solubility effects in aqueous ethanol pre-equilibrated with benzene can be seen in Figure 14. The benzene drop is able to retain its original size and shape in the solvent even after 4.5 hours. These observations clearly suggest that compositional effects on IFT in partially soluble regions can be eliminated by the use of fully saturated or pre-equilibrated fluids during the experiments.

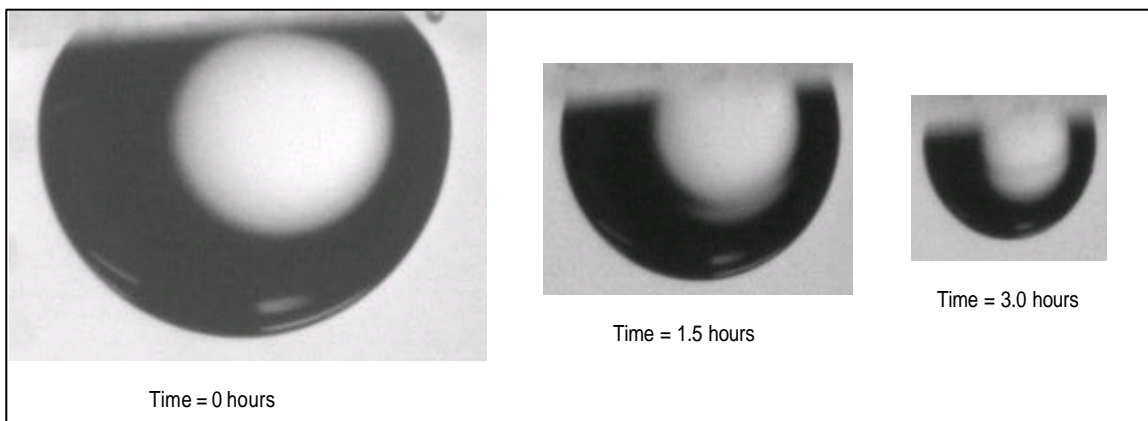


**Figure 13: Photographs Showing the Effect of Benzene Dissolution in Non-Equilibrated Aqueous Ethanol Solvent at 30% Ethanol Enrichment**

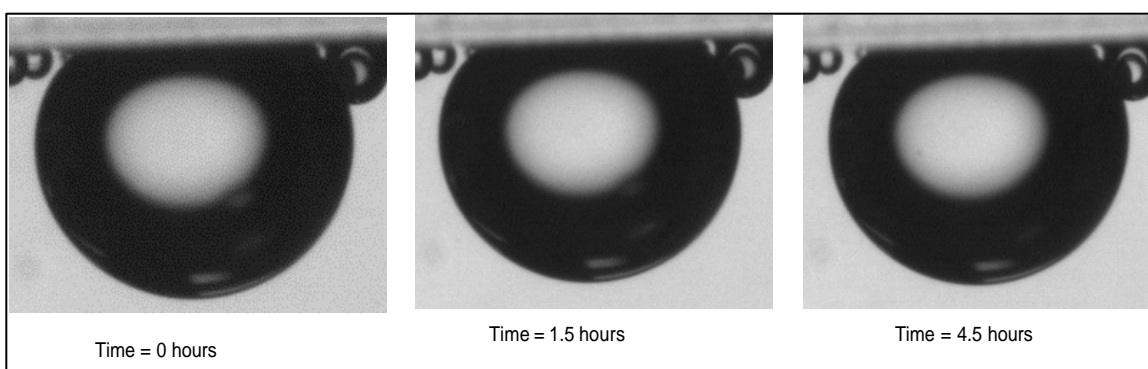


**Figure 14: Photographs Showing the Absence of Benzene Dissolution in Pre-Equilibrated Aqueous Ethanol Solvent at 30% Ethanol Enrichment**

Thus IFT dependence on feed solvent-oil ratio for non-equilibrated fluids in partially soluble regions appears to be due to benzene dissolution in aqueous ethanol. Therefore, the slight changes in IFT observed with non-equilibrated solutions in partially soluble regions at ethanol enrichments above 30% at different solvent-oil ratios in the feed (Table 5 and Figure 12) can be attributed mainly to benzene solubility effects and not to solvent-oil ratio in the feed mixture. For further verification, IFT measurements were repeated using the fully saturated pre-equilibrated fluids at 30% and 40% ethanol enrichments in

aqueous phase for various solvent-oil ratios in the feed. The results are summarized in Table 6 and shown in Figure 15.

**Table 6: Measured Benzene IFT's in Pre-Equilibrated Aqueous Ethanol at 30% and 40% Ethanol Enrichments and Various Feed Compositions**

Solvent (Mole%)		Feed Composition (Mole%)		Benzene IFT (mN/m)
Ethanol	Water	Solvent	Benzene	
30	70	100.0	0.0	$2.94 \pm 0.048$
		96.6	3.4	$2.94 \pm 0.055$
		82.5	17.5	$3.12 \pm 0.023$
40	60	100.0	0.0	$0.09 \pm 0.004$
		96.2	3.8	$0.09 \pm 0.004$
		80.7	19.3	$0.09 \pm 0.004$

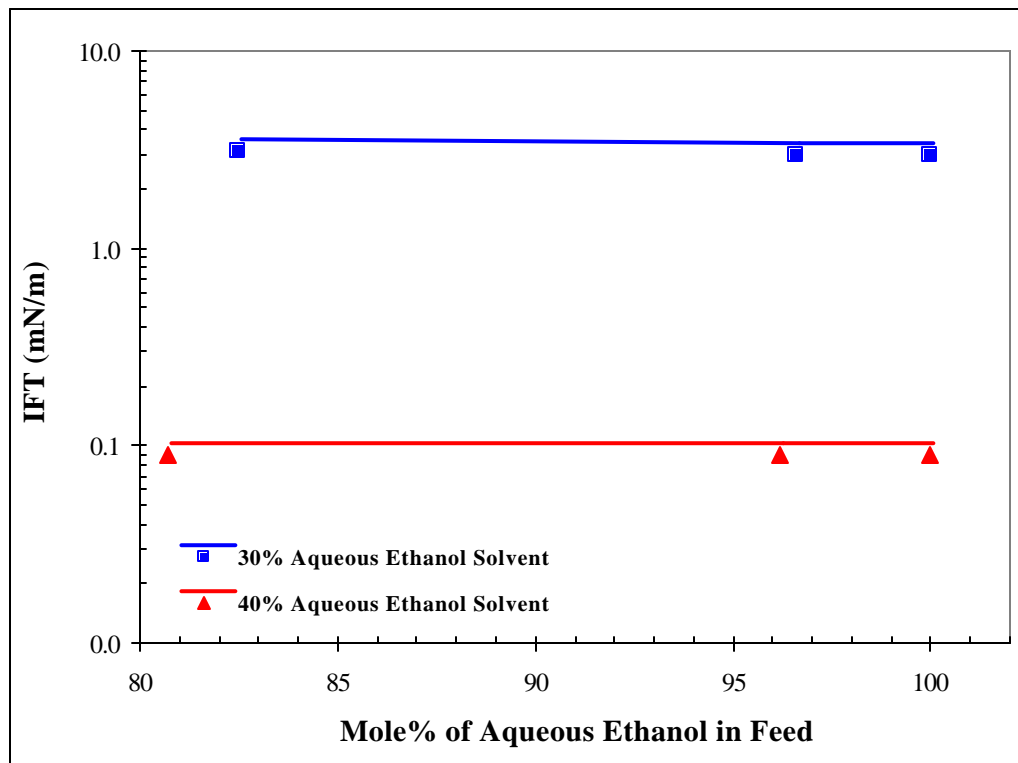


**Figure 15: Effect of Feed Solvent-Oil Ratio on IFT in Pre-Equilibrated Aqueous Ethanol Solvents**

From Table 6 and Figure 15, it can be seen that no noticeable changes in IFT were observed for various solvent-oil ratios in the feed at these ethanol enrichments of pre-equilibrated fluids. Therefore, it can be concluded that the use of pre-equilibrated solutions in the partially soluble regions for IFT measurements eliminates the compositional effects on IFT thereby rendering the IFT independent of solvent-oil ratio in the feed. This clearly indicates that the miscibilities determined using interfacial tension measurements in the VIT technique do not depend on solvent-oil ratio in the feed mixtures, provided that mutual saturation between the two fluid phases is attained prior to IFT measurements.

#### **4.1.3 IFT Measurements Using Capillary Rise Technique**

This technique was adapted to measure low IFT's that could not be measured using drop shape analysis technique at ethanol enrichments above 40%. At first, this technique was calibrated for a known low IFT standard fluid pair of n-butanol and water, using two different capillary sizes. IFT values of 1.72 and 1.79 mN/m were obtained for inner capillary glass tube radii of 0.09 and 0.025 cm, respectively. These values were in good agreement with the value of 1.8 mN/m reported by Mannhardt [75] for this standard fluid system.

All the measured capillary heights and the densities of the equilibrated fluid phases using the capillary rise technique at ethanol enrichments above 40% in benzene, ethanol, water standard ternary liquid system are summarized in Table 7. From Table 7, it can be seen that as the ethanol enrichment in aqueous phase increases from 50 to 75%, the density difference between the fluid phases decreases from 0.0128 gm/cc to 0.0003 gm/cc. Contrarily, an increase in capillary rise from 0.53 cm to 0.98 cm can be seen as

the ethanol enrichment in aqueous phase is increased. This indicates an inverse correlation between the density difference and the capillary rise and hence a good precision of IFT measurement can be made even in low IFT regions using this technique due to easily measurable rises in the capillary tube.

**Table 7: Benzene IFT's in Pre-Equilibrated Aqueous Ethanol Solvent at Ethanol Enrichments above 40%**

Ethanol Enrichment (Mole%)	Phase Densities (gm/cc)		Contact Angle (degrees)	Capillary Rise (cm)	IFT (mN/m)
	Solvent	Oil			
50	0.8725	0.8597	25	0.53	0.3301
60	0.8641	0.8579	25	0.59	0.1780
70	0.8612	0.8594	25	0.68	0.0596
75	0.8579	0.8576	25	0.98	0.0143

The equilibrium benzene contact angles measured for IFT calculations in capillary rise technique at different ethanol enrichments in aqueous phase are given in Table 8 and shown in Figure 16. From Table 8 and Figure 16, it can be seen that, the benzene equilibrium contact angles gradually decrease from 48° at 0 % ethanol enrichment to 26° at 20 % ethanol enrichment in aqueous phase and then remains unchanged (25°) for ethanol enrichments of 30% and 40%. Therefore, it is reasonable to assume that there will be no change in benzene equilibrium contact angles from 25° with ethanol enrichment at ethanol enrichments above 30%. Hence, an equilibrium contact angle of 25° was used in capillary rise IFT calculations at all ethanol enrichments above 40%, as indicated by the extrapolated line in Figure 16. The summary of all the measured parameters used in the IFT calculations of the capillary rise technique at ethanol enrichments above 40% is

shown in Table 7. As can be seen in Table 7, an IFT value as low as 0.014 mN/m was measured at 75% ethanol enrichment in aqueous phase with this technique.

**Table 8: Measured Equilibrium Benzene Contact Angles at Various Ethanol Enrichments in Aqueous Phase**

Ethanol Enrichment (Mole%)	Equilibrium Time (hrs)	Benzene Contact Angle ( ° )
0	24	48
10	24	33
20	24	26
30	24	25
40	24	25

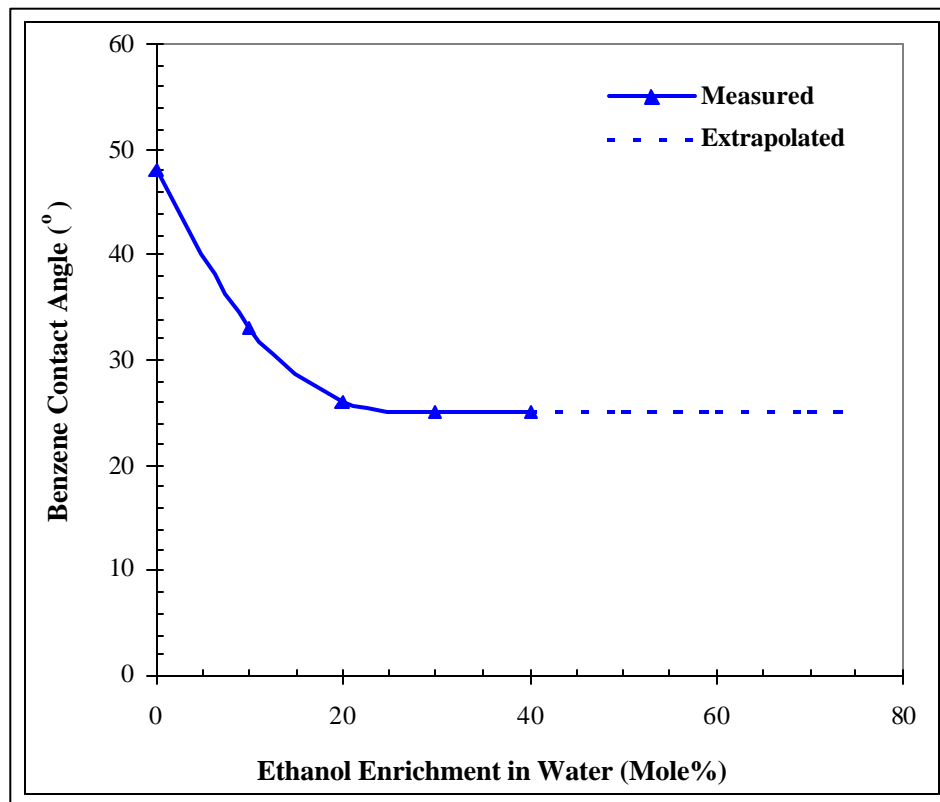


**Figure 16: Benzene Equilibrium Contact Angles Against Ethanol Enrichment in Aqueous Phase**

#### 4.1.4 Correlation of Solubility and Miscibility with IFT

The correlation among all the three thermodynamic properties of solubility, miscibility and IFT in the standard ternary liquid system is shown in Figure 17. The measured IFT's of benzene in aqueous ethanol using both the pendent drop and capillary rise techniques and the reported solubility values of benzene are plotted against ethanol enrichment in aqueous phase to correlate solubility, miscibility and IFT. From Figure 17, it can be seen that IFT decreases exponentially as the ethanol enrichment in aqueous phase is increased and reduces to a low value of 0.014 mN/m at 75% enrichment, as miscibility is approached. The regression equation obtained is  $IFT = 32.58 e^{(-0.0928 * \text{Mole\% of Ethanol})}$  with a coefficient of determination ( $R^2$ ) = 0.9811.

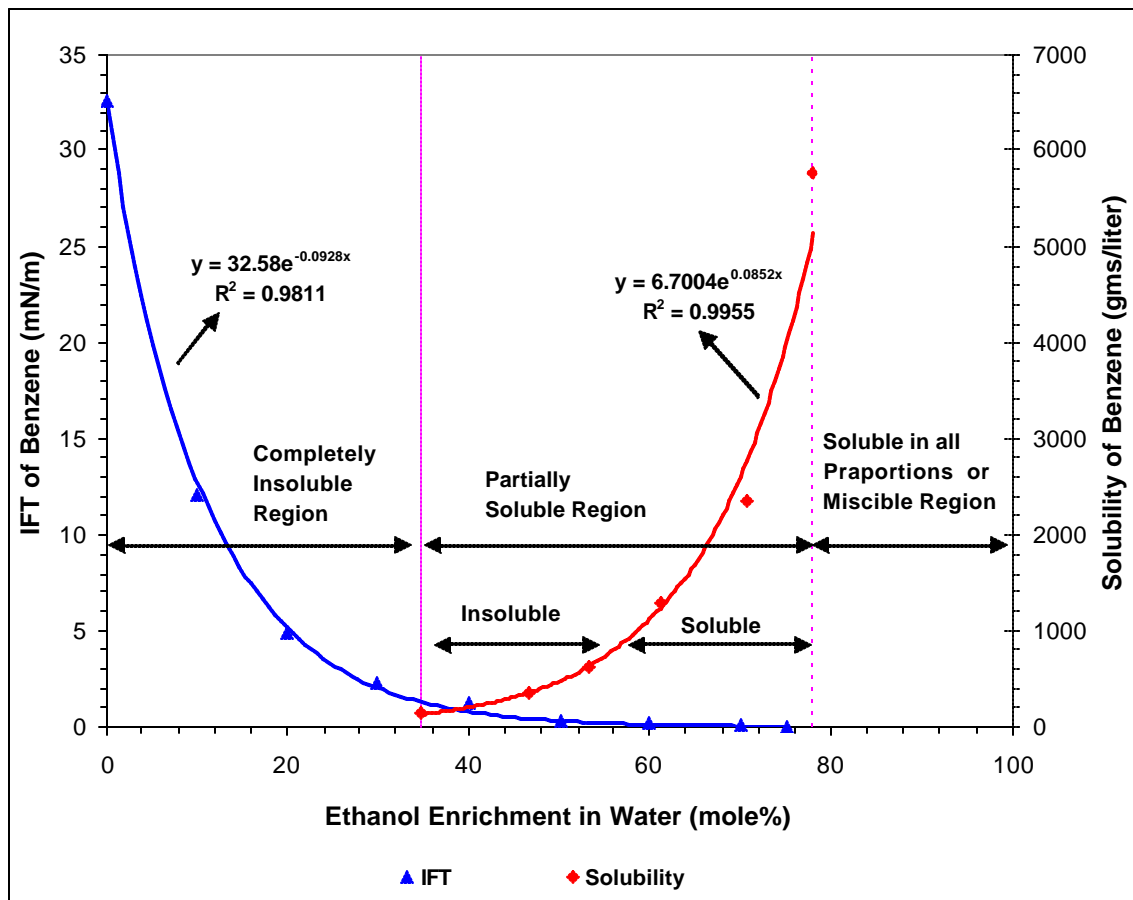
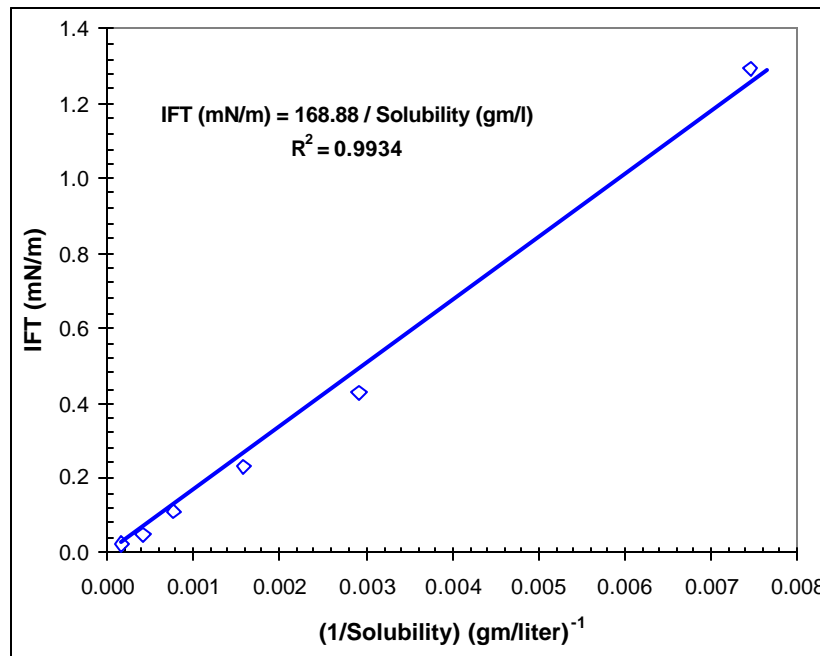


Figure 17: Correlation of Solubility and Miscibility with IFT

Solubility of benzene is also exponentially correlated to ethanol enrichment by the regression equation,  $\text{solubility} = 6.7004 e^{(0.0852 * \text{Mole\% of Ethanol})}$  with a coefficient of determination ( $R^2$ ) = 0.9955. The positive slope in the exponential relationship between the solubility and ethanol enrichment shows an exponential growth. This is contrary to the negative slope of exponential decay obtained in the exponential correlation between IFT and ethanol enrichment. Furthermore, almost similar absolute values of the slope can be seen in both these exponential regression equations. These observations indicate a possible perfect inverse correlation between solubility and interfacial tension in ternary liquid systems.

In order to determine such an inverse correlation between solubility and IFT, solubility is plotted against  $1/\text{IFT}$  in Figure 18. The IFT values from the exponential regression equation of IFT vs. ethanol enrichment are used at ethanol enrichments corresponding to the solubility values in the plot.



**Figure 18: Correlation between IFT and Solubility**

As can be seen in Figure 18, solubility is linearly correlated to (1/IFT), indicating a strong mutual relationship between these two thermodynamic properties. The relationship obtained is  $\text{solubility} = 168.88 / \text{IFT}$  with a determination coefficient ( $R^2$ ) = 0.9934. Therefore, the correlation between solubility and IFT in ternary liquid systems can be generalized as  $\text{solubility} = c / \text{IFT}$  where  $c$  is a system dependent constant. Thus solubility is strongly correlated to IFT and hence can be used for IFT predictions in soluble regions.

#### 4.1.5 Determination of VIT Miscibility

All the IFT measurements obtained in the standard ternary liquid system of benzene, ethanol and water at various ethanol enrichments were fitted using a hyperbolic function to determine the miscibility using the VIT technique. The results are summarized in Figure 19.

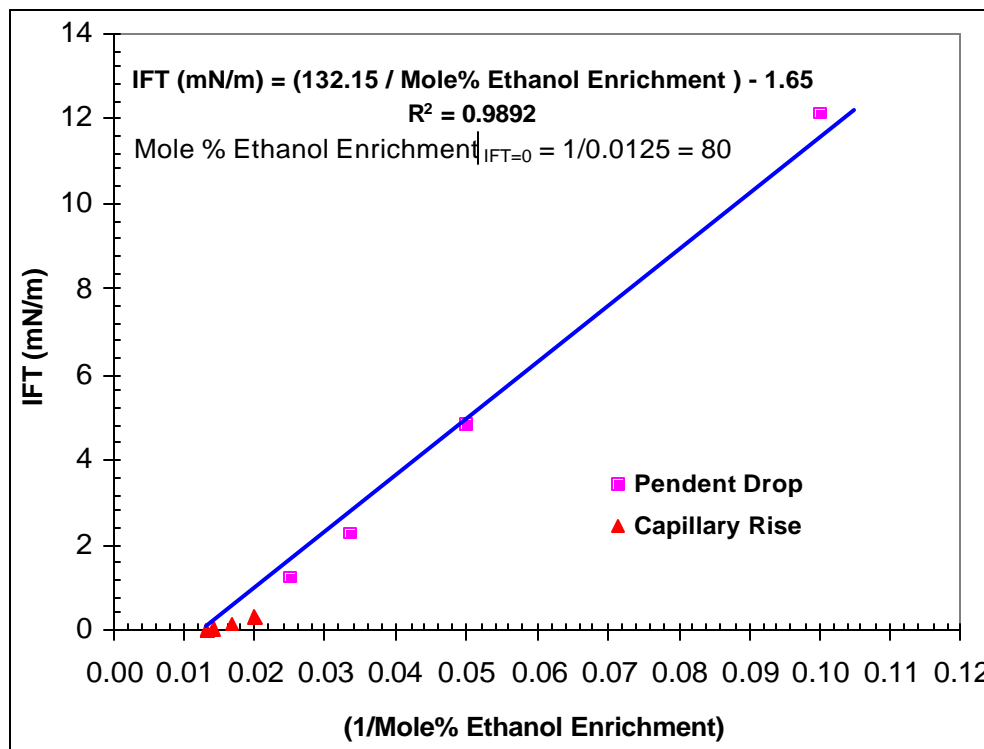


**Figure 19: Plot of IFT vs. Ethanol Enrichment to Determine Miscibility**

A good linear relationship between IFT and the reciprocal of ethanol enrichment can be seen with a determination coefficient ( $R^2$ ) of 0.989. The regression equation obtained is shown in Figure 19. The regression equation is then extrapolated to zero IFT, as required in the VIT technique, to determine miscibility in this standard ternary liquid system. A miscibility condition of 80 mole% ethanol enrichment was obtained with the VIT technique, which agrees well with the miscibility conditions obtained from the phase diagram (83%) and solubility data (>78%). This clearly demonstrates the sound conceptual basis of the VIT technique and hence validates the use of VIT technique to determine the conditions of fluid-fluid miscibility in ternary liquid systems.

## **4.2 IFT Measurements in Standard Gas-Oil Systems of n-Decane-CO<sub>2</sub> and Synthetic Live Oil-CO<sub>2</sub>**

### **4.2.1 Bubble Point Pressure Estimation of Synthetic Live Oil**

The plot of cumulative volume of water collected (which is an accurate representation of the expansion in the volume of live oil in the vessel) against the pressure obtained during the bubble point pressure measurement of live oil containing 25 mole% n-C<sub>1</sub>, 30 mole% n-C<sub>4</sub> and 45 mole% n-C<sub>10</sub> is shown in Figure 20. The two different linear sections of the plot were identified and fitted separately using linear regression. The coefficients of determination ( $R^2$ ) values of above 99% obtained for both the linear sections indicate good fits. The two regression equations obtained are indicated in Figure 20.

The two regression equations were then solved to determine the point of their intersection as the bubble point pressure of the live oil. An experimental bubble point pressure of 1011 psi was obtained for the synthetic live oil mixture at 160 °F. This experimental value matches well with the bubble point pressure of 1045 psi obtained from PR-EOS calculations, using the commercial simulator Winprop [124].

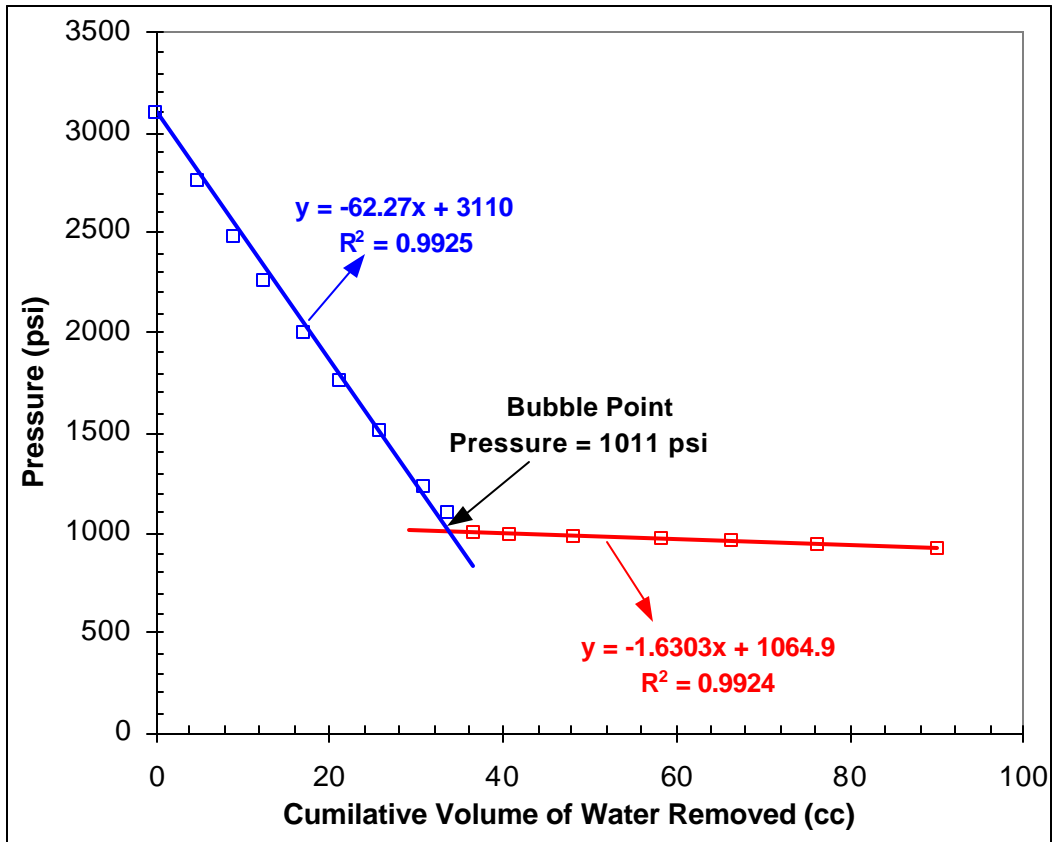


**Figure 20: Bubble Point Pressure Determination of Live Synthetic Oil at 160° F**

#### 4.2.2 Density Meter Calibration and Density Measurements of Pure Fluids

The density meter is calibrated for density measurements at 100° F and 160° F by measuring the densities of pure CO<sub>2</sub> gas at different pressures and comparing the measurements with those obtained from PR-EOS calculations of the commercial simulator, Winprop [124]. The measured densities of CO<sub>2</sub> gas and their comparison with PR-EOS calculations are shown in Figures 21 and 22, respectively at the temperatures 100° F and 160° F. A good match between the measurements and calculations can be seen at both the temperatures, which indicates good calibration of the density meter used.

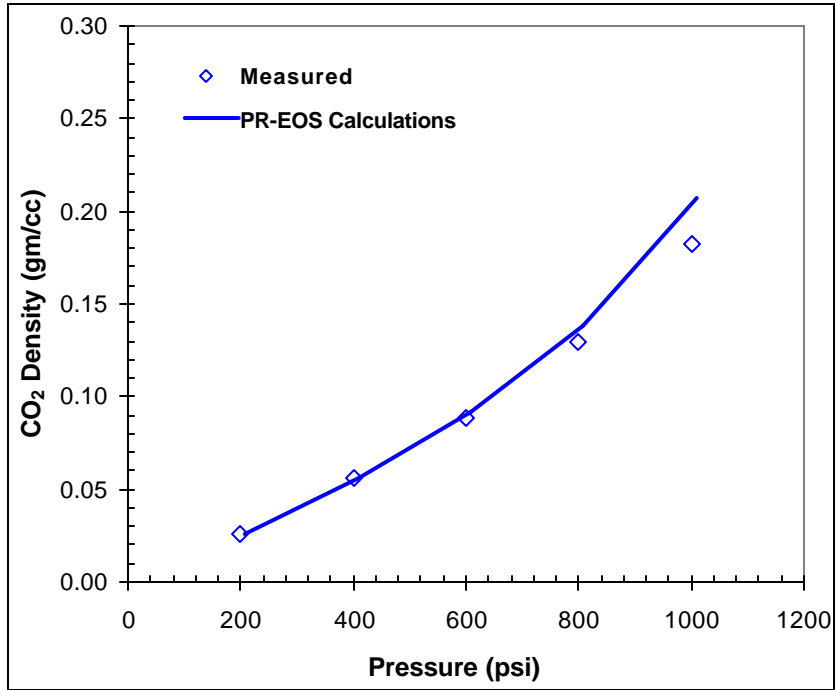


**Figure 21: Comparison between Measured and PR-EOS Calculated CO<sub>2</sub> Densities at 100° F**

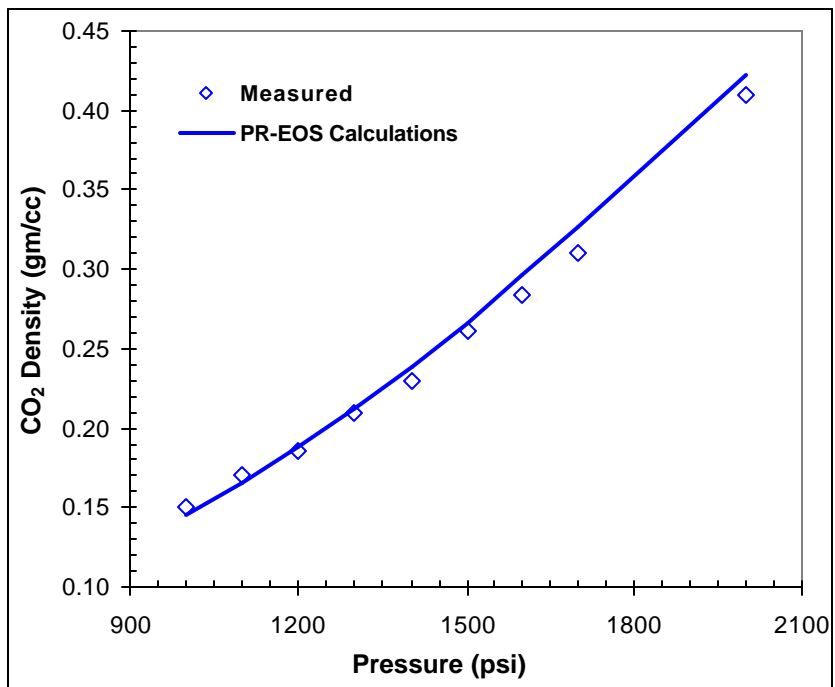


**Figure 22: Comparison between Measured and PR-EOS Calculated CO<sub>2</sub> Densities at 160° F**

Now, the densities of the pure liquids, n-decane and synthetic live oil mixture were measured at 100 °F and 160° F, respectively at different pressures (pressures above the bubble point pressure for synthetic live oil). The measured fluid densities were shown in Figure 23 for n-decane at 100° F and Figure 24 for synthetic live oil at 160° F. The measured density data were then fitted using linear regression for both the fluids. The regression equations obtained are also indicated in Figures 23 and 24. The coefficients of determination ( $R^2$ ) values above 99.7% obtained for both the liquids indicate good fits and hence these equations can be used for density predictions of n-decane and synthetic live oil mixture within the range of pressures and the temperatures used.

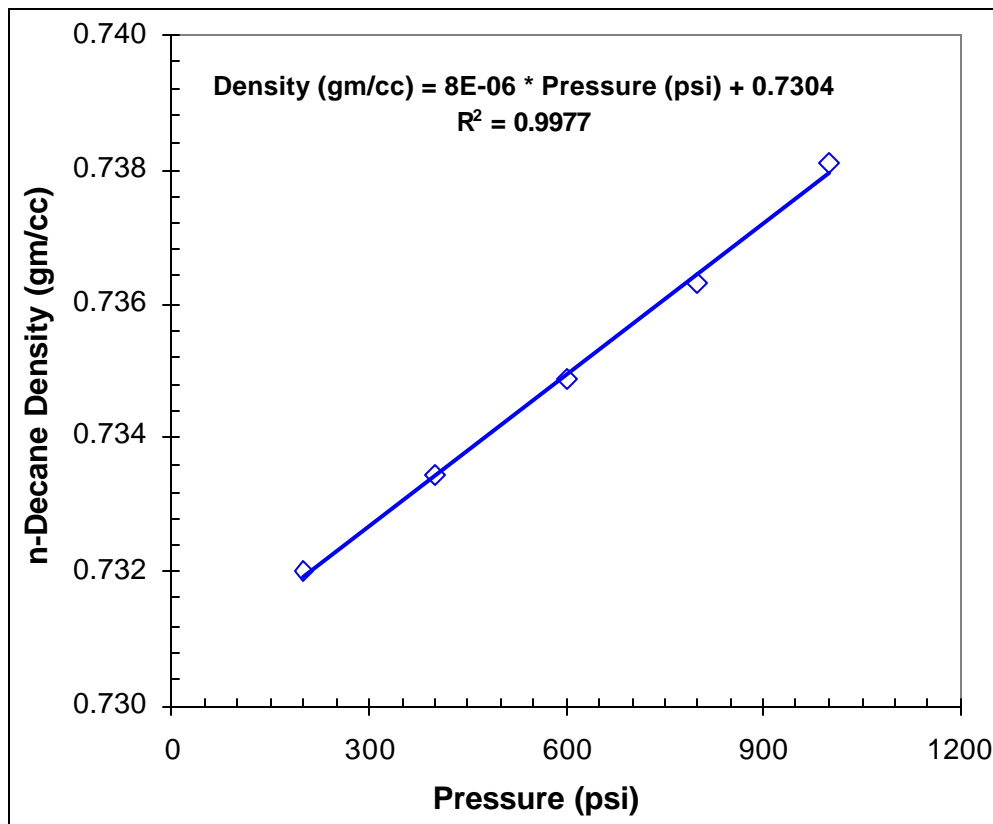


**Figure 23: Measured Densities of Pure n-Decane at 100° F**

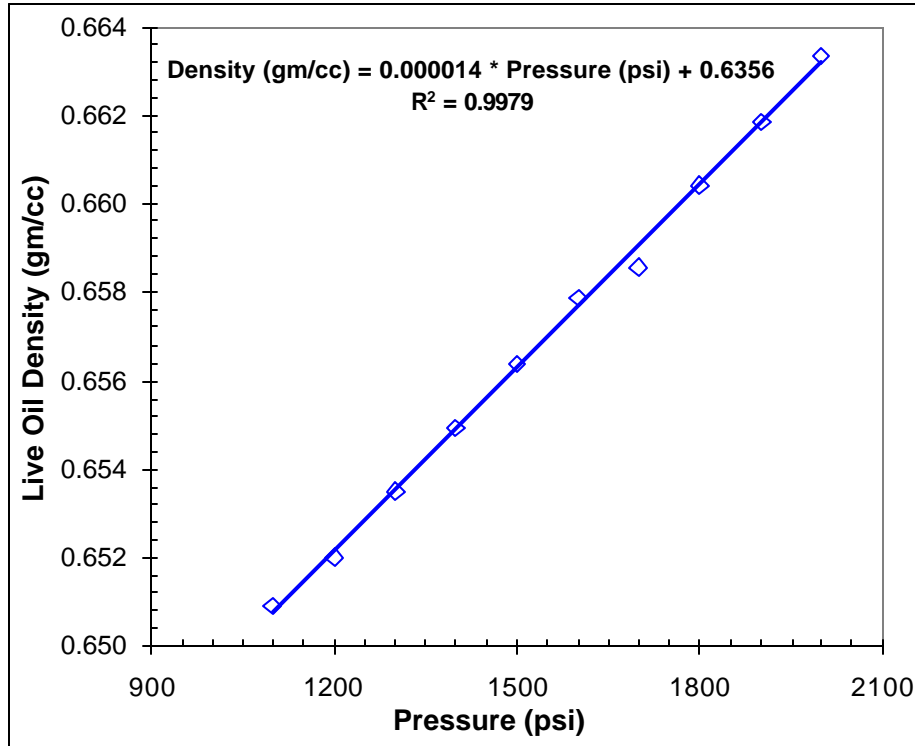


**Figure 24: Measured Densities of Pure Synthetic Live Oil at 160° F**

#### **4.2.3 IFT Measurements in n-Decane-CO<sub>2</sub> System at 100° F**

This standard gas-oil system of n-C<sub>10</sub>/CO<sub>2</sub> has a reported slim-tube miscibility of 1250 psi [10] and a rising-bubble miscibility of 1280 psi [10] at 100° F. The IFT measurements in this gas-oil system at 100°F and at various pressures were carried out using the capillary rise and pendent drop techniques. Three different molar feed compositions of 100 mole% oil, 40/60 mole% gas and oil, and 80/20 mole% gas and oil were used during the experiments to study the effect of gas-oil ratio on miscibility. The IFT measurements at the feed composition of 100 mole% oil were conducted using pendent drop technique. Both the pendent drop and capillary rise techniques were used for IFT measurements at the feed composition of 40/60 mole% gas and oil, while only capillary rise technique was used for IFT measurements at the molar feed composition of

80/20 mole% gas and oil. The densities of the equilibrated fluid phases and the capillary rise heights measured at molar feed compositions of 40/60 mole% gas and oil and 80/20 mole% gas and oil are summarized in Table 9.

**Table 9: Summary of Equilibrated Fluid Densities and Capillary Rise Heights Measured in n-Decane-CO<sub>2</sub> System at 100° F**

Pressure (psi)	Equilibrated Fluid Densities (gm/cc)		Capillary Height (cm)	
	Oil	Gas	40/60 Mole% Gas and Oil	80/20 Mole% Gas and Oil
0	0.719	0.0091	0.712	0.717
200	0.722	0.0185	0.640	0.649
400	0.720	0.0432	0.539	0.544
600	0.678	0.0698	0.380	0.383
800	0.663	0.1159	0.248	0.252
1000	0.698	0.2203	0.178	0.159
1100	0.482	0.2998	0.041	0.041

From Table 9, it can be seen that the equilibrated oil phase density is gradually decreasing while the equilibrated gas phase density is gradually increasing with pressure. This indicates simultaneous counter-directional mass transfer of components between oil and gas phases to attain thermodynamic equilibrium. The gradual decrease of capillary rise with pressure can be seen at both the gas-oil ratios used. The summary of all the IFT's measured at different gas-oil ratios and at various pressures using both the pendent drop and capillary rise techniques is given in Table 10 and shown in Figure 25.

**Table 10: Summary of IFT's measured in n-Decane-CO<sub>2</sub> System at Various Pressures and Gas-Oil Ratios in the Feed**

Pressure (psi)	100 Mole% Oil	40/60 Mole% Gas and Oil		80/20 Mole% Gas and Oil
	Pendent Drop IFT (mN/m)	IFT (mN/m)		Capillary Rise IFT (mN/m)
		Pendent Drop	Capillary Rise	
0	22.29 ± 0.245	21.95 ± 0.054	22.29	22.45
200	19.70 ± 0.172	19.27 ± 0.121	19.86	20.13
400	15.76 ± 0.118	15.36 ± 0.051	16.09	16.24
600	11.29 ± 0.166	10.38 ± 0.098	10.19	10.27
800	8.24 ± 0.139	7.28 ± 0.103	5.97	6.07
1000	3.57 ± 0.138	3.28 ± 0.257	3.75	3.34
1100			0.33	0.33

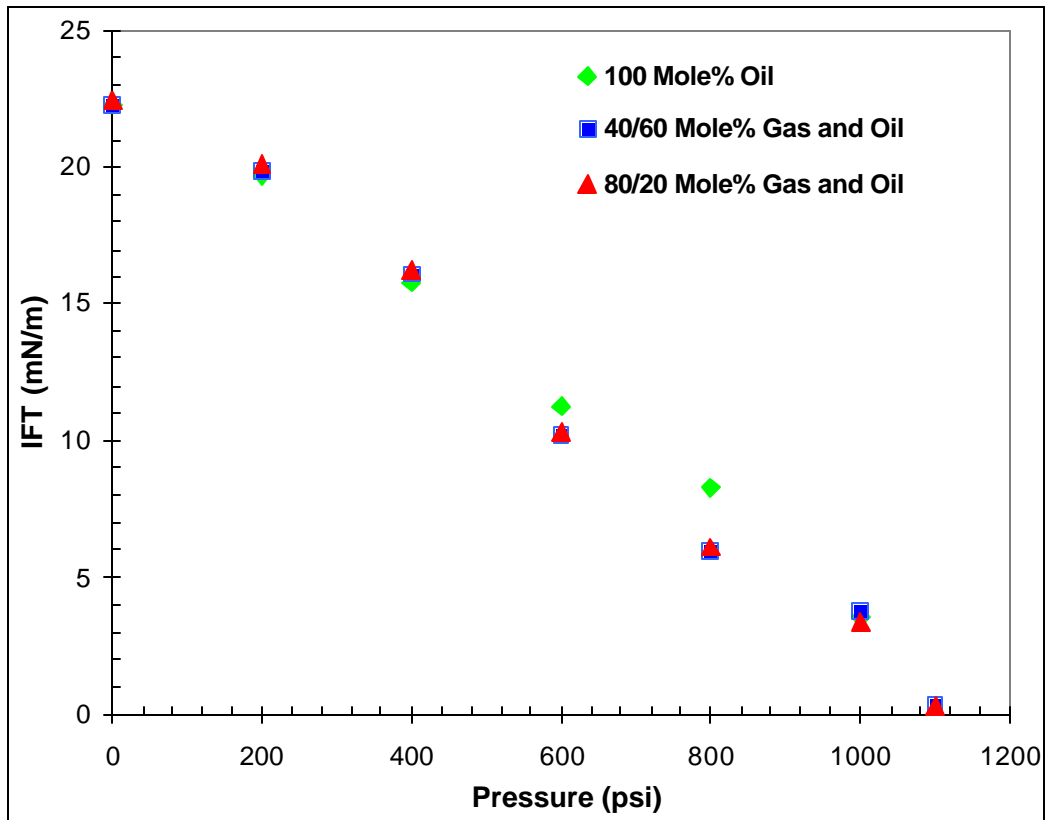


**Figure 25: Effect of Gas-Oil Ratio on IFT in n-Decane-CO<sub>2</sub> System at 100°F**

From Table 10, a good match of IFT's between capillary rise and pendent drop techniques can be seen at 40/60 gas-oil ratio in the feed. This validates the newly used capillary rise technique for IFT measurements at elevated pressures and temperatures. As can be seen in Table 10 and Figure 25, almost similar IFT values are obtained at each of the pressures for all the three gas-oil ratios used, which clearly indicates the absence of gas-oil ratio effects on IFT and hence on miscibility. This once again confirms that the miscibilities determined from the VIT technique do not depend on gas-oil ratios in the feed mixture.

Therefore, the average values of IFT's measured at each pressure for different gas-oil ratios is plotted against pressure to determine miscibility using the VIT technique and is shown in Figure 26.

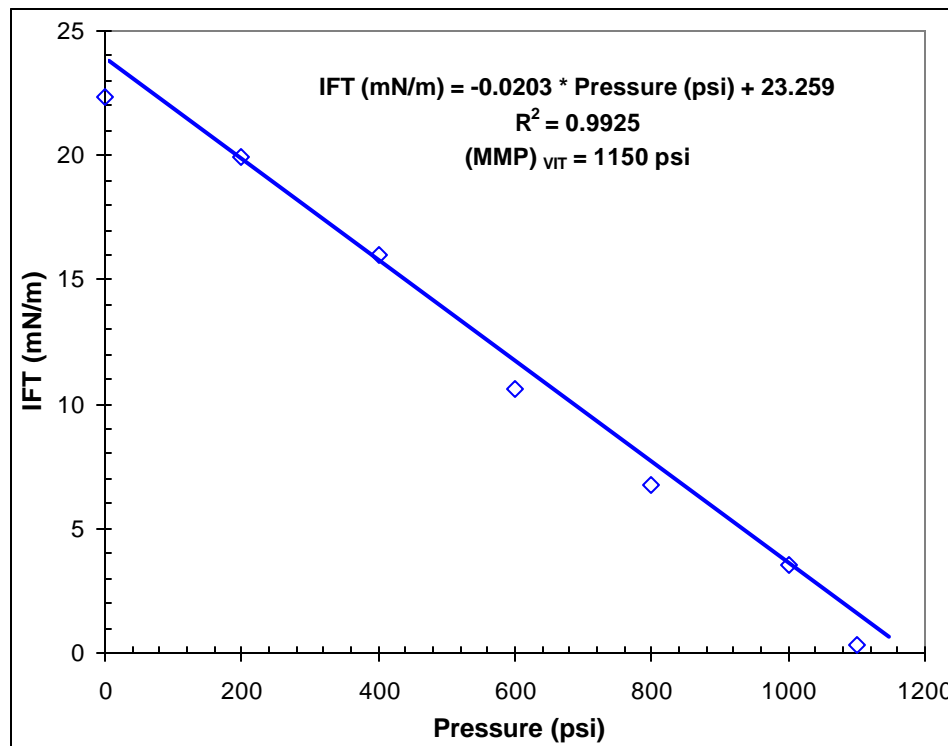


**Figure 26: Determination of VIT Miscibility in n-Decane-CO<sub>2</sub> System at 100°F**

As can be seen in Figure 26, a good linear correlation was obtained between IFT and pressure in the standard n-decane-CO<sub>2</sub> system at 100° F. The linear regression equation obtained is shown in Figure 26. The coefficient of determination (R<sup>2</sup>) value of 99.25% obtained indicates a good fit. The extrapolation of the regression equation to zero IFT gives a VIT miscibility of 1150 psi. This VIT miscibility is in good agreement with the reported miscibilities from slim-tube (1250 psi) and rising-bubble (1280 psi) experimental techniques. Considering the variabilities normally encountered in slim-tube and rising-bubble measurements, this can be treated as an excellent match. Thus, this VIT experiment conducted using the standard gas-oil system of n-decane-CO<sub>2</sub> at 100°F serves as one more validation of the VIT technique to measure fluid-fluid miscibility.

#### **4.2.4 IFT Measurements in Synthetic Live Oil-CO<sub>2</sub> System at 160° F**

This standard gas-oil system has been reported to have a slim-tube minimum miscibility pressure (MMP) of 1700 psia at 160° F [125]. This miscibility pressure is further reproduced with phase diagram measurements [125] and analytical model predictions [30, 35]. The IFT measurements in this gas-oil system at 160° F and at various pressures were carried out using the capillary rise technique. Two different molar feed compositions of 80/20 mole% gas and oil, and 20/80 mole% gas and oil were used during the experiments to examine the effect of gas-oil ratio on miscibility of this system as well. The summary of measured equilibrated fluid phase densities and capillary rise heights at the two different gas-oil ratios used is given in Table 11.

From Table 11, it can be seen that the equilibrated gas phase densities are increasing significantly with pressure, while very little change in equilibrated oil phase densities with pressure is observed. This indicates pronounced mass transfer of lighter components

(n-C<sub>1</sub> and n-C<sub>4</sub>) from oil to gas phase. The steady decline of capillary rise with pressure can be seen at both the gas-oil ratios used.

**Table 11: Summary of Equilibrated Fluid Densities and Capillary Rise Heights Measured in Synthetic Live Oil - CO<sub>2</sub> System at 160° F**

Pressure (psi)	Equilibrated Fluid Phase Densities (gm/cc)		Capillary Height (cm)	
	Oil	Gas	20/80 Mole% Gas and Oil	80/20 Mole% Gas and Oil
1100	0.6495	0.2743	0.440	0.442
1150	0.6509	0.3028	0.406	0.409
1200	0.6520	0.3325	0.341	0.346
1250	0.6538	0.3543	0.322	0.332
1300	0.6553	0.3726	0.292	0.295
1350	0.6571	0.4060	0.291	0.291
1400	0.6590	0.4276	0.242	0.242
1500	0.6630	0.4586	0.225	0.223
1550	0.6641	0.4813	0.196	0.198
1600	0.6677	0.5186	0.166	0.156
1650	0.6703	0.5334	0.130	0.132
1700	0.6717	0.6252	0.105	0.109
1750	0.6765	0.6502	0.068	0.068

The summary of IFT's measured at both the gas-oil ratios and at various pressures in this standard gas-oil system at 160° F is given in Table 12 and shown in Figure 27.

**Table 12: Summary of IFT's Measured in Synthetic Live Oil – CO<sub>2</sub> System at Various Pressures and Gas-Oil Ratios in the Feed**

Pressure (psi)	20/80 Mole% Gas and Oil	80/20 Mole% Gas and Oil
	IFT (mN/m)	IFT (mN/m)
1100	4.048	4.061
1150	3.458	3.490
1200	2.672	2.712
1250	2.361	2.437
1300	2.023	2.041
1350	1.790	1.791
1400	1.371	1.373
1500	1.125	1.115
1550	0.878	0.887
1600	0.606	0.571
1650	0.435	0.441
1700	0.120	0.125
1750	0.044	0.044

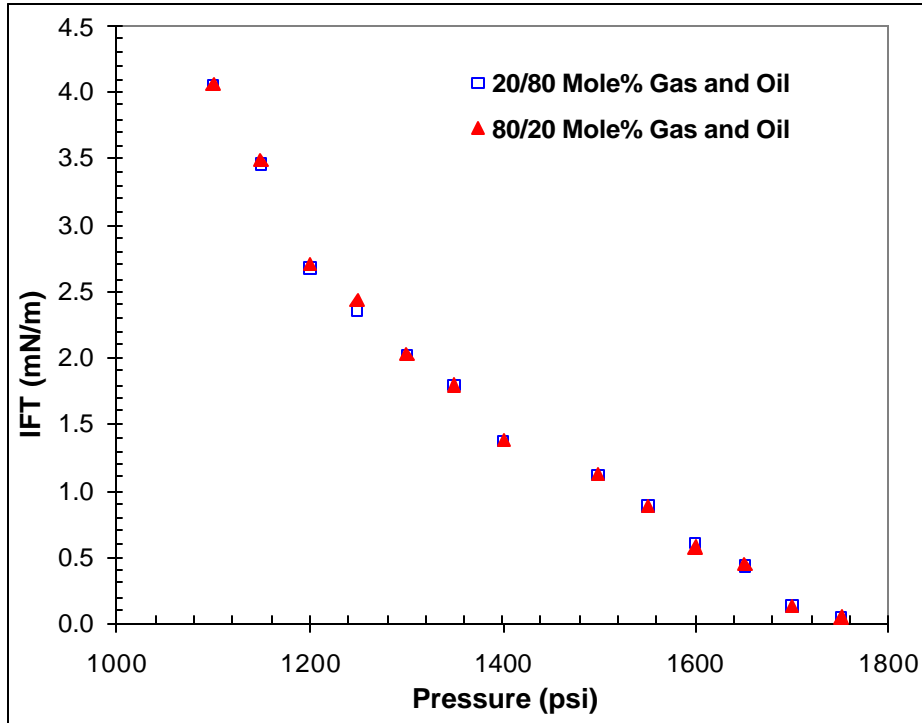


**Figure 27: Effect of Gas-Oil Ratio on IFT in Synthetic Live Oil-CO<sub>2</sub> System at 160° F**

From Table 12 and Figure 27, it can be seen that IFT is not changing with gas-oil ratio at all the pressures used. This clearly indicates the absence of gas-oil ratio effects on IFT and hence on miscibility. This further substantiates the compositional independence of miscibilities determined using the VIT technique, due to varying gas-oil ratios in the feed mixtures.

Since IFT's are found to be independent of gas-oil ratio, the average values of IFT's measured at each pressure for the two gas-oil ratios are used to determine miscibility using the VIT technique. The IFT measurements were fitted against pressure using a hyperbolic function. This function was used especially to fit the curvature to the data due to almost one order of magnitude reduction in IFT observed near miscibility. This plot is shown in Figure 28.

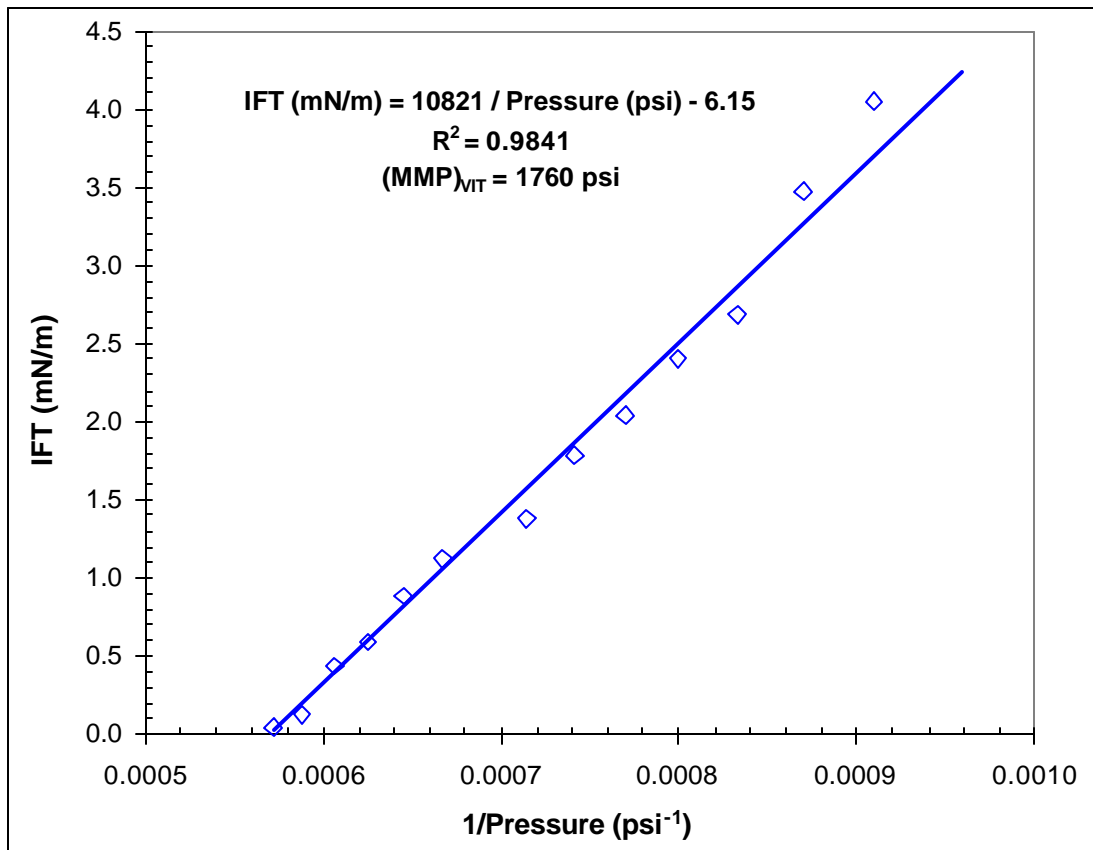


**Figure 28: Determination of VIT Miscibility in Synthetic Live Oil-CO<sub>2</sub> System at 160° F**

A good linear relationship between IFT and the reciprocal pressure can be seen in Figure 28 with a determination coefficient ( $R^2$ ) of 0.9841. The regression equation obtained is shown in Figure 28. This regression equation is then extrapolated to zero IFT to determine MMP. A miscibility pressure of 1760 psi was obtained with the VIT technique, which agrees well with the miscibility pressure of 1700 psia reported from the slim-tube, phase diagram and analytical models. Thus, this VIT experiment conducted using the standard gas-oil system of synthetic oil mixture-CO<sub>2</sub> at 160° F provides the third validation for the VIT technique to measure fluid-fluid miscibility conditions in multicomponent hydrocarbon systems.

#### 4.2.5 Effect of Gas-Oil Ratio on Dynamic Interfacial Tension

The effect of gas-oil ratio on dynamic interfacial tension was studied by measuring the changes in capillary rise heights with time in the synthetic live oil-CO<sub>2</sub> system at 1100 psi and 160° F. The two gas-oil ratios of 20/80 mole% gas and oil and 80/20 mole% gas and oil were used. Since capillary rise is an independent variable that affects interfacial tension, it is reasonable to assume that the changes in capillary rise with time measured are representative of changes in dynamic interfacial tension. The effect of gas-oil ratio on dynamic interfacial behavior is shown in Figure 29.

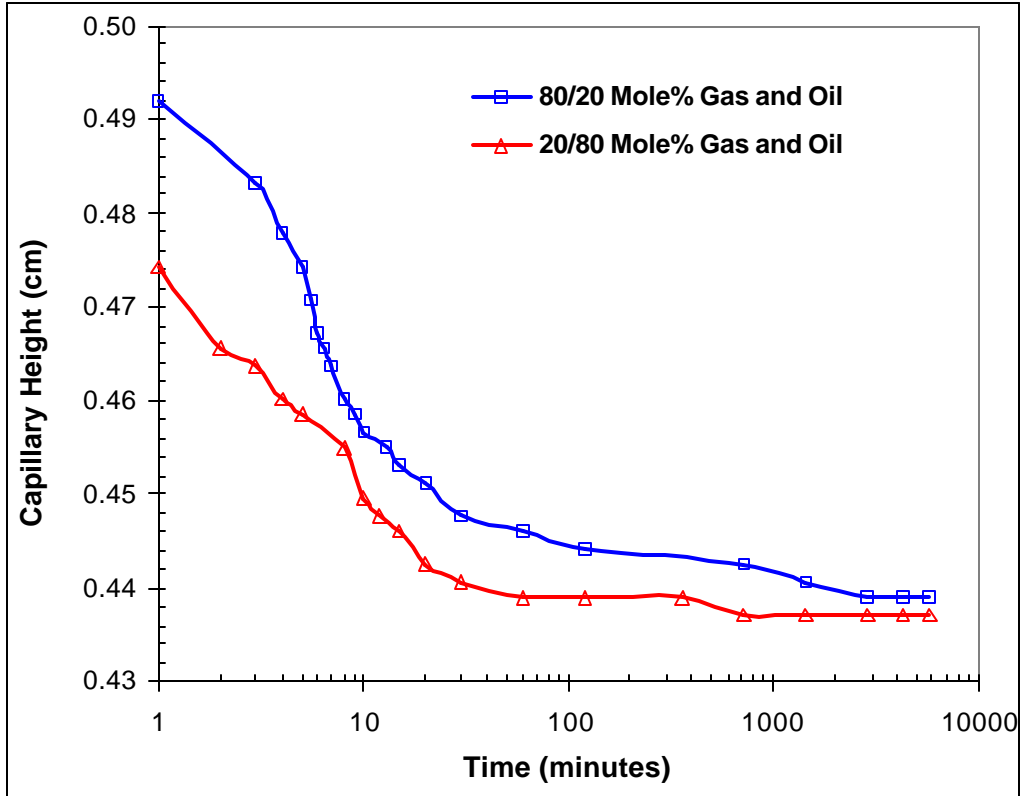


**Figure 29: Effect of Gas-Oil Ratio on Dynamic Interfacial Behavior**

From Figure 29, the dynamic nature of interfacial tension can be clearly seen at both the gas oil ratios used. The interfacial tension is gradually decreasing with time for both the gas-oil ratios due to mass transfer interactions taking place between the fluid phases

to reach the thermodynamic equilibrium. Such a phenomenon of dynamic interfacial tension will be more pronounced especially in multicomponent hydrocarbon systems. The dynamic nature of interfacial tension in multicomponent systems was first discovered experimentally by Plateau [126] long time ago.

As can be seen in Figure 29, the changes in interfacial tension with time are much more rapid at 20/80 gas-oil ratio, when compared to 80/20 gas-oil ratio. The influence of changes in interfacial tension has more pronounced effects on mass transfer rates than the effect of variations in the static properties such as density, viscosity and diffusivity [127]. Therefore, the rapid changes in interfacial tension observed at 20/80 gas-oil ratio can be attributed to higher mass transfer rates between the two fluid phases. The possible reasons for the higher mass transfer rates at 20/80 gas-oil ratio in the feed mixture are explained below.

The synthetic live oil mixture contains significant amount of lighter components (55 mole%  $n\text{-C}_1$  and  $n\text{-C}_4$ ), which more easily tend to diffuse from oil to gas phase. Hence, the components  $n\text{-C}_1$  and  $n\text{-C}_4$  in oil can be considered as solutes for mass transfer between oil and gas phases. At 20/80 gas-oil ratio, higher amounts of lighter components (solute) are available in oil to initiate the mass transfer and hence higher mass transfer rates, resulting in quicker thermodynamic equilibrium.

However, near thermodynamic equilibrium, the interfacial tensions become almost similar for both the gas-oil ratios used. This clearly indicates that once both the fluid phases approach equilibrium, IFT becomes independent of gas-oil ratio. Thus the gas-oil ratio in the feed mixture has no effect on near equilibrium IFT values, but it determines the rate at which the thermodynamic equilibrium state is attained. In other words, gas-oil

ratio has an impact on how fast the thermodynamic equilibrium can be reached when two immiscible fluid phases containing multiple components are brought into contact with each other. The following important observations can be made from the dynamic capillary rise measurements shown in Figure 29.

The capillary rise first decreases rapidly with time up to 10 minutes and then slowly until 100 minutes for both the gas-oil ratios used. For 20/80 gas-oil ratio, much smaller changes in capillary rise were observed from 100-700 minutes and then capillary rise becomes almost constant after 700 minutes. However, for 80/20 gas-oil ratio, much smaller changes in capillary rise were observed until 3000 minutes and then it appeared to stay constant. We believe that, even after such long aging periods between the two fluid phases, very minute changes in capillary rise may occur, but are not measurable with the available experimental instrumentation. This hypothesis can be well understood using the schematic diagram of solute concentration profiles shown in Figure 30. Figure 30 depicts the changes in the concentration profile of a diffusing component in the bulk liquid, bulk vapor and at the interface due to mass transfer between the liquid and vapor phases in both vaporizing and condensing modes of mass transfer in a gas liquid system.

The initial concentrations of the diffusing component A in gas and liquid phases are  $C_{A, gi}$  and  $C_{A, li}$ , respectively. In the vaporizing drive mechanism, mass transfer of component A takes place from liquid to gas by vaporization and in condensing mechanism, mass transfer of component A takes place from gas to liquid by condensation. In both these modes of mass transfer, the component A immediately reaches its equilibrium composition at the gas-liquid interface due to instantaneous mass transfer across the interface.  $C_{A, sge}$  and  $C_{A, sle}$  represent the equilibrium compositions of

component A in the gas and liquid phases, respectively, at the interface. However, these equilibrium compositions of the component A at the interface seem to be different from the equilibrium compositions of component A in the bulk liquid and vapor phases,  $C_{A, ble}$  and  $C_{A, bge}$ , respectively. As a result, prolonged intra-phase mass transfer of component A takes place within the bulk fluid phases for much longer times so as to attain thermodynamic equilibrium.

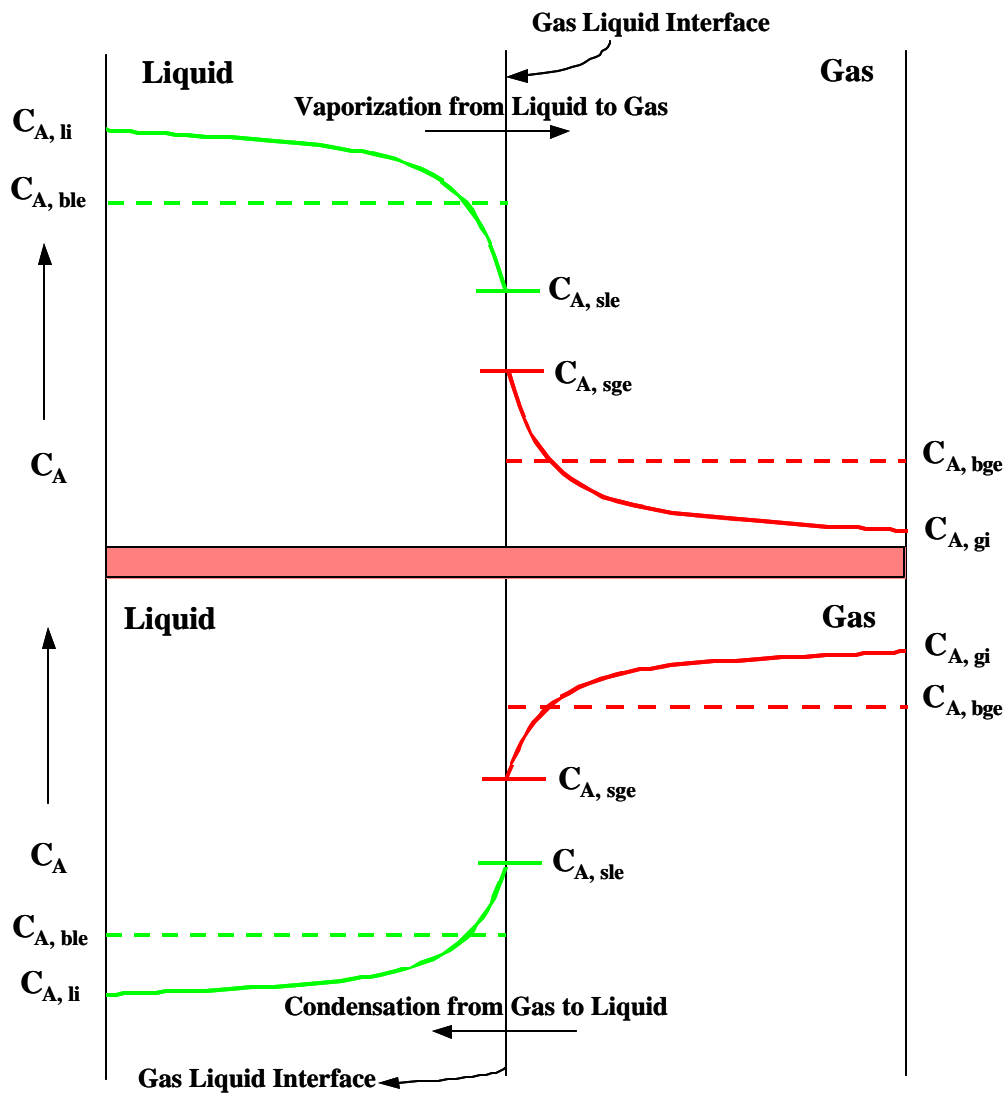


**Figure 30: Concentration Profiles of a Diffusing Component in Gas-Liquid Systems**

Therefore, we postulate that it is not possible to measure true equilibrium interfacial tensions with finite amounts of aging period between the fluid phases (as it was noted earlier that IFT changes were observed even after 3000 minutes). These dynamic effects of interfacial tension will be especially significant in the complex hydrocarbon systems consisting of multicomponent crude oil and gas phases. Crude oils contain thousands of chemical compounds [128] and hence it is difficult to attain thermodynamic equilibrium compositions of these various components within short aging periods. Therefore, in such systems, even after aging for much longer times, there may be still some infinitesimal amounts of mass transfer interactions occurring between the fluid phases to reach the ultimate thermodynamic equilibrium. However, after certain finite aging periods, the changes in interfacial tension with time become so minute that it is reasonable to approximate these interfacial tensions to near equilibrium interfacial tension. These near equilibrium interfacial tensions appear to be amenable to calculations using the diffusivity included Parachor model proposed in this study (Section 4.5) and hence can be used to predict fluid-fluid miscibility using the VIT technique.

### **4.3 Comparison of VIT Experiments of RKR and Terra Nova Reservoir Fluids with EOS Model Computations**

In this section, the VIT experimental results of MMP's reported for Rainbow Keg River (RKR) and Terra Nova Reservoir fluids [1 – 3] were compared with EOS calculations based on PR-equation of state [17]. The EOS calculations were carried out using the commercial simulator, Winprop [124].

#### **4.3.1 EOS Tuning**

The reservoir fluids compositions, reservoir temperatures and saturation pressures used in VIT experiments as well as in EOS calculations are described in Tables 13 and

14. The effect of tuning equations of state on EOS calculations was examined by tuning the EOS to match the saturation pressures, as done by several researchers before [37, 129].

**Table 13: Composition of Rainbow Keg River Fluids Used**

Reservoir Temperature: 188° F    Saturation Pressure: 2486.7 psia  
 Reservoir Pressure: 2538.6 psia    (bubble point)

Component	Mol % in live oil	Mol % in lean gas (Primary)	Mol % in rich gas (Makeup)
Hydrogen Sulfide	1.37	0	0
Carbon Dioxide	0.82	1.24	0.8
Nitrogen	0.57	1.76	0.4
Methane	35.13	81.01	14.73
Ethane	10.15	11.14	21.34
Propane	6.95	3.95	41.83
iso-Butane	1.1	0.5	7.35
n-Butane	3.16	0.34	11.67
iso-Pentane	2.29	0	0
n-Pentane	1.74	0.07	1.89
Hexanes	3.68	0	0
Heptanes plus	33.04	0	0
Total	100	100	100
CO <sub>2</sub> + C <sub>2+</sub>	62.93	17.24	84.88

**C<sub>7+</sub> Properties:**  
 Specific Gravity: 0.8397  
 Molecular Weight: 205

**Table 14: Composition of Terra Nova Fluids Used**

Reservoir Temperature: 212° F    Saturation Pressure: 3595 psia  
 Reservoir Pressure: 5516 psia    (bubble point)

Component	Mol % in live oil	Mol % in lean gas (Primary)	Mol % in rich gas (Makeup)
Nitrogen	0.15	0.33	0.21
Carbon dioxide	0.69	1.1	1.18
Methane	45.06	90.11	51.55
Ethane	5.37	6.01	12.8
Propane	5.44	2.09	16.31
<i>i</i> - Butane	0.98	0.12	2.63
<i>n</i> - Butane	2.85	0.21	6.71
<i>i</i> - Pentane	1.24	0.02	2.12
<i>n</i> -Pentane	1.8	0	2.35
<i>n</i> -Hexane	9.13	0	3.86
Heptanes plus	27.29	0	0.29
Total	100	100	100
CO <sub>2</sub> + C <sub>2+</sub>	54.79	9.56	48.24

**C<sub>7+</sub> Properties:**  
 Specific Gravity: 0.879  
 Molecular Weight: 241

Before tuning the EOS, the heptanes plus fraction was characterized using the two-stage exponential distribution [130]. Then, the PR-EOS was tuned to match the saturation pressures using different tuning approaches. The parameters tuned are:

1. The critical temperature,  $T_c$ , of the heaviest component in the characterized heptanes plus fraction
2. The critical pressure,  $P_c$ , of the heaviest component in the characterized heptanes plus fraction
3. The acentric factor,  $\omega$ , of the heaviest component in the characterized heptanes plus fraction
4. The binary interaction coefficient (BIC),  $K_{ij}$ , between methane and the heaviest component in the characterized heptanes plus fraction
5. Volume shift parameter,  $S$ , of the heaviest component in the characterized heptanes plus fraction
6. EOS parameter,  $\Omega_b$ , of the heaviest component in the characterized heptanes plus fraction
7. Molecular weight of the heaviest component in the characterized heptanes plus fraction

The initial and final values of tuned parameters and predicted saturation pressures obtained using different tuning approaches for the two reservoir crude oils of RKR and Terra Nova are given in Tables 15 and 16, respectively.

**Table 15: Comparison of MMP's from VIT Technique and EOS Calculations Using Various Tuning Approaches for Rainbow Keg River Reservoir Fluids**

Parameter	Initial Value	Tuned Value	P <sub>sat</sub> (psia)	Deviation (%)	Solvent #1 (C <sub>2+</sub> =51.0%) MMP (MPa)	Solvent #2 (C <sub>2+</sub> =52.5%) MMP (MPa)	Solvent #3 (C <sub>2+</sub> =59.7%) FCM (MPa)
Experimental (VIT)	-	-	2486.7	0	14.8	14	14.8
No tuning and without C <sub>7+</sub> characterization	-	-	2563	3	17.8	16.7	19.5
No tuning and with C <sub>7+</sub> characterization	-	-	2512	1	15.6	16.4	24.7
T <sub>c</sub> (K)	940.947	915.46	2486.9	0	21.8	23.7	22.3
P <sub>c</sub> (atm)	10.2318	9.7738	2485.5	0.05	21.8	23.6	23.5
ω	1.09313	1.04037	2486.8	0	21.9	21.7	22.7
Volume Shift Parameter, S	0.085167	0.035171	2512.9	1	15.6	16.4	24.7
K <sub>ij</sub> (C <sub>1</sub> - C <sub>27+</sub> )	0.111198	0.105836	2487	0.01	15.9	23.6	23.6
Ω <sub>b</sub>	0.077796	0.079139	2487	0.01	24.1	23.7	23.1
M <sub>w</sub> (g/mole)	480.611	480.611	2512.9	1	15.6	16.4	24.7

Best Choice



**Table 16: Comparison of MMP's from VIT Technique and EOS Calculations Using Various Tuning Approaches for Terra Nova Reservoir Fluids**

Parameter	Initial Value	Tuned Value	P <sub>sat</sub> (psia)	Deviation (%)	Solvent #1 (C <sub>2+</sub> =9.56%) MMP (MPa)	Solvent #2 (C <sub>2+</sub> =21.4%) MMP (MPa)	Solvent #3 (C <sub>2+</sub> =29.4%) MMP (MPa)	Solvent #4 (C <sub>2+</sub> =32.3%) MMP (MPa)	Solvent #5 (C <sub>2+</sub> =41.2%) MMP (MPa)
Experimental (VIT)	-	-	3595	0	62.85	57.8	31.8	-	-
Visible MMP	-	-	-	-	60.7	55	30.6	30	26.2
No tuning and without C <sub>7+</sub> characterization	-	-	3805	5.8	56.2	54.8	44.4	40	29.3
No tuning and with C <sub>7+</sub> characterization	-	-	3724	3.5	38	38	31.5	35.95	34.59
T <sub>c</sub> (K)	1014.6	996.228	3699	2.9	38.7	38.7	32.87	37.32	34.93
P <sub>c</sub> (atm)	9.3298	8.1739	3613	0.5	39.04	38.7	38.01	37.32	34.58
ω	1.20948	1.16924	3697	2.8	38.7	38.4	31.85	36.64	34.93
Volume Shift Parameter, S	0.07201	0.122	3724	3.5	38	38	31.5	35.95	34.59
K <sub>ij</sub> (C <sub>1</sub> - C <sub>31+</sub> )	0.119124	0.106069	3600	0.14	38.7	38.7	30.48	37.32	34.24
Ω <sub>b</sub>	0.077796	0.082574	3601	0.16	39.4	39.4	38.4	36.64	34.6
M <sub>w</sub> (g/mole)	577.624	606.549	3724	3.5	38	38	37.67	35.95	34.58

Best Choice



From Tables 15 and 16, it can be seen that the deviations of EOS predicted saturation pressures without tuning and without heptanes plus characterization from experimental values were reasonable (less than 5%). The tuning of volume shift parameter and molecular weight of the heaviest component in  $C_{7+}$  fraction were ineffective in improving the match of EOS predictions. The EOS predictions from the tuned parameters of critical temperature, critical pressure, binary interaction coefficient, acentric factor and  $\Omega_b$  of the heaviest component in  $C_{7+}$  fractions matched well with the experimental saturation pressure. The best fit of saturation pressures were obtained with the tuned parameter of binary interaction coefficient (BIC) for both the reservoir crude oils studied. Furthermore, in order to match the experimental saturation pressure, an absolute change of less than 5% was needed in all these parameters. Knowing the uncertainty in the experimental measurements, these variations in EOS parameters can be considered reasonable. Thus, good match of saturation pressures was obtained for both the reservoir crude oils without much change in the tuned parameters and hence it is reasonable to assume decent EOS tuning for both the crude oils.

#### **4.3.2 Gas-Oil Miscibility Determination Using EOS Model**

The compositions of the lean and rich gases used for making up the solvent and the compositions of various solvents used in VIT experiments as well as in EOS calculations are shown in Tables 13, 14, 17 and 18 for RKR and Terra Nova reservoir fluids, respectively.

**Table 17: Composition (in Mole %) of Solvents Used in VIT Tests as well as in EOS Calculations for Rainbow Keg River Reservoir Fluids**

Component	Solvent #1	Solvent #2	Solvent #3
Hydrogen Sulfide	0	0	0
Carbon Dioxide	1.01	1	0.96
Nitrogen	1.06	1.03	0.89
Methane	46.93	45.47	38.46
Ethane	16.38	16.61	17.69
Propane	23.42	24.26	28.27
iso-Butane	4.02	4.17	4.9
n-Butane	6.16	6.41	7.61
iso-Pentane	0	0	0
n-Pentane	1.01	1.05	1.24
Hexanes	0	0	0
Heptanes plus	0	0	0
Total	100	100	100
C <sub>2+</sub>	51	52.5	59.7
Makeup (%)	51.417	53.621	64.198

**Table 18: Composition (in Mole %) of Solvents Used in VIT Tests as well as in EOS Calculations for Terra Nova Reservoir Fluids**

Component	Solvent #1	Solvent #2	Solvent #3	Solvent #4	Solvent #5
Nitrogen	0.33	0.2933	0.2684	0.2594	0.2318
Carbon dioxide	1.1	1.1245	1.141	1.1471	1.1654
Methane	90.11	78.306	70.3285	67.4085	58.5642
Ethane	6.01	8.0894	9.4932	10.0071	11.5635
Propane	2.09	6.4444	9.3848	10.4611	13.7211
<i>i</i> - Butane	0.12	0.8886	1.4076	1.5976	2.173
<i>n</i> - Butane	0.21	2.2004	3.5445	4.0365	5.5266
<i>i</i> - Pentane	0.02	0.663	1.0973	1.2562	1.7377
<i>n</i> -Pentane	0	0.7196	1.2055	1.3834	1.9222
<i>n</i> -Hexane	0	1.182	1.9802	2.2723	3.1573
Heptanes plus	0	0.0888	0.1488	0.1707	0.2372
Total	100	100	100	100	100
CO <sub>2</sub> + C <sub>2+</sub>	9.56	21.4	29.4	32.33	41.2
Makeup (%)	0	30.62	51.3	58.87	81.8

The following steps are followed in the commercial simulator, Winprop [124] to calculate the minimum miscibility pressures at a given temperature.

1. An initial pressure below MMP is chosen to start the computation.
2. The reservoir temperature, crude oil composition, primary and makeup gas compositions, makeup gas fraction, pressure increment, solvent to oil ratio increment, equilibrium gas/original oil mixing ratio and equilibrium liquid/original solvent mixing ratio are then provided as inputs to the program.
3. The composition of solvent obtained by mixing of primary and makeup gases is then calculated using the specified ratio.
4. Solvent is added to the crude oil at specified solvent to oil molar ratio increments and flash calculations are performed until two-phase region is detected. The absence of two-phase region implies first contact miscibility and the program stops.
5. For the presence of two- phase region, the program checks the relative positions of solvent and crude oil compositions with respect to limiting tie line. If the solvent composition is to the left, while that of crude oil to the right of limiting tie line, then the process is a vaporizing gas drive. Otherwise, the process is a condensing gas drive [131].
6. For vaporizing gas drive, using the first point in the two-phase region detected in step 4, the flashed vapor is mixed with the original oil at the specified ratio of equilibrium gas to original oil and the flash calculation is performed.
7. For condensing gas drive, using the first point in the two-phase region detected in step 4, the flashed liquid is mixed with the original solvent at the specified ratio of equilibrium liquid to original solvent and the flash calculation is performed.

8. The procedure is repeated until the liquid composition is same as the vapor composition and MMP is the pressure at which this occurs and the program stops.
9. Otherwise, the pressure is increased at specified pressure increment and the steps 4 to 8 are repeated.

The results of MMP calculations from EOS model and their comparison with the VIT experiments for the two reservoir fluids of Rainbow Keg River (RKR) and Terra Nova are summarized below.

- **Rainbow Keg River (RKR) Reservoir**

Figure 31 (for a pressure of 16.7 MPa) shows the development of multiple contact miscibility by condensing drive mechanism at a  $C_{2+}$  concentration of 52.5% in the solvent, as an example case. Since the 7<sup>th</sup> contact-line between solvent (A) and the liquid phase ( $L_7$ ) lies outside the two-phase envelope, the MMP is 16.7 MPa. The summary of VIT experimental results and EOS calculations for different tuning approaches is shown in Table 15. The comparison is shown in Figure 32, which indicates that the MMP predictions from untuned PR-EOS and without  $C_{7+}$  characterization were consistently higher by about 3-5 MPa than VIT measurements at all  $C_{2+}$  enrichments. This is in good agreement with the other published reports [23, 24] that EOS calculations generally yield more conservative results than laboratory measurements.

As can be seen in Table 15, the MMP predictions from tuned EOS of critical temperature, critical pressure, acentric factor, binary interaction coefficient and  $\Omega_b$  parameter are nearly the same. Interestingly, all these tuned parameters also resulted in similar saturation pressure predictions. But these MMP predictions significantly differed

from the VIT experimental values. Thus, in spite of matching the saturation pressure with acceptable change in EOS parameters, the significantly different MMP predictions from tuned EOS compared to VIT experiments clearly indicate that tuning of EOS may not be always suitable for miscibility determination. However, it also raises question as to the effect of choosing another measured property to match, other than the saturation pressure, on MMP prediction.

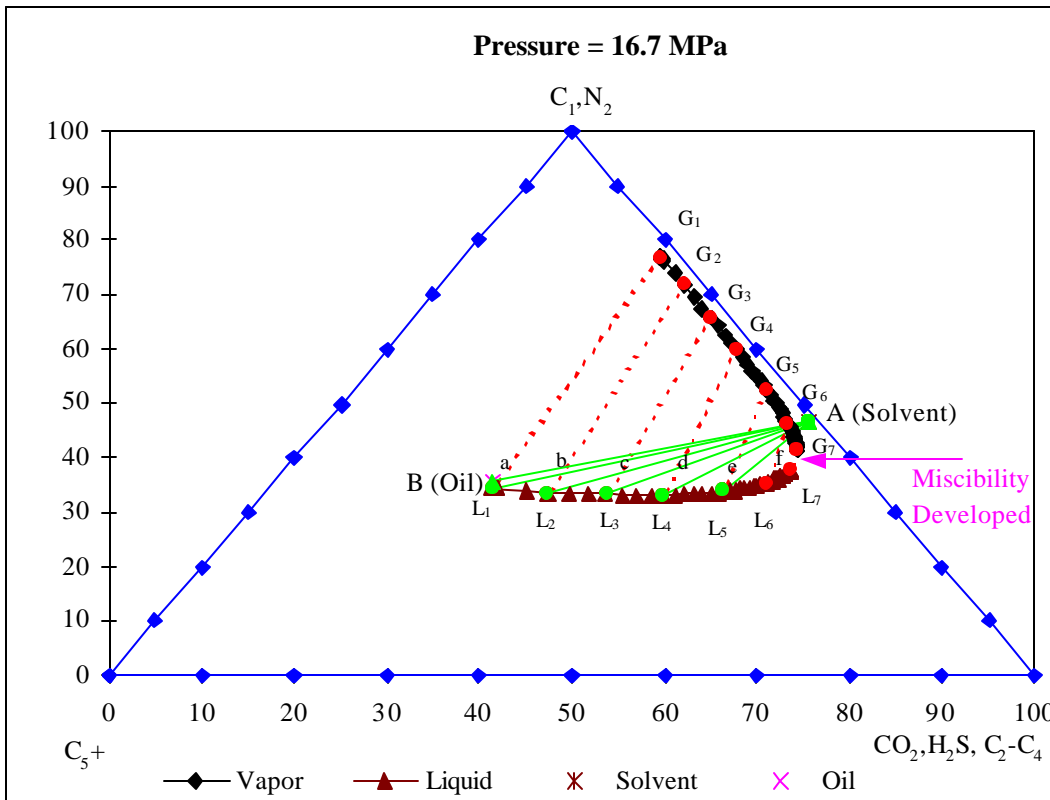


**Figure 31: Representation of Condensing Drive Mechanism on a Pseudo-Ternary Diagram for RKR Fluids at a  $C_{2+}$  Concentration of 52.5% in Solvent**

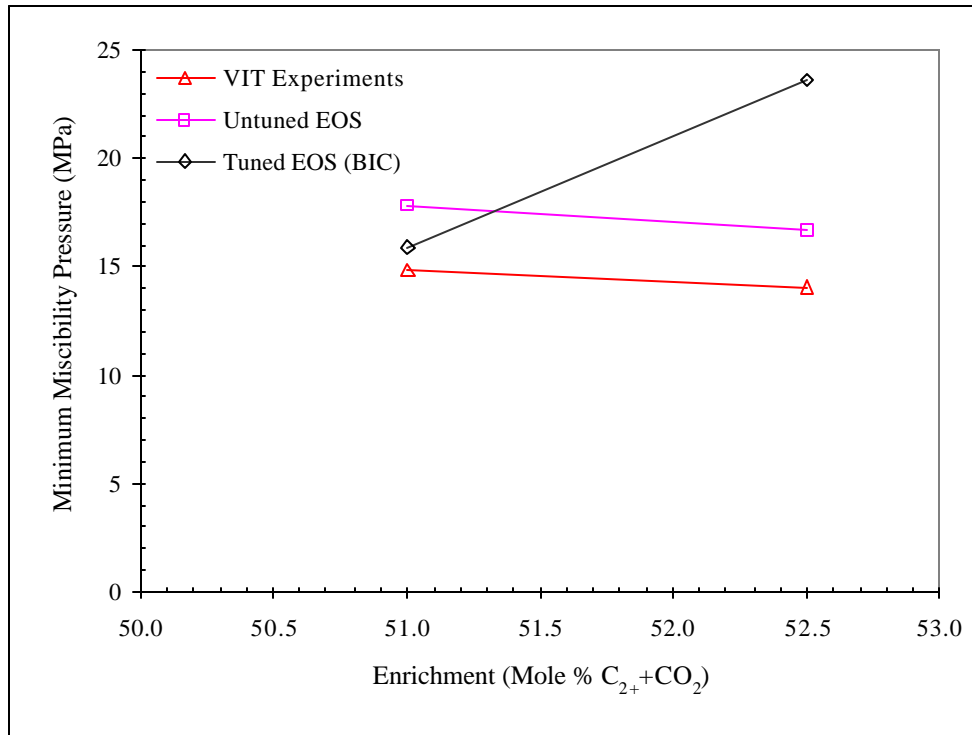


**Figure 32: Comparison of Miscibility Conditions of RKR Fluids Obtained from VIT Experiments and EOS Calculations**

- **Terra Nova Reservoir**

Table 16 shows the summary of VIT experimental values and EOS calculations for this reservoir fluids system. The comparison between various experimental techniques and EOS calculations is shown in Figure 33. The following important observations can be made from Table 16 and Figure 33.

- ❖ Large differences exist between untuned and tuned EOS at low C<sub>2+</sub> enrichments below 25%.
- ❖ Untuned EOS prediction is much closer to VIT and visible MMP experimental values than tuned EOS predictions.
- ❖ Sharp decline in MMP is indicated at C<sub>2+</sub> enrichments above 21.4% by almost all the techniques including VIT, visible observations, untuned and tuned EOS.

- ❖ Both tuned and untuned EOS indicate that calculated MMP's are insensitive to enrichment when the  $C_{2+}$  enrichment level is between 9.5-21.4%. This does not appear to be reasonable, since the doubling of enrichment should be expected to yield a significant drop in MMP.

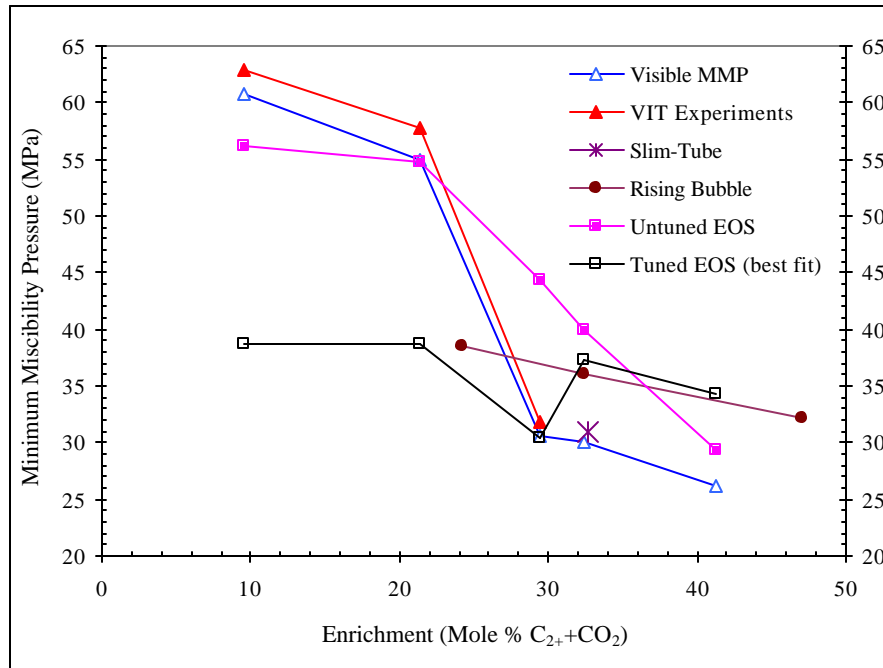


**Figure 33: Comparison of Miscibility Conditions of Terra Nova Fluids Obtained from VIT Experiments and EOS Calculations**

In three out of a total of five cases studied, the predicted MMP's from untuned PR-EOS and without  $C_{7+}$  characterization reasonably matched the visible MMP's from VIT experiments. Interestingly, the  $C_{2+}$  concentration in the solvent is around 30% for the two particular cases where the strong disagreement is observed. In one out of three cases where reasonable match is obtained, the EOS prediction is about 3.0 MPa higher than the VIT experimental value. The  $C_{2+}$  concentration in the solvent for this case is around 40%. Similar situation was observed at 50%  $C_{2+}$  concentration in the RKR reservoir case.

Furthermore, the slim-tube measurement lies close to the line joining the visible MMP experimental points (Figure 33).

The comparison of predicted MMP's from different tuning approaches for Terra Nova reservoir fluids is shown in Figure 34. The overall range of predicted MMP's from tuned EOS was from 30 to 40 MPa within the range of enrichments studied. However, the VIT experimental MMP's ranged from 31.8-62.85 MPa. The untuned EOS prediction did cover the same range as experimental data. While critical temperature, acentric factor and binary interaction coefficient show a sharp decline in predicted MMP at a  $C_{2+}$  concentration above 21.4%, the remaining tuned parameters did not show such a decline. This clearly points out that any MMP value within the range of 30 to 40 MPa can be matched by suitably choosing a tuning parameter, which in turn raises questions about the utility of such non-unique results from EOS tuning.

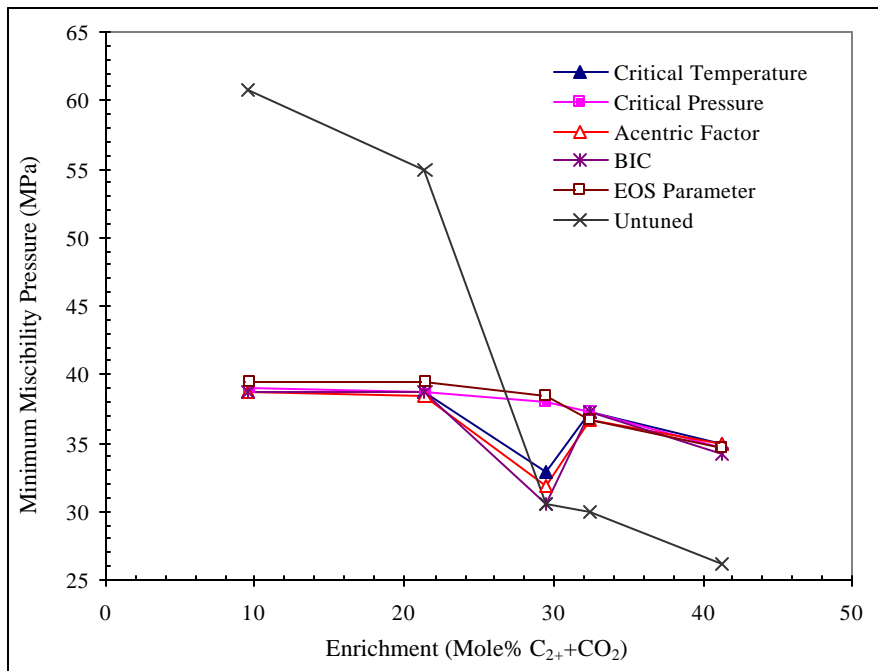


**Figure 34: Effect of Tuning on EOS MMP Predictions for Terra Nova Fluids**

### 4.3.3 Reality Check

The best tuning parameter (binary interaction coefficient) obtained in this study that matched the saturation pressures for both the reservoir crude oils perfectly was used to predict the laboratory PVT data as a reality check. The weight factors proposed by Coats and Smart [18], Coats [19] and Behbahaninia [20], as discussed in Section 2.6.1, were used to improve the PR-EOS predictive capabilities. These predictions were then compared against the actual laboratory PVT measurements of the reservoir crude oil samples. The comparisons of tuned PR-EOS predictions against the PVT experimental data for RKR and Terra Nova reservoir crude oils are shown in the Figure 35 and Figure 36, respectively. From these Figures, it can be seen that, the best tuned EOS parameter was unable to predict other important PVT measurements such as oil specific gravity, gas compressibility factor and gas-oil ratio as accurately as the saturation pressure, for the two reservoir crude oils considered. This raises another question: Is tuning an EOS based on saturation pressure alone enough to provide capability to predict other PVT properties and miscibility calculations?

Thus, this study has provided examples of several non-unique results from EOS tuning and also questions the utility of EOS tuning based on only saturation pressure for reliable phase behavior calculations. This study also suggests alternate ways of choosing another measured property other than saturation pressure to match while tuning EOS for MMP calculations. Therefore, it can be concluded that the untuned EOS is best suited for miscibility predictions of the two reservoir fluids considered. Only small disagreements observed between the miscibilities of untuned EOS calculations and VIT experiments further validate VIT technique for fluid-fluid miscibility determination.

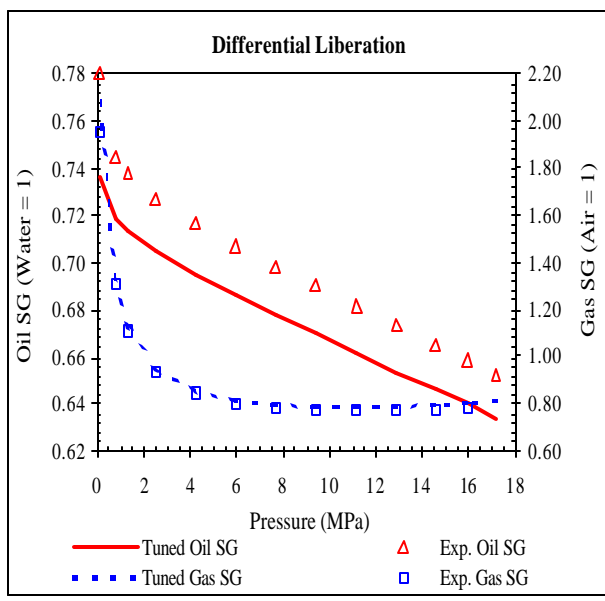
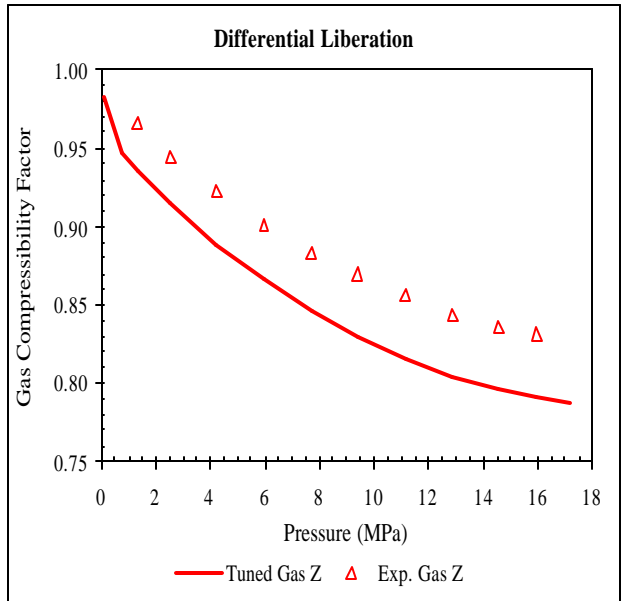
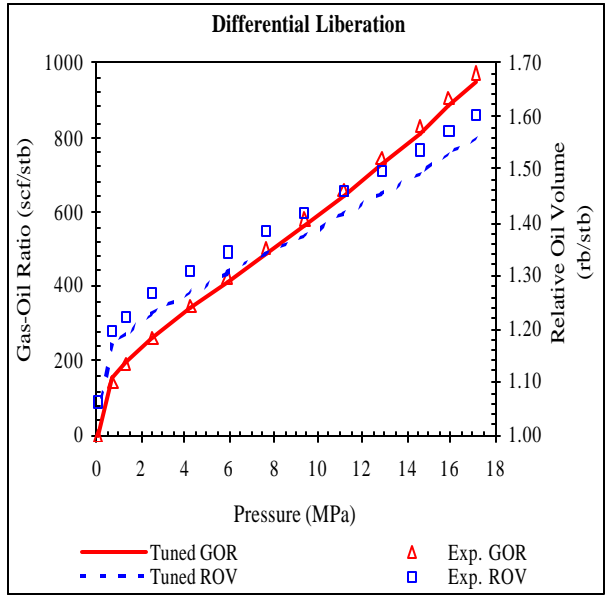
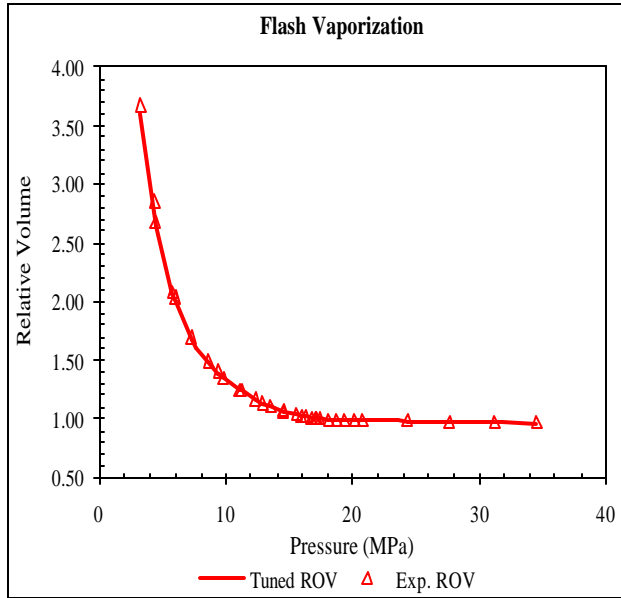


**Figure 35: Comparison of Tuned PR-EOS Predictions with Experimental PVT Data of RKR Reservoir Crude Oil**

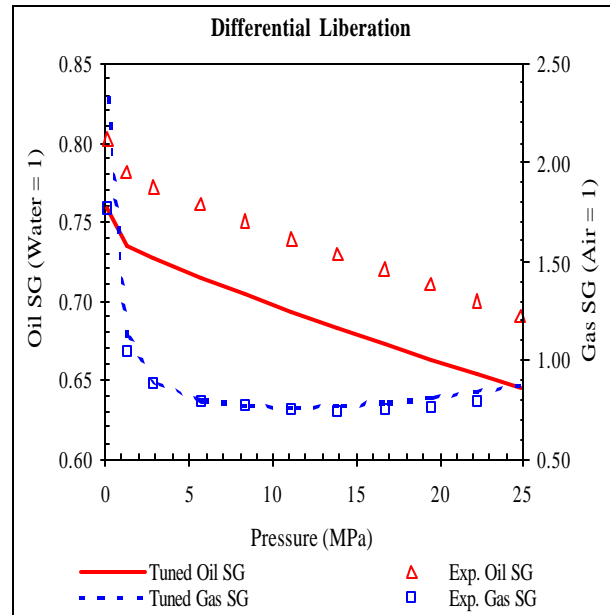
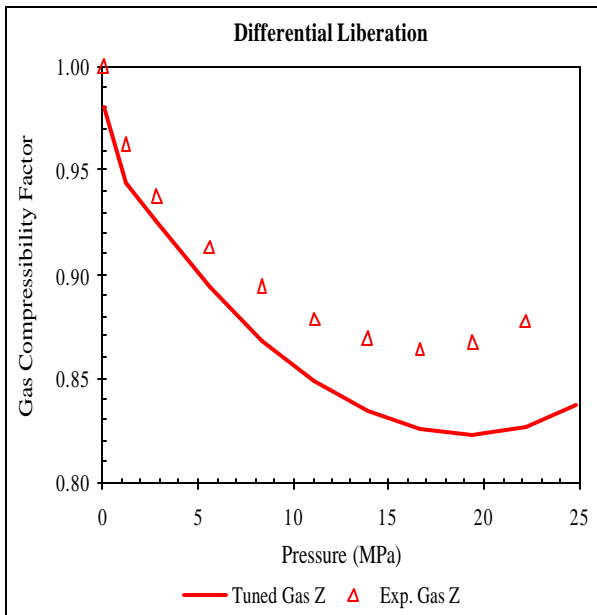
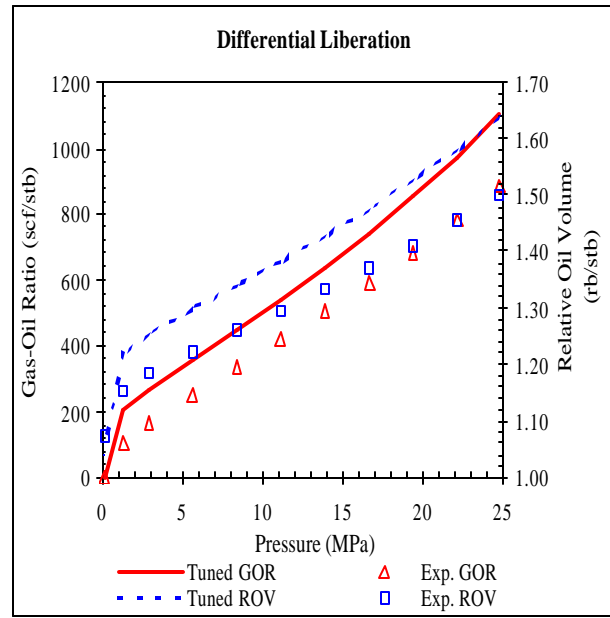
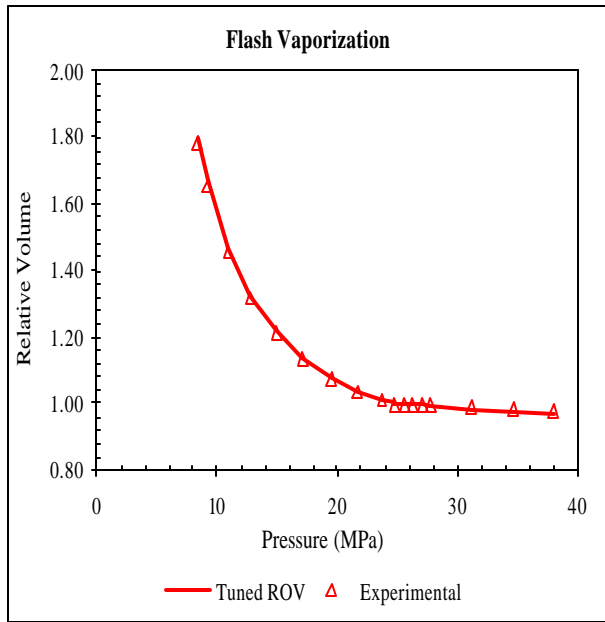


**Figure 36: Comparison of Tuned PR-EOS Predictions with Experimental PVT Data of Terra Nova Reservoir Crude Oil**

#### **4.4 Application of Parachor IFT Model to Predict Fluid-Fluid Miscibility**

In this section, the VIT experimental results of minimum miscibility pressures reported for Rainbow Keg River (RKR) reservoir fluids [1] were compared with the miscibility predictions of the conventional Parachor IFT model [76, 77]. Just as the VIT experimental technique, this model is also based on the concept of zero interfacial tension at miscibility. In this model, the interfacial tension between the fluids is calculated using Weinaug and Katz's [85] Parachor method at reservoir temperature as a function of pressure or gas enrichment. Then the extrapolation of the plot between interfacial tension and pressure or enrichment to zero interfacial tension yields the conditions of miscibility. The reservoir fluid and solvent compositions for RKR reservoir given in Tables 13 and 17, respectively, were used in Parachor model computations.

##### **4.4.1 Gas – Oil IFT Calculations**

A mixture consisting of 10 mole% of crude oil and 90 mole% of solvent is used as the feed composition in the Parachor computational model to match the composition used in VIT experiments. Flash calculations are performed with the mixed feed using PR-EOS [17] and the commercial simulator, Winprop [124] at the specified pressure and reservoir temperature at varying  $C_{2+}$  enrichments in solvent. QNSS/Newton algorithm [132] was used to perform the flash calculations. The resultant molar liquid, vapor densities, equilibrium liquid and vapor compositions of different components along with their pure component Parachors reported in the literature [81 - 84] are then used in Eq. 14 to compute the gas-oil interfacial tension.

The summary of experimental IFT's and the calculated IFT's using the Parachor computational model for RKR fluids at different  $C_{2+}$  enrichments in solvent is given in

Table 19 for pressures of 14.8 MPa and 14.0 MPa. Similar trends are observed at both the pressures. Parachor model under-predicts the interfacial tension at all  $C_{2+}$  enrichments. The calculated IFT's are then plotted against  $C_{2+}$  enrichment to determine MME's in Figures 37 and 38, for pressures of 14.8 MPa and 14.0 MPa, respectively. As can be seen in these figures, conservative estimates of MME's are obtained with Parachor model when compared to experimental MME's (by about 3.2-3.4%) at both the pressures.

**Table 19: Comparison of Measured IFT's with Parachor Model Predictions for RKR Reservoir Fluids**

Pressure = 14.8 MPa			Pressure = 14.0 MPa		
Enrichment (Mole% $C_{2+}+CO_2$ )	IFT (mN/m)		Enrichment (Mole% $C_{2+}+CO_2$ )	IFT (mN/m)	
	Experimental [1] (Rao, 1997)	Parachor Model		Experimental [1] (Rao, 1997)	Parachor Model
17.79	4.26	2.91	32.68	2.86	1.88
21.64	3.89	2.59	37.55	1.89	1.46
25.85	3.27	2.21	41.45	1.51	1.14
30.57	2.69	1.81	42.61	1.39	1.04
33.86	2.13	1.54	47.48	0.70	0.68
37.70	1.52	1.24			
43.07	0.97	0.85			
48.39	0.53	0.50			
49.28	0.27	0.48			

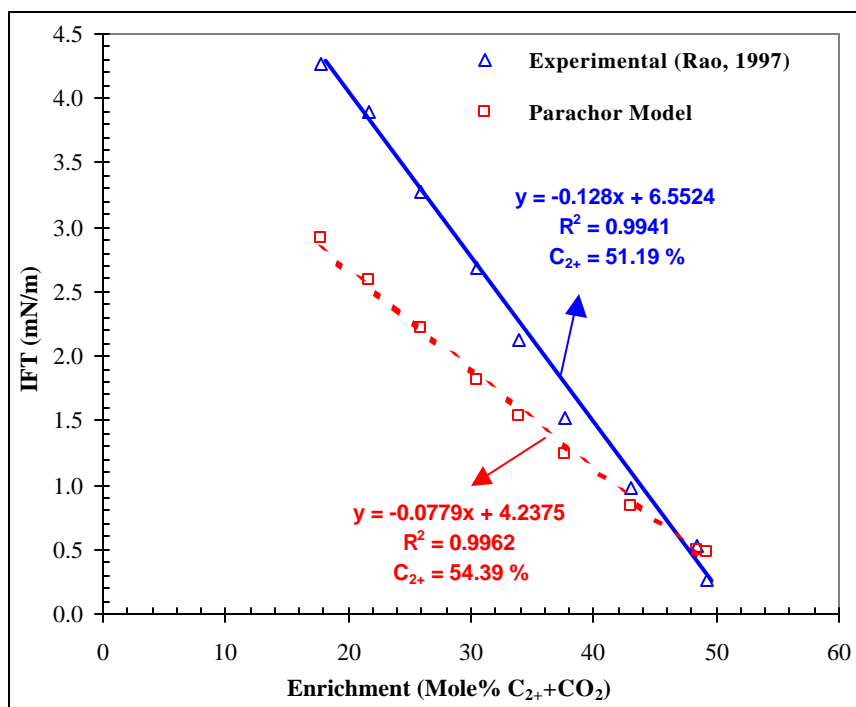


**Figure 37: Comparison of Experimental IFT's with Parachor Model for RKR Fluids at a Pressure of 14.8 MPa**

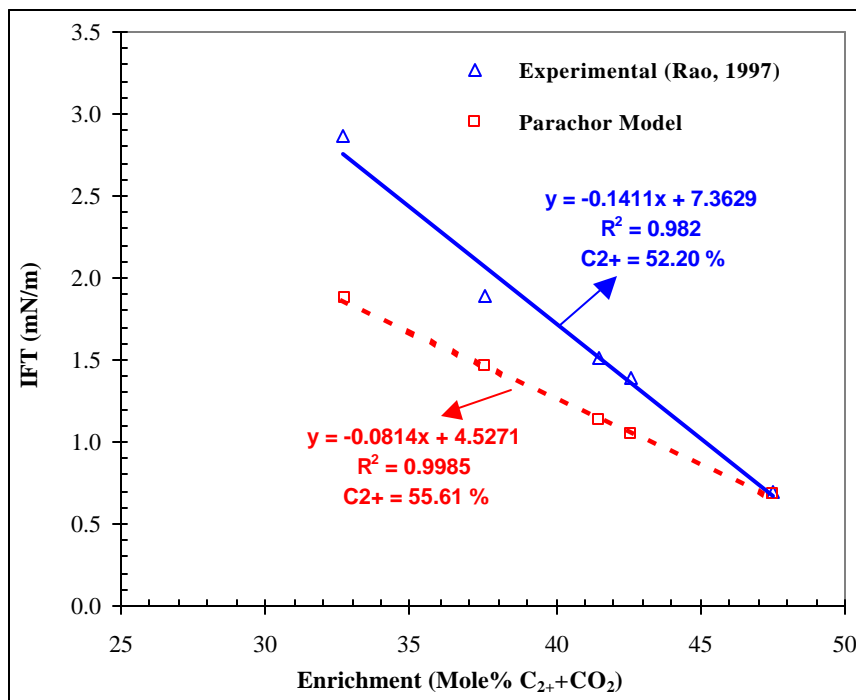


**Figure 38: Comparison of Experimental IFT's with Parachor Model for RKR Fluids at a Pressure of 14.0 MPa**

#### 4.4.2 Gas - Oil Miscibility Calculations

The sequence of steps followed in MMP calculation procedure using Parachor computational model are:

1. Oil composition, solvent composition, reservoir temperature, mole fraction of oil in the feed, pressure and the pressure increment are provided as inputs to the model.
2. Flash calculations are performed with mixed feed at reservoir temperature and specified pressure using QNSS/Newton Algorithm [132].
3. The resulting molar liquid, vapor densities, equilibrium liquid and vapor compositions of different components along with their pure component Parachors are used in Eq. 14 to calculate the IFT's.
4. The pressure is incremented at the specified pressure increment and steps 2 and 3 are repeated.
5. In the low interfacial tension region, pressure is incremented in smaller steps to clearly identify the point of vanishing IFT pressure. Then this vanishing IFT pressure becomes the MMP for the reservoir fluids system.

The comparison between VIT experimental MMP's and the calculated MMP's from Parachor computational model for RKR fluids at  $C_{2+}$  enrichments of 51.0% and 52.5% in solvent is shown in Figure 39. The gas-oil miscibility predictions from the untuned EOS calculations at these  $C_{2+}$  enrichments are also included in the Figure for better comparison. The calculated IFT's using the Parachor model at both the  $C_{2+}$  enrichments are plotted against pressure to determine MMP's in Figure 40.

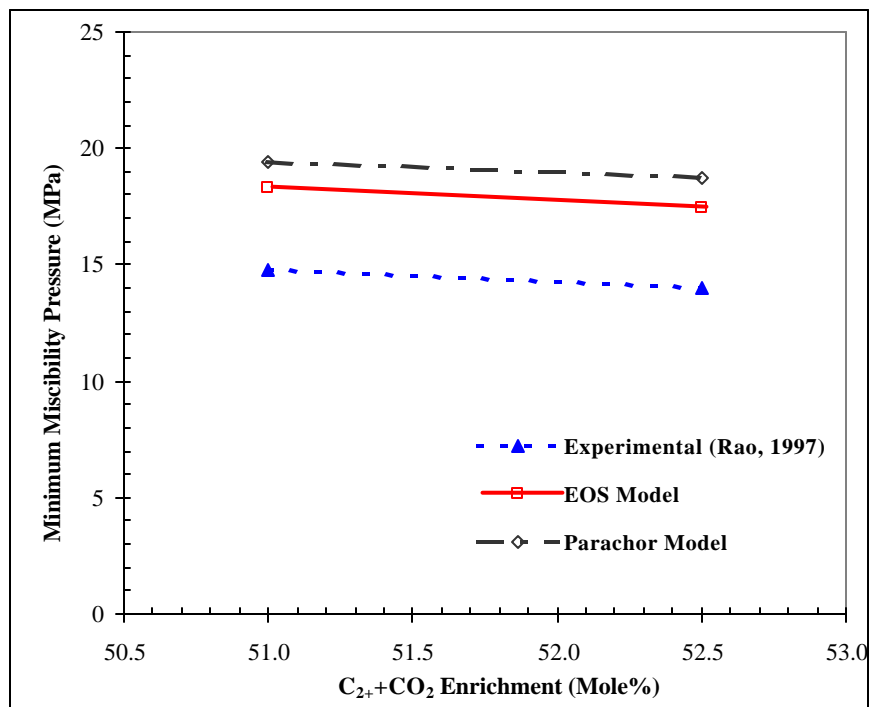


**Figure 39: Comparison of VIT Miscibility of RKR Fluids with EOS Calculations and Parachor Model**

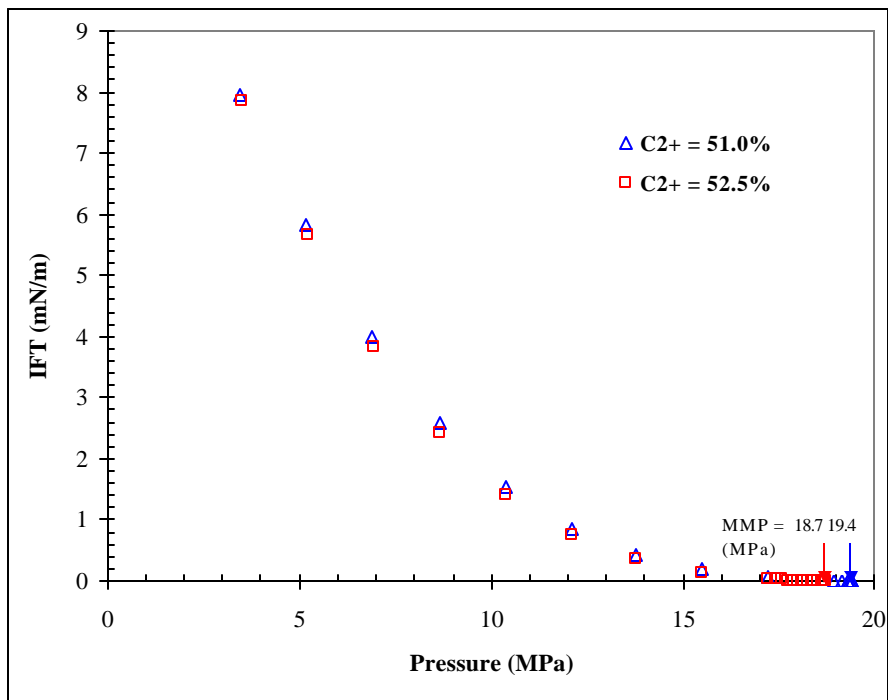


**Figure 40: MMP Determination using Parachor Computational Model for RKR Fluids**

From Figure 39, it can be seen that the Parachor computational model has resulted in MMP over-predictions by about 4.5 MPa, when compared to VIT experiments. Miscibility over-predictions of about 3.5 MPa are obtained from EOS calculations. Thus, the miscibility over-predictions from the Parachor model are greater than those obtained from the EOS model (by about 1.0 MPa or 145 psi).

#### **4.4.3 Mass Transfer Effects on Fluid-Fluid Miscibility**

Since IFT, a good indicator of mass transfer effects, was used to interpret miscibility in this study, the reasons for the miscibility over-predictions by the computational models appear to be the following.

In VIT experiments, equilibrated fluids are used in IFT measurements. Hence various types of mass transfer mechanisms are allowed to take place between the fluids (condensing gas drive, vaporizing gas drive and combined condensing/vaporizing gas drive). Thus VIT measurements include all the mass transfer effects and hence predict true MMP's. In EOS calculations, mass transfer effects are taken into account only through either condensing gas drive or vaporizing gas drive, which is quite evident in the MMP calculation procedure of EOS model, as discussed in Section 4.3. This limited mass transfer resulted in MMP over-predictions (about 3.5 MPa) by the EOS model. In Parachor computational model, the Parachor values are based on surface tension measurements of pure compounds. Hence these values are incorporated in the computational model considering each component of the mixture as if all the others were absent. Because of this assumption, this model does not incorporate any of the mass transfer effects in the calculation procedure. This appears to be responsible for over-predictions of MMP (about 4.5 MPa) by the Parachor model.

Therefore, it can be concluded that mass transfer has significant effect on fluid-fluid miscibility and that the combined vaporizing/condensing mechanism involving simultaneous counter-directional mass transfer of components between the fluid phases is the main mechanism that controls fluid-fluid miscibility in multicomponent hydrocarbon systems. This is in good agreement with the experimental observations of Zick [16]. Thus the ability of any miscibility computational procedure to account for the counter-directional mass transfer effects between the fluids governs the extent of agreement with miscibility pressures and enrichments determined from VIT experiments. This clearly demonstrates the importance of mass transfer effects in fluid-fluid miscibility computations and hence identifies the need to develop methods to incorporate all the mass transfer effects in the models used to compute miscibility.

#### **4.5 Newly Proposed Mechanistic Parachor Model for Prediction of Dynamic IFT and Miscibility in Multicomponent Hydrocarbon Systems**

From the literature review provided in Section 2.7.3, it is quite evident that almost all the currently available IFT models have been extensively tested for either pure compounds or binary mixtures. The use of these models to predict interfacial tension in complex hydrocarbon systems involving multicomponents in both the phases is only limited and not well reported. Furthermore, none of these models provides information on mass transfer interactions governing fluid phase equilibria. Several studies by eminent researchers in literature reported the effect of interfacial tension on mass transfer in various chemical engineering applications [126, 127, 133] such as in distillation and extraction operations. These studies prompted us to investigate the utility of interfacial tension to infer information on mass transfer mechanisms taking place between the fluid phases. Hence, we proposed a mechanistic Parachor model, based on the Parachor

method to predict interfacial tension and to infer information on mass transfer mechanisms governing fluid phase equilibria in complex multicomponent hydrocarbon systems.

#### **4.5.1 Background on Development of Proposed Mechanistic Parachor Model**

In the application of the original Parachor model to multicomponent mixtures, Parachor values of pure components are used in IFT predictions, considering each component of the mixture as if all the others were absent. Because of this assumption, this model does not incorporate all the mass transfer effects and this appears to be the main reason for poor IFT predictions from the original Parachor model in complex multicomponent hydrocarbon systems.

Therefore, a mechanistic Parachor model has been proposed, in which, the ratio of diffusivity coefficients between the fluid phases raised to an exponent is introduced into the Parachor model to incorporate mass transfer effects. The mass transfer interactions for phase equilibria between fluid phases take place by diffusion due to concentration gradient and by dispersion. Hence diffusivities are used in the mechanistic model to account for mass transfer effects. Furthermore, only diffusivities can reasonably represent mass transfer interactions in complex systems like crude oil-hydrocarbon gas mixtures involving multicomponents in both the phases. This is further substantiated with the fact that several investigators [134 - 137] used diffusivity coefficients in their proposed models to predict dynamic interfacial tension in brine – crude oil – surfactant systems. The ratio of diffusivities in both directions (vaporizing and condensing) between the fluid phases raised to an exponent used in the mechanistic model, enables the retention of the

same dimensions of the original Parachor model. The proposed mechanistic model is therefore given by:

$$s^{1/4} = \left( \frac{D_{os}}{D_{so}} \right)^n (\mathbf{r}_M^L \sum x_i P_i - \mathbf{r}_M^V \sum y_i P_i) \dots\dots\dots (37)$$

Where,  $D_{os}$  is the diffusivity of oil in gas (solvent),  $D_{so}$  is the diffusivity of gas (solvent) in oil and  $n$  is the exponent, whose sign and value characterize the type and extent of governing mass transfer mechanism for fluid phase equilibria. In the discussion on mass transfer effects on fluid-fluid miscibility provided in Section 4.4.3, it is clearly shown that the simultaneous counter directional mass transfer of components between the fluid phases (combined vaporizing and condensing drive) is the main mechanism responsible for attaining fluid phase equilibria. Therefore, the sign and the value of the exponent in the proposed mechanistic model characterize the type and extent of the dominant mass transfer mechanism (either vaporizing or condensing) in that combined vaporizing and condensing mass transfer drive mechanism.

If  $n > 0$ , the governing mass transfer mechanism for fluid phase equilibria in the combined vaporizing and condensing drive mechanism is the vaporization of lighter components from the oil to the gas phase. If  $n < 0$ , the governing mass transfer mechanism in the combined vaporizing and condensing drive mechanism for fluid phase equilibria is condensation of intermediate to heavy components from the gas to the crude oil. The value of  $n$  equal to zero ( $n \approx 0$ ) indicates equal proportions of both vaporizing and condensing drive mechanisms in the combined vaporizing and condensing drive mechanism. This condition of equal extent of vaporizing and condensing mechanisms appears to be most common in binary mixtures where the original Parachor model has

shown to result in reasonable accurate interfacial tension predictions ( $n = 0$  in the mechanistic Parachor model). The higher the numerical value of  $n$  (irrespective of its sign), the greater is the extent of that governing mass transfer mechanism.

The gas-oil IFT calculations in this section using Parachor model were carried out using the procedure described in Section 4.4.1. Sigmund [138] used Wilke equation [139] for comparison with the experimental data of diffusivities between two nine-component gas mixtures and found that Wilke equation is capable of giving good estimates of diffusivities even for the cases where one mixture diffuses into another mixture. Fayers [140] compared the diffusivity data of multicomponent systems at reservoir conditions obtained from various correlations with experiments and concluded that Wilke-Chang equation [141] is the best available empirical correlation to compute the diffusivities in multicomponent hydrocarbon systems. Hence, the diffusivities between the fluid phases are computed, using the empirical correlation of Wilke and Chang [141, 142], given by:

$$D_{AB} = \frac{(117.3 \times 10^{-18})(j M_B)^{0.5} T}{\mu_A^{0.6}} \dots\dots\dots (38)$$

Where  $D_{AB}$  = diffusivity of solute A in very dilute solution in solvent B,  $m^2/sec$

$M_B$  = molecular weight of the solvent, kg/kmol

$T$  = temperature, K

$\mu$  = solution viscosity, kg/msec

$v_A$  = solute molal volume at normal boiling point,  $m^3/kmol$

$\phi$  = association factor for solvent, set equal to unity since the solvents used in this study are unassociated.

Eq. 38 is extended to multicomponent hydrocarbon mixtures, using:

$$M_B = \sum x_{Bi} M_{Bi} \dots\dots\dots (39)$$

$$n_A = \sum x_{Ai} n_{Ai} \dots\dots\dots (40)$$

Where,  $x_i$  is the mole fraction of the component  $i$  in the mixture,  $M_{Bi}$  is the molecular weight of the component  $i$  and  $n_{Ai}$  is the molal volume of the component  $i$  at normal boiling point.

An objective function ( $\Delta$ ) is defined as the sum of weighted squared deviations between the original Parachor model predictions and experimental IFT values and is given by:

$$\Delta = \sum_{j=1}^N \left[ w_j \left( \frac{\sigma_j^{pred}(X) - \sigma_j^{exp}}{\sigma_j^{exp}} \right) \right]^2 \dots\dots\dots (41)$$

Where, each element of the objective function expresses the weighted difference between the predicted and experimental interfacial tension values,  $\sigma^{pred}$  and  $\sigma^{exp}$ , respectively;  $w$  is the weighting factor and  $N$  represents the number of measured data points to be fitted;  $X$  designates the correction factor to the original Parachor model prediction.

The mass transfer enhancement parameter ( $k$ ), a correction to the original Parachor model to account for mass transfer effects, is then defined as the correction factor ( $X$ ) at which the objective function ( $\Delta$ ) becomes the minimum. The mechanistic Parachor model is now given by:

$$\sigma^{1/4} = (k)(r_M^L \sum x_i P_i - r_M^V \sum y_i P_i) \dots\dots\dots (42)$$

From Eqs. 37 and 42, the exponent  $n$ , characterizing the governing mass transfer mechanism for fluid phase equilibria, can be computed using:

$$k = \left( \frac{D_{os}}{D_{so}} \right)^n \dots\dots\dots (43)$$

#### 4.5.2 Application of the Proposed Mechanistic Model to Crude Oil - Gas Systems

##### (a) Rainbow Keg River Reservoir

The crude oil and hydrocarbon gas compositions and the temperature from Rao [1] are used in IFT computations for this reservoir. The IFT measurements at various C<sub>2+</sub> enrichments in hydrocarbon gas phase and at various pressures reported by Rao [1] are used for comparison with model predictions. A mixture consisting of 10 mole% of crude oil and 90 mole% of hydrocarbon gas is used as the feed composition in the computations to match the composition used in the reported experiments.

The comparison of IFT predictions by the original Parachor model with experiments at various C<sub>2+</sub> enrichments in gas phase is given in Tables 20 and 21, for pressures 14.8 MPa and 14.0 MPa, respectively. These results are also shown in Figures 41 and 42, respectively for pressures 14.8 MPa and 14.0 MPa.

**Table 20: Comparison of IFT Measurements with Parachor Model for RKR Fluids at 87 °C and 14.8 MPa**

Enrichment (Mole% C <sub>2+</sub> +CO <sub>2</sub> )	IFT (mN/m)		Weighted Squared Deviation
	Experimental (Rao, 1997)	Parachor Model	
17.79	4.26	2.91	0.1000
21.64	3.89	2.59	0.1124
25.85	3.27	2.21	0.1043
30.57	2.69	1.81	0.1065
33.86	2.13	1.54	0.0762
37.70	1.52	1.24	0.0347
43.07	0.97	0.85	0.0166
48.39	0.53	0.50	0.0028
49.28	0.27	0.48	0.0061
Objective Function (Δ) =			0.5595

**Table 21: Comparison of IFT Measurements with Parachor Model for RKR Fluids at 87 °C and 14.0 MPa**

Enrichment (Mole% C <sub>2+</sub> +CO <sub>2</sub> )	IFT (mN/m)		Weighted Squared Deviation
	Experimental (Rao, 1997)	Parachor Model	
32.68	2.86	1.88	0.1167
37.55	1.89	1.46	0.0518
41.45	1.51	1.14	0.0610
42.61	1.39	1.04	0.0620
47.48	0.70	0.68	0.0007
Objective Function (Δ) =			0.2921

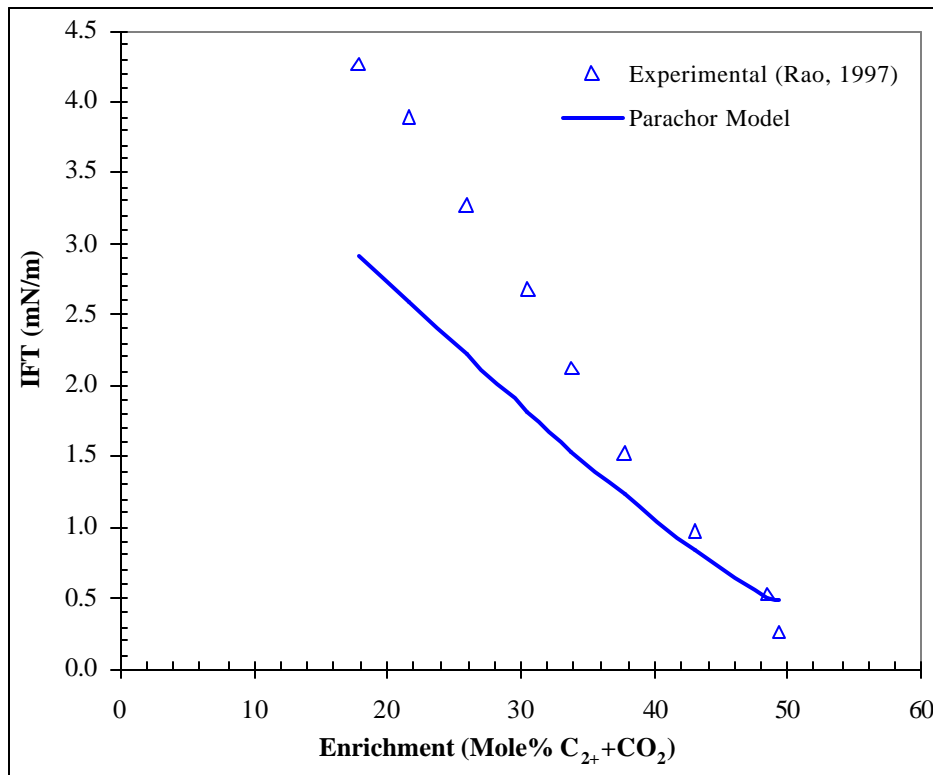


**Figure 41: Comparison between IFT Measurements and Parachor Model for RKR Fluids at 87 °C and 14.8 MPa**

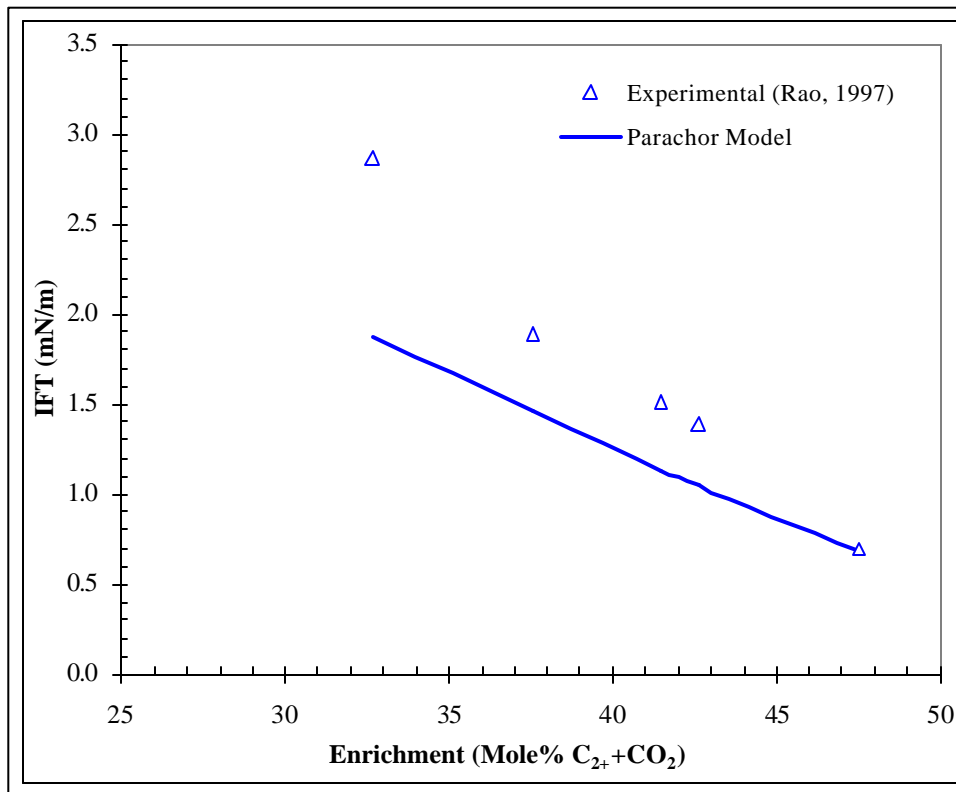


**Figure 42: Comparison between IFT Measurements and Parachor Model for RKR Fluids at 87 °C and 14.0 MPa**

As can be seen in Tables 20-21 and Figures 41-42, similar trends in IFT are observed for both the pressures. The match between the experiments and the model predictions is not good and IFT under-predictions are obtained with the Parachor model. This is in agreement with Cornelisse et al. [116], who made similar observations for n-Decane and carbon dioxide systems.

The disagreement between the experiments and the model predictions, as seen in Figures 41 and 42, are attributed mainly to the absence of complete mass transfer effects in the original Parachor model. Hence correction factors are used for original Parachor model predictions to minimize the objective function ( $\Delta$ ), which is the sum of weighted squared deviations between the model predictions and experimental values. The correction factors and the resulting objective functions for this crude oil-gas system are

shown in Figure 43. The mass transfer enhancement parameters ( $k$ ), the correction factors at which objective function becomes the minimum, are estimated to be 1.30 and 1.26, respectively for pressures of 14.8 MPa and 14.0 MPa.

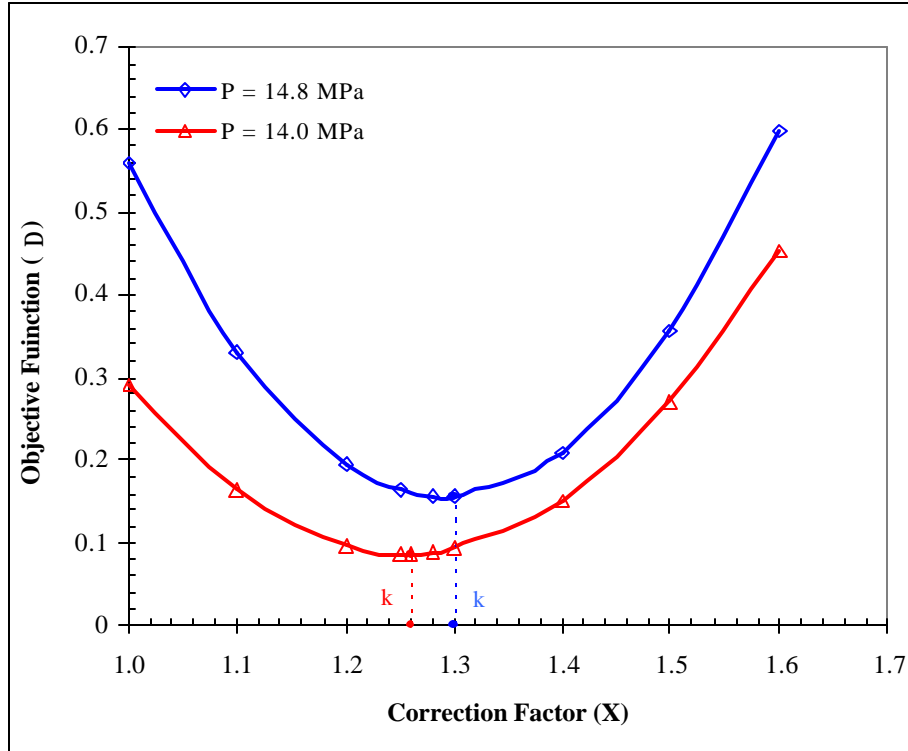


**Figure 43: Determination of Mass Transfer Enhancement Parameters for RKR Reservoir Fluids**

The computed diffusivities between the fluid phases at various  $C_{2+}$  enrichments in hydrocarbon gas phase for RKR fluids at pressures of 14.8 MPa and 14.0 MPa are given in Table 22. From Table 22, it can be seen that the mass transfer interactions between the fluid phases declined slightly as the  $C_{2+}$  enrichment in hydrocarbon gas phase is increased for both the pressures. However, the ratio of diffusivities in both directions (oil to gas and gas to oil) remains almost the same at all  $C_{2+}$  enrichments in gas phase. The average

ratios of diffusivities between the fluids at all  $C_{2+}$  enrichments are 3.70 and 3.92, respectively for pressures 14.8 MPa and 14.0 MPa.

**Table 22: Diffusivities between Oil and Gas at Various  $C_{2+}$  Enrichments for RKR Reservoir Fluids at 87° C**

14.8 MPa				14.0 MPa			
(Mole% $C_{2+} + CO_2$ )	$D_{os}$ (m <sup>2</sup> /s)	$D_{so}$ (m <sup>2</sup> /s)	$D_{os}/D_{so}$	(Mole% $C_{2+} + CO_2$ )	$D_{os}$ (m <sup>2</sup> /s)	$D_{so}$ (m <sup>2</sup> /s)	$D_{os}/D_{so}$
17.79	3.45E-08	9.69E-09	3.56	32.68	3.44E-08	8.67E-09	3.97
21.64	3.45E-08	9.40E-09	3.68	37.55	3.34E-08	8.39E-09	3.98
25.85	3.42E-08	9.11E-09	3.75	41.45	3.21E-08	8.18E-09	3.93
30.57	3.36E-08	8.81E-09	3.81	42.61	3.17E-08	8.12E-09	3.91
33.86	3.29E-08	8.62E-09	3.82	47.48	2.99E-08	7.89E-09	3.79
37.70	3.19E-08	8.41E-09	3.80				
43.07	3.03E-08	8.14E-09	3.73				
48.39	2.85E-08	7.89E-09	3.61				
49.28	2.83E-08	7.88E-09	3.59				
Average =			3.70	Average =			3.92

Using the mass transfer enhancement parameters and the average ratios of diffusivities between the fluid phases in Eq. 43, the exponent (n) characterizing the governing mass transfer mechanism is found to be +0.20 and +0.17, respectively for pressures 14.8 MPa and 14.0 MPa. These values of n being greater than zero indicate that the vaporization of components from the crude oil into the gas phase is the primary mass transfer mechanism in the combined vaporizing and condensing drive mechanism that governs the fluid phase equilibria of these reservoir fluids. This can be attributed to the presence of significant amounts of lighter components (52 mole%  $C_1$  to  $C_3$ ) in the crude oil of this reservoir [1].

The comparison between the IFT predictions of proposed mechanistic Parachor model with experiments at various  $C_{2+}$  enrichments in gas phase is given in Tables 23 and 24, respectively, for pressures 14.8 MPa and 14.0 MPa. These results are shown in

Figures 44 and 45, respectively, at these pressures. Since the optimization of the mass transfer enhancement parameter ( $k$ ) is based on minimizing the sum of squared deviations between the experimental and calculated values, the mechanistic model predictions matched well with the experiments for both the pressures.

**Table 23: Comparison of IFT Measurements with Mechanistic Parachor Model for RKR Fluids at 87 °C and 14.8 MPa**

Enrichment (Mole% C <sub>2+</sub> +CO <sub>2</sub> )	IFT (mN/m)		Weighted Squared Deviation
	Experimental (Rao, 1997)	Mechanistic Parachor Model	
17.79	4.26	3.79	0.0123
21.64	3.89	3.36	0.0184
25.85	3.27	2.88	0.0144
30.57	2.69	2.36	0.0155
33.86	2.13	2.00	0.0035
37.70	1.52	1.61	0.0034
43.07	0.97	1.10	0.0175
48.39	0.53	0.65	0.0535
49.28	0.27	0.63	0.0173
Objective Function ( $\Delta$ ) =			0.1558

**Table 24: Comparison of IFT Measurements with Mechanistic Parachor Model for RKR Fluids at 87 °C and 14.0 MPa**

Enrichment (Mole% C <sub>2+</sub> +CO <sub>2</sub> )	IFT (mN/m)		Weighted Squared Deviation
	Experimental (Rao, 1997)	Mechanistic Parachor Model	
32.68	2.86	2.37	0.0290
37.55	1.89	1.84	0.0007
41.45	1.51	1.43	0.0026
42.61	1.39	1.32	0.0029
47.48	0.70	0.86	0.0518
Objective Function ( $\Delta$ ) =			0.0871

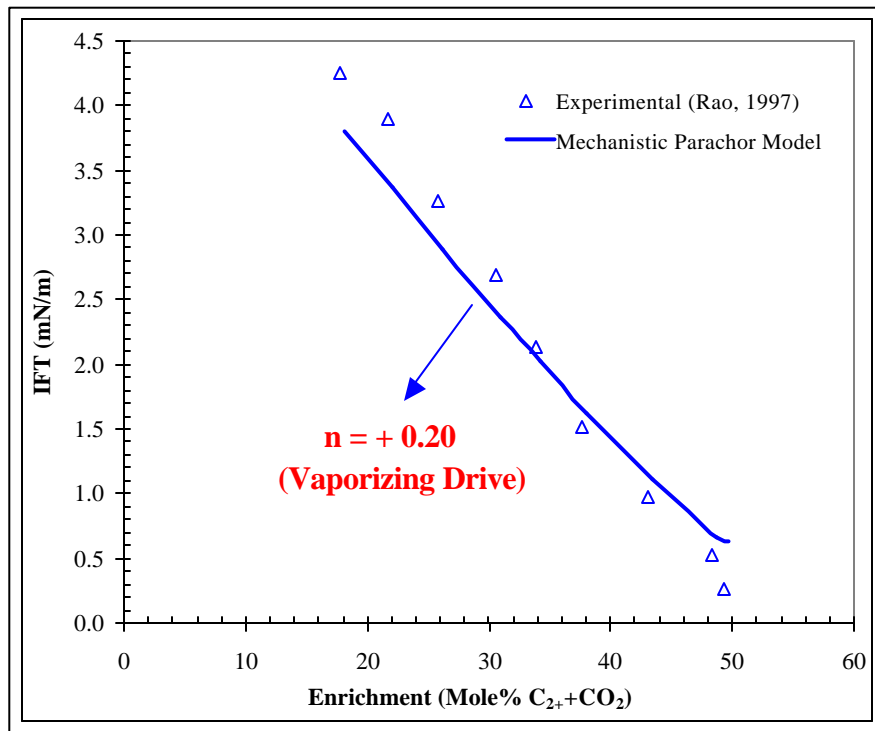


**Figure 44: Comparison between IFT Measurements and Mechanistic Parachor Model for RKR Fluids at 87 °C and 14.8 MPa**

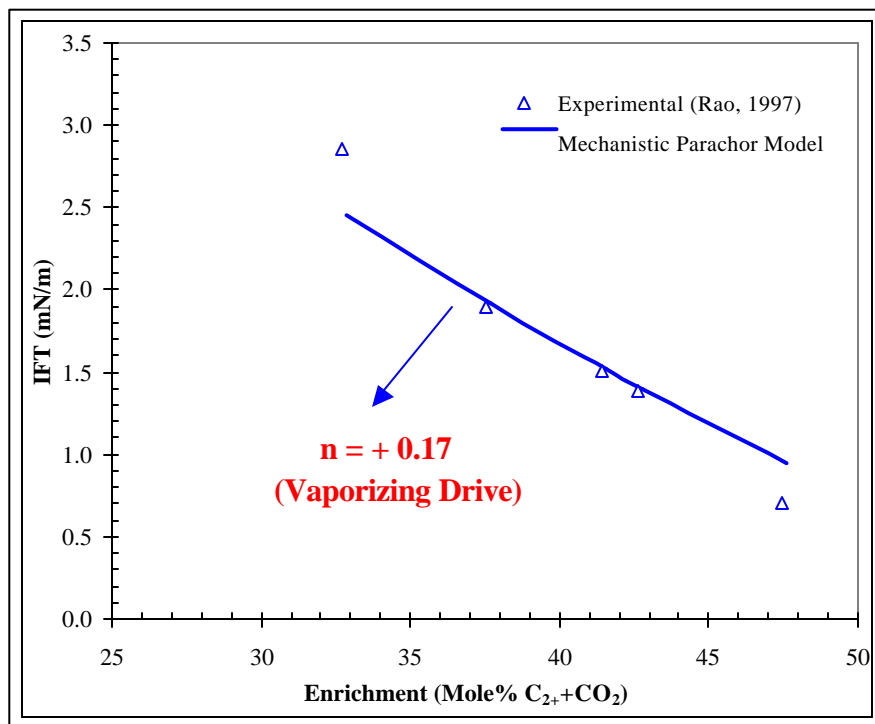


**Figure 45: Comparison between IFT Measurements and Mechanistic Parachor Model for RKR Fluids at 87 °C and 14.0 MPa**

**(b) Terra Nova Reservoir**

The crude oil and gas compositions and the temperature from Rao and Lee [2] are used in IFT computations of these reservoir fluids. IFT measurements, at various  $C_{2+}$  enrichments in hydrocarbon gas, from Rao and Lee [2], are used for comparison with model predictions. A mixture consisting of 8 mole% of crude oil and 92 mole% of gas is used as the feed composition in the calculations in order to match the composition used in experiments.

The comparison of experimental IFT's with original Parachor model predictions at different  $C_{2+}$  enrichments in gas phase and at a pressure of 30 MPa is given in Table 25 and shown in Figure 46.

**Table 25: Comparison of IFT Measurements with Parachor Model for Terra Nova Fluids at 96 °C and 30.0 MPa**

Enrichment (Mole% $C_{2+}+CO_2$ )	IFT (mN/m)		Weighted Squared Deviation
	Experimental (Rao and Lee, 2002)	Parachor Model	
9.49	3.19	0.78	0.5694
11.79	3.09	0.66	0.6204
14.22	2.60	0.58	0.6052
18.57	2.02	0.41	0.6376
24.64	1.07	0.23	0.6147
27.77	0.73	0.15	0.6265
Objective Function ( $\Delta$ ) =			3.6738

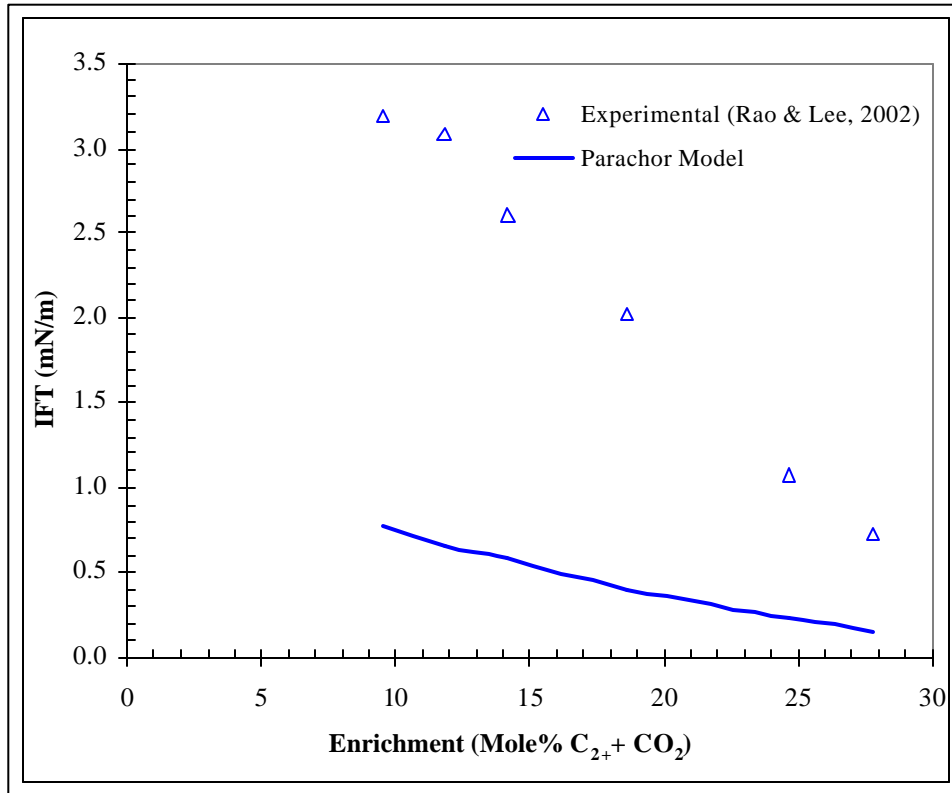


**Figure 46: Comparison between IFT Measurements and Parachor Model for Terra Nova Fluids at 96 °C and 30.0 MPa**

As can be seen in Table 25 and Figure 46, the match between the experiments and the model predictions is very poor and large IFT under-predictions are obtained with the Parachor model. This appears to be mainly due to the absence of mass transfer effects in the Parachor model. Therefore, as before, correction factors are used for Parachor model predictions to minimize the objective function ( $\Delta$ ), the sum of weighted squared deviations between the model predictions and experimental values. The correction factors and the resulting objective functions for this crude oil-gas system are shown in Figure 47. The mass transfer enhancement parameter ( $k$ ), the correction factor at which objective function becomes the minimum, is found to be 4.58.

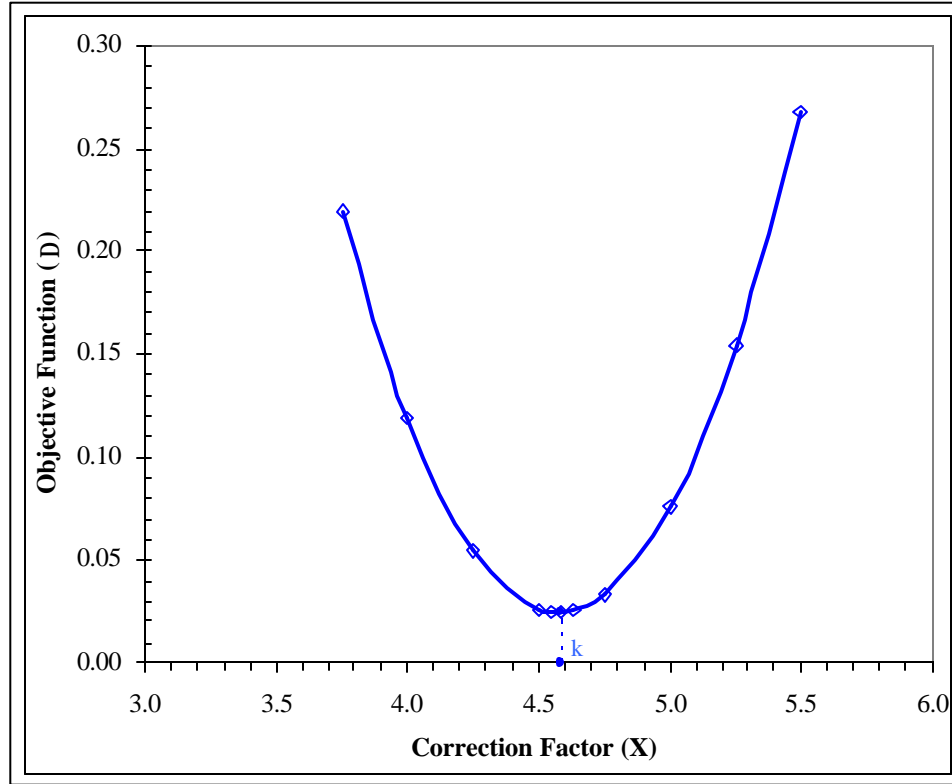


**Figure 47: Determination of Mass Transfer Enhancement Parameter for Terra Nova Reservoir Fluids**

The calculated diffusivities between the fluid phases at different  $C_{2+}$  enrichments in gas phase for Terra Nova fluids at a pressure of 30 MPa are given in Table 26.

**Table 26: Diffusivities between Oil and Gas at Various  $C_{2+}$  Enrichments for Terra Nova Reservoir Fluids at 96° C and 30.0 MPa**

(Mole% $C_{2+} + CO_2$ )	$D_{os}$ (m <sup>2</sup> /s)	$D_{so}$ (m <sup>2</sup> /s)	$D_{os}/D_{so}$
9.49	2.39E-08	7.39E-09	3.23
11.79	2.34E-08	7.14E-09	3.28
14.22	2.32E-08	7.05E-09	3.29
18.57	2.24E-08	6.77E-09	3.31
24.64	2.12E-08	6.44E-09	3.29
27.77	2.04E-08	6.25E-09	3.27
Average =			3.28

As can be seen in Table 26, the mass transfer interactions between the fluids decreased slightly as the  $C_{2+}$  enrichment in gas is increased. However, the ratio of diffusivities between the fluids remains nearly constant irrespective of  $C_{2+}$  enrichment in gas phase. These findings are similar to those observed with RKR reservoir fluids. The average ratio of diffusivities between the fluids at various  $C_{2+}$  enrichments is computed to be 3.28. Using the mass transfer enhancement parameter and the average ratio of diffusivities between the fluid phases in Eq. 43, the exponent (n) characterizing the governing mass transfer mechanism is found to be +1.28. The positive sign of n indicates that even for these reservoir fluids, vaporization of components from the crude oil into the gas phase is the controlling mass transfer mechanism in the combined vaporizing and condensing drive mechanism for attaining the fluid phase equilibria. Furthermore, relatively higher value of n obtained for this reservoir crude oil-gas system compared to RKR reservoir fluids imply more pronounced vaporization mass transfer effects in the Terra Nova reservoir fluids. This can be attributed to the presence of relatively larger amounts of lighter components (56 mole%  $C_1$  to  $C_3$ ) in the Terra Nova crude oil compared to 52 mole%  $C_1$  to  $C_3$  in RKR crude oil [1, 2].

The comparison between the mechanistic Parachor model IFT predictions and the experiments at various  $C_{2+}$  enrichments in gas phase is given in Table 27 and shown in Figure 48 for a pressure of 30 MPa. As expected, an excellent match is obtained between the experiments and the mechanistic model predictions.

**Table 27: Comparison of IFT Measurements with Mechanistic Parachor Model for Terra Nova Fluids at 96 °C and 30.0 MPa**

Enrichment (Mole% C <sub>2+</sub> +CO <sub>2</sub> )	IFT (mN/m)		Weighted Squared Deviation
	Experimental (Rao and Lee, 2002)	Mechanistic Parachor Model	
9.49	3.19	3.59	0.0154
11.79	3.09	3.00	0.0008
14.22	2.60	2.64	0.0003
18.57	2.02	1.86	0.0060
24.64	1.07	1.06	0.0001
27.77	0.73	0.70	0.0020
Objective Function ( $\Delta$ ) =			0.0245

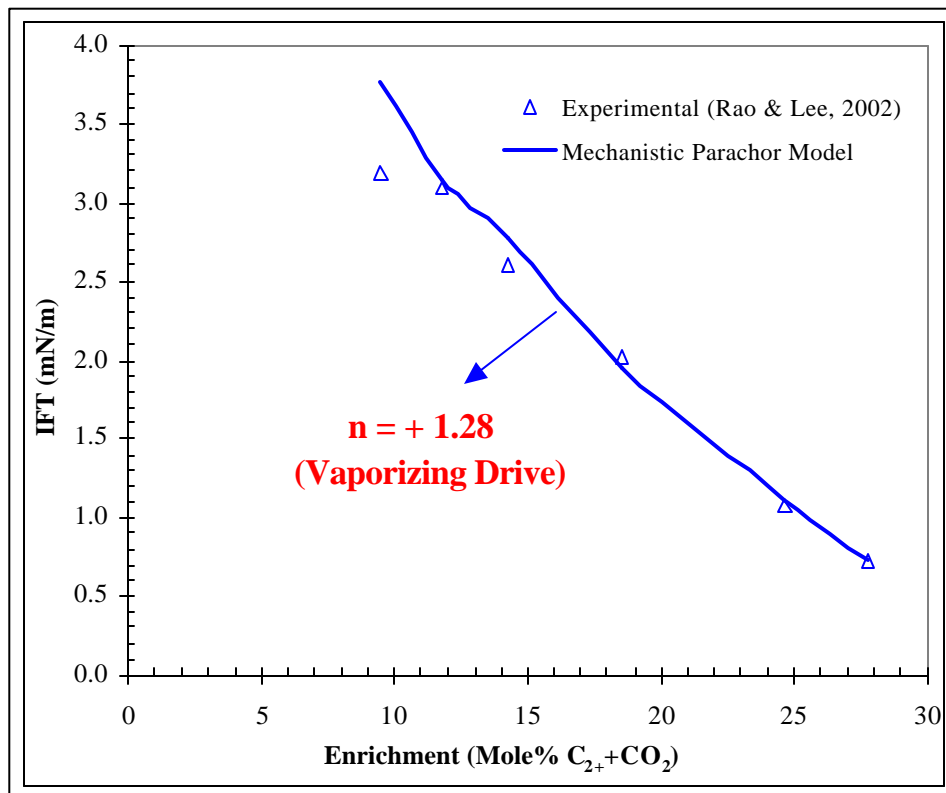


**Figure 48: Comparison between IFT Measurements and Mechanistic Parachor Model for Terra Nova Fluids at 96 °C and 30.0 MPa**

**(c) Schrader Bluff Reservoir**

The crude oil and gas compositions and the temperature and pressures from Sharma et al. [143] are used in IFT calculations of this reservoir. Experimental data on IFT is not available for these reservoir fluids to compare with model predictions. However, the crude oil of this reservoir is experimentally shown to be miscible with the gas mixtures at a minimum miscibility enrichment (MME) of 15 mole% natural gas (NGL) in CO<sub>2</sub>/NGL mixture and 50 mole% NGL in Prudhoe Bay gas (PBG)/NGL mixture at reservoir conditions [143]. Review of literature shows that the zero IFT is a necessary and sufficient condition to attain miscibility [6 – 9]. But, the gas-oil interfacial tension can be measured to a very low value of only about 0.001 mN/m with the available experimental methods [86]. Hence, the interfacial tensions between oil and the gas are presumed to be 0.001 mN/m at the minimum miscibility enrichments of the two gas mixtures for comparison with model predictions. A mixture consisting of 5 mole% of crude oil and 95 mole% of solvent is used as the feed composition in IFT calculations.

The Parachor model IFT predictions for Schrader Bluff crude oil at different NGL enrichments in PBG/NGL solvent is given in Table 28 and shown in Figure 49.

**Table 28: Parachor and Mechanistic Parachor Model IFT Predictions for Schrader Bluff Reservoir Fluids at 82° F and 1300 psi**

(PBG + NGL) Solvents			(CO <sub>2</sub> + NGL) Solvents		
NGL (Mole%)	IFT (mN/m)		IFT (mN/m)		
	Parachor	Mechanistic Parachor	NGL (Mole%)	Parachor	Mechanistic Parachor
0	5.40	0.00124	0	0.197	0.0045
30	4.77	0.00109	10	0.078	0.0018
40	4.72	0.00108	15	0.044	0.0010
50	4.73	0.00108			

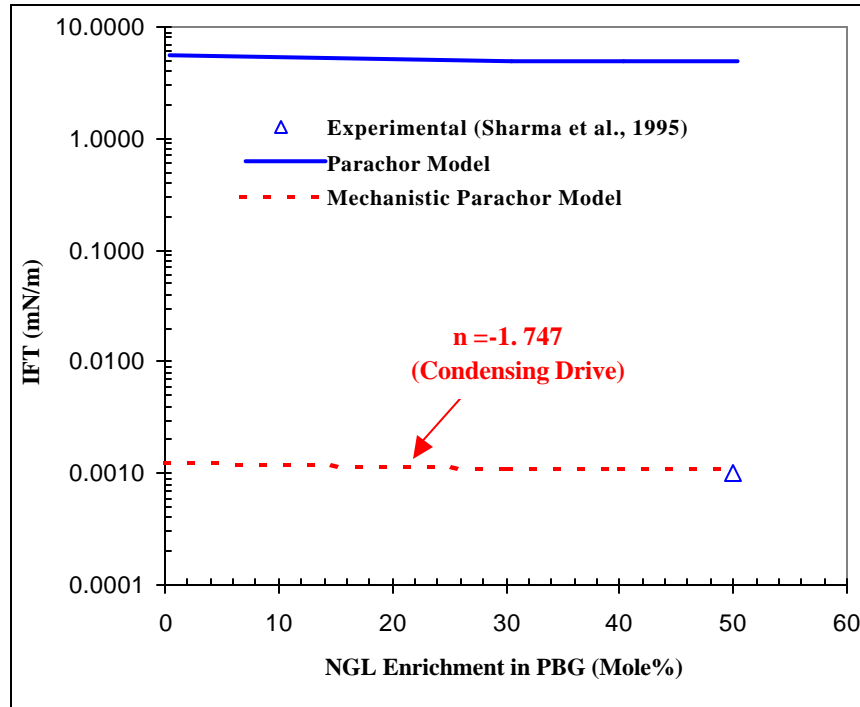


**Figure 49: Comparison of IFT Measurements with Parachor and Mechanistic Parachor Models for Schrader Bluff Crude Oil with (PBG + NGL) Solvents at 82°F and 1300 psi**

As can be seen in Table 28 and Figure 49, the predicted IFT at the MME of 50 mole% NGL in the PBG/NGL solvent is 4.73 mN/m, much higher than the presumed experimental value of 0.001 mN/m at this enrichment. Hence, correction factor (X) is used for Parachor model prediction to determine the mass transfer enhancement parameter (k) as before and is computed to be 0.00023. The computed diffusivities between the fluids at different NGL enrichments in PBG/NGL solvent at reservoir conditions are given in Table 29. The average ratio of diffusivities for all NGL enrichments in PBG/NGL solvent is 120.91 (Table 29). Using the average ratio of diffusivities and the mass transfer enhancement parameter in Eq. 43, the exponent (n) characterizing the governing mass transfer mechanism is determined as  $-1.747$ . The value of n less than zero indicates that the condensation of heavier components from

solvent to oil phase is the controlling mass transfer mechanism in the combined vaporizing and condensing drive mechanism for fluid phase equilibria of these reservoir fluids. The proposed mass transfer enhanced mechanistic model IFT predictions for this crude oil-solvent system at different NGL enrichments in solvent are shown in Table 28 and Figure 49.

**Table 29: Diffusivities between Oil and Solvent at Various NGL Enrichments in Solvent for Schrader Bluff Reservoir Fluids at 82°F and 1300 psi**

(PBG + NGL) Solvents				(CO <sub>2</sub> + NGL) Solvents			
NGL (Mole%)	D <sub>os</sub> (m <sup>2</sup> /s)	D <sub>so</sub> (m <sup>2</sup> /s)	D <sub>os</sub> /D <sub>so</sub>	NGL (Mole%)	D <sub>os</sub> (m <sup>2</sup> /s)	D <sub>so</sub> (m <sup>2</sup> /s)	D <sub>os</sub> /D <sub>so</sub>
0	2.05E-08	9.38E-11	218.38	0	7.57E-09	1.05E-10	72.42
30	8.75E-09	8.25E-11	106.09	10	6.47E-09	8.97E-11	72.15
40	5.51E-09	6.37E-11	86.47	15	5.94E-09	8.41E-11	70.67
50	5.19E-09	7.15E-11	72.69				
Average			120.91	Average			71.75

The Parachor model IFT predictions for Schrader Bluff crude oil at different NGL enrichments in CO<sub>2</sub>/NGL solvent is given in Table 28 and shown in Figure 50. As can be seen in Table 28 and Figure 50, the predicted IFT at the MME of 15 mole% NGL in CO<sub>2</sub>/NGL solvent is 0.044 mN/m, higher than the experimental value of 0.001 mN/m at this enrichment. Hence, as done before, correction factor (X) is used for Parachor model prediction to compute the mass transfer enhancement parameter (k) and is determined to be 0.023. The calculated diffusivities between the fluid phases at different NGL enrichments in CO<sub>2</sub>/NGL solvent at reservoir conditions are given in Table 29. The average ratio of diffusivities for all NGL enrichments in CO<sub>2</sub>/NGL solvent is 71.75

(Table 29). Using the average ratio of diffusivities and the mass transfer enhancement parameter in Eq. 43, the exponent ( $n$ ) characterizing the mass transfer mechanism is computed as  $-0.883$ . The negative sign of  $n$  indicates that the condensation of heavier components from solvent to oil phase is the governing mass transfer mechanism in the combined vaporizing and condensing drive mechanism for the attainment of fluid phase equilibria of these fluids. The proposed mechanistic Parachor model IFT predictions for this crude oil-solvent system at different NGL enrichments in solvent are given in Table 28 and shown in Figure 50.

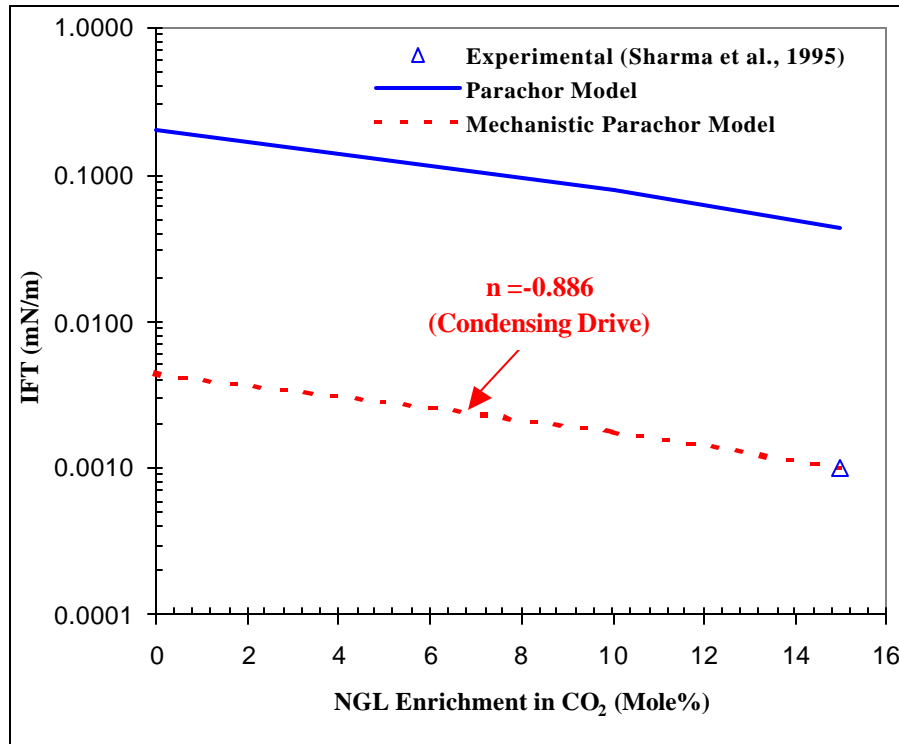


**Figure 50: Comparison of IFT Measurements with Parachor and Mechanistic Parachor Models for Schrader Bluff Crude Oil with (CO<sub>2</sub> + NGL) Solvents at 82°F and 1300 psi**

The governing mass transfer mechanism of condensation as identified by the proposed mechanistic model for fluid phase equilibria of Schrader Bluff fluids is

substantiated by the presence of only limited amount of lighter components i.e. 26.64 mole%  $C_1$  to  $C_2$  in the crude oil of this reservoir [143]. Furthermore, relatively higher absolute value of exponent (n) in the proposed mechanistic model for crude oil-solvent system with PBG/NGL solvents, when compared to that with  $CO_2$ /NGL solvents indicate more pronounced condensation mass transfer effects in the crude oil-solvent system containing PBG/NGL solvents. This can be attributed to the presence of relatively larger amounts of heavier components in PBG/NGL solvents when compared to  $CO_2$ /NGL solvents [143].

#### 4.5.3 Application of the Proposed Mechanistic Model to Crude Oil Systems

The proposed mechanistic Parachor model has been further extended to three more reservoir crude oil systems namely crude oil A, crude oil C and crude oil D. The crude oil compositions and the experimentally measured interfacial tensions between the equilibrium vapor and liquid phases of these crude oils at different pressures and at reservoir temperature from Firoozabadi et al. [69] are used for comparison with the proposed model predictions.

These three crude oils were from different reservoirs with gravities ranging from 31 to 35° API (0.87 to 0.85 gm/cc). The key physical characteristics of the crude oils used are described in Table 30.

**Table 30: Physical Properties of Crude Oils Used**

Crude Oil	Saturation Pressure (psi)	Temperature (°F)	( $C_1$ - $C_3$ ) Mole%	$C_{7+}$ M.wt	$C_{7+}$ Sp.gravity
A	2155	130	46.52	227.4	0.870
C	4589	180	64.64	217.0	0.838
D	2573	170	51.18	234.3	0.868

From the Table 30, it can be seen that the crude oil C is the lightest when compared to the other two crude oils A and D, as it has higher  $C_1$ - $C_3$  molar composition and lower  $C_{7+}$  molecular weight.

The comparison of the experimental IFT measurements with the original Parachor model and the proposed mechanistic model IFT predictions are shown in Tables 31-33 and Figures 51-53 respectively, for crude oil A, crude oil C and crude oil D.

**Table 31: Comparison of IFT Measurements with Parachor and Mechanistic Parachor Model Predictions for Crude Oil A**

Pressure (psia)	Exp. IFT (mN/m)	Parachor Model		Mechanistic Parachor Model	
		IFT (mN/m)	Abs. Dev. (%)	IFT (mN/m)	Abs. Dev. (%)
2150	5.5	3.03	44.91	4.76	13.50
1650	6.7	4.61	31.19	7.24	8.02
1150	10.1	6.73	33.37	10.57	4.61
185	19.5	12.16	37.64	19.09	2.09
Average			36.78		7.06

**Table 32: Comparison of IFT Measurements with Parachor and Mechanistic Parachor Model Predictions for Crude Oil C**

Pressure (psia)	Exp. IFT (mN/m)	Parachor Model		Mechanistic Parachor Model	
		IFT (mN/m)	Abs. Dev. (%)	IFT (mN/m)	Abs. Dev. (%)
3815	1.3	0.54	58.62	1.25	3.98
3315	2.3	0.89	61.48	2.06	10.62
2815	3.3	1.42	56.97	3.29	0.16
2315	4.6	2.23	51.52	5.17	12.46
Average			57.15		6.81

**Table 33: Comparison of IFT Measurements with Parachor and Mechanistic Parachor Model Predictions for Crude Oil D**

Pressure (psia)	Exp. IFT (mN/m)	Parachor Model		Mechanistic Parachor Model	
		IFT (mN/m)	Abs. Dev. (%)	IFT (mN/m)	Abs. Dev. (%)
2010	6.0	2.73	54.50	5.26	12.33
1610	8.5	4.16	51.06	8.01	5.76
1110	10.3	6.08	40.97	11.70	13.63
Average			48.84		10.57

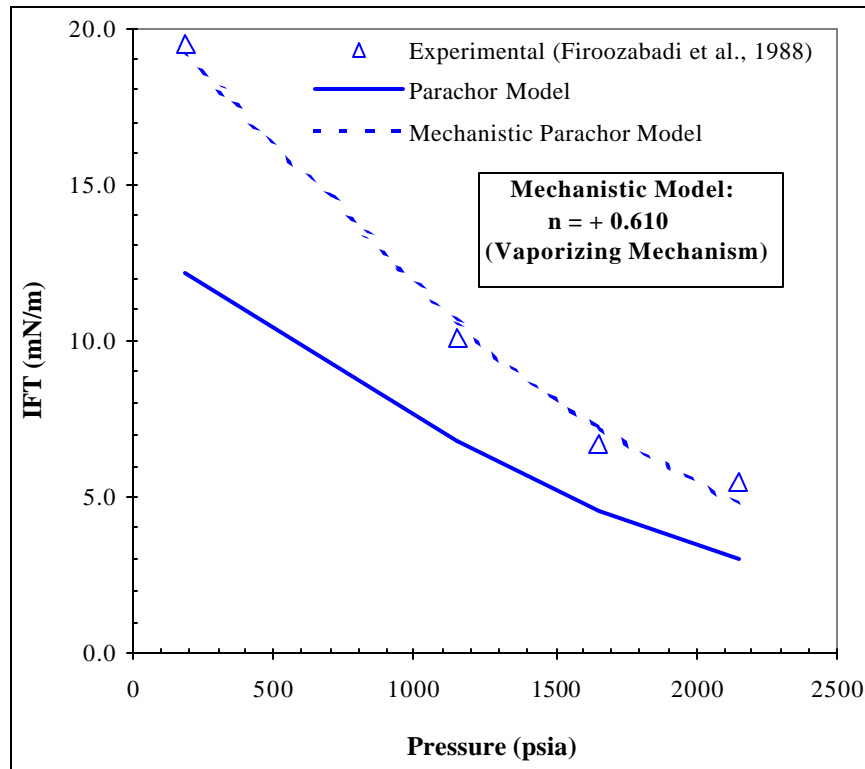


**Figure 51: Comparison of IFT Measurements with Parachor and Mechanistic Parachor Model Predictions for Crude Oil A**

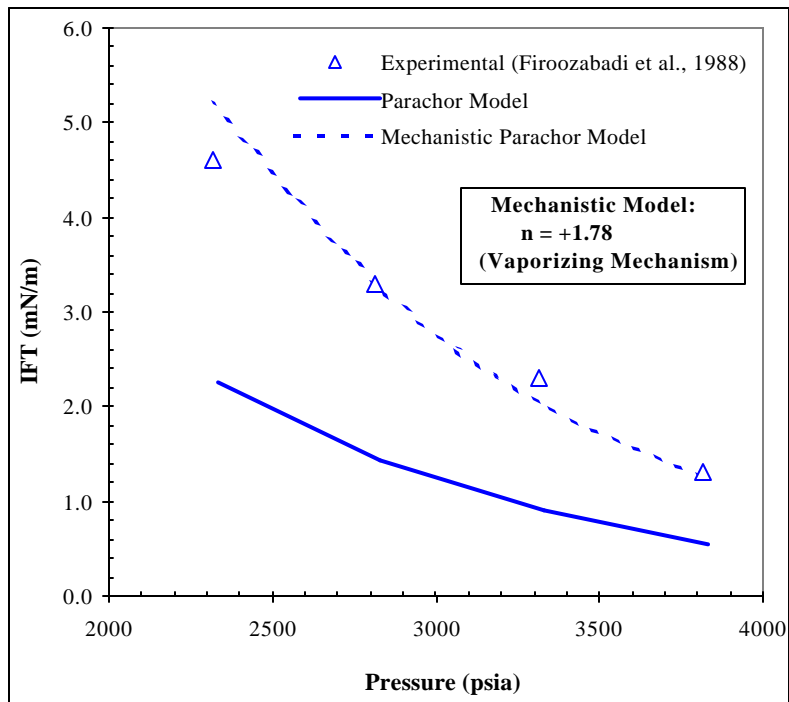


**Figure 52: Comparison of IFT Measurements with Parachor and Mechanistic Parachor Model Predictions for Crude Oil C**

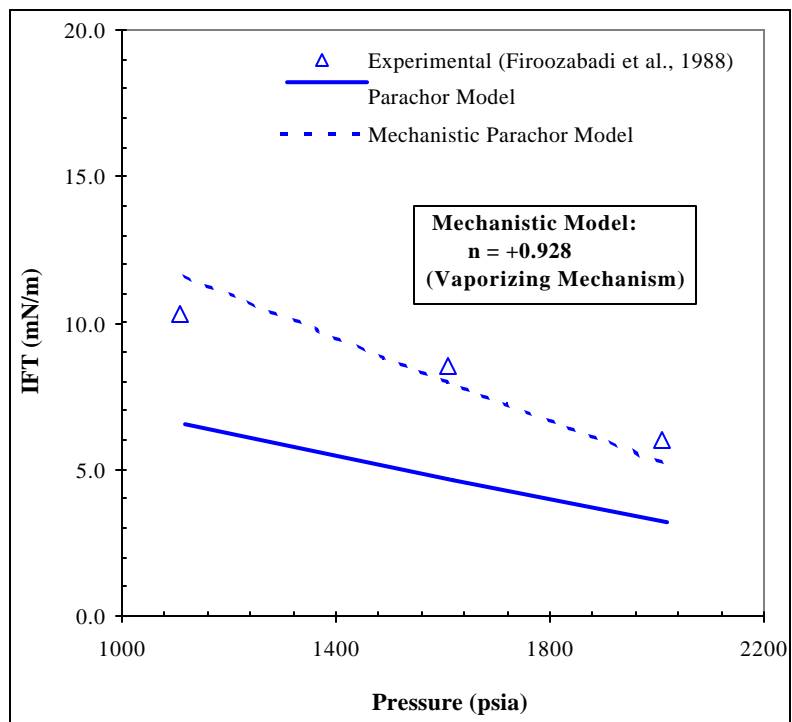


**Figure 53: Comparison of IFT Measurements with Parachor and Mechanistic Parachor Model Predictions for Crude Oil D**

From the Tables 31-33 and Figures 51-53, it can be seen that the match between the experiments and the original Parachor model is poor and significant IFT under-predictions are obtained with Parachor model for all the three crude oil systems studied. The average absolute deviations between the Parachor model and the experimental data for the three crude oils ranged from 36.8% to 57.2%. Contrarily, excellent match between the proposed mechanistic model and the experimental data can be seen for the three crude oil systems considered. The average absolute deviations ranging from 6.8% to 10.6% are obtained between the proposed mechanistic model and the experiments for all the three crude oil systems.

The exponents of +0.61, +1.78, and +0.928 are obtained in the proposed mechanistic model for crude oils A, C and D, respectively to best fit the experimental data. The positive exponents in the mechanistic model indicate that vaporization of lighter components ( $C_1$ - $C_3$ ) from crude oil is the governing mass transfer mechanism for the attainment of fluid phase equilibria between the equilibrium liquid and vapor phases of these crude oils. This is substantiated by the fact that these three crude oil systems contain only crude oil in the feed and hence the vaporization of lighter components from the crude oil is responsible for forming the equilibrium vapor phase.

#### **4.5.4 Sensitivity Studies on Proposed Mechanistic Parachor Model**

Sensitivity studies were carried out for RKR and Terra Nova reservoir fluids to determine the effect of number of experimental IFT measurement data points on the proposed mechanistic model results. The exponents obtained by using different single experimental IFT measurements in the mechanistic model are shown in Table 34 and Table 35 for RKR and Terra Nova reservoir fluids, respectively. The comparison of IFT

predictions from the mechanistic model obtained by using three different single IFT measurements namely high IFT, medium IFT and low IFT with the original Parachor model and the mechanistic model with all the available IFT experimental data are shown in Figures 54 and 55 for RKR and Terra Nova fluids, respectively.

**Table 34: Model Exponents for Different Single Experimental IFT Measurement Points in the Mechanistic Parachor Model for RKR Fluids at 14.8 MPa**

Enrichment ( $C_{2+}$ %)	IFT (mN/m)			C.F (k)	$D_{os}/D_{so}$	n
	Experimental	Parachor	Mechanistic Parachor			
17.79	4.26	2.910	4.26	1.46	3.56	0.30
21.64	3.89	2.590	3.89	1.50	3.68	0.31
25.85	3.27	2.210	3.27	1.47	3.75	0.29
30.57	2.69	1.810	2.69	1.48	3.81	0.29
33.86	2.13	1.540	2.13	1.39	3.82	0.25
37.70	1.52	1.240	1.52	1.23	3.80	0.16
43.07	0.97	0.850	0.97	1.15	3.73	0.11
48.39	0.53	0.500	0.53	1.10	3.61	0.07

**Table 35: Model Exponents for Different Single Experimental IFT Measurement Points in the Mechanistic Parachor Model for Terra Nova Fluids at 30.0 MPa**

Enrichment ( $C_{2+}$ %)	IFT (mN/m)			C.F (k)	$D_{os}/D_{so}$	n
	Experimental	Parachor	Mechanistic Parachor			
9.49	3.19	0.783	3.19	4.08	3.23	1.20
11.79	3.09	0.656	3.09	4.71	3.28	1.30
14.22	2.60	0.577	2.60	4.51	3.29	1.27
18.57	2.02	0.407	2.02	4.97	3.31	1.34
24.64	1.07	0.231	1.07	4.63	3.29	1.29
27.77	0.73	0.152	0.73	4.80	3.27	1.33

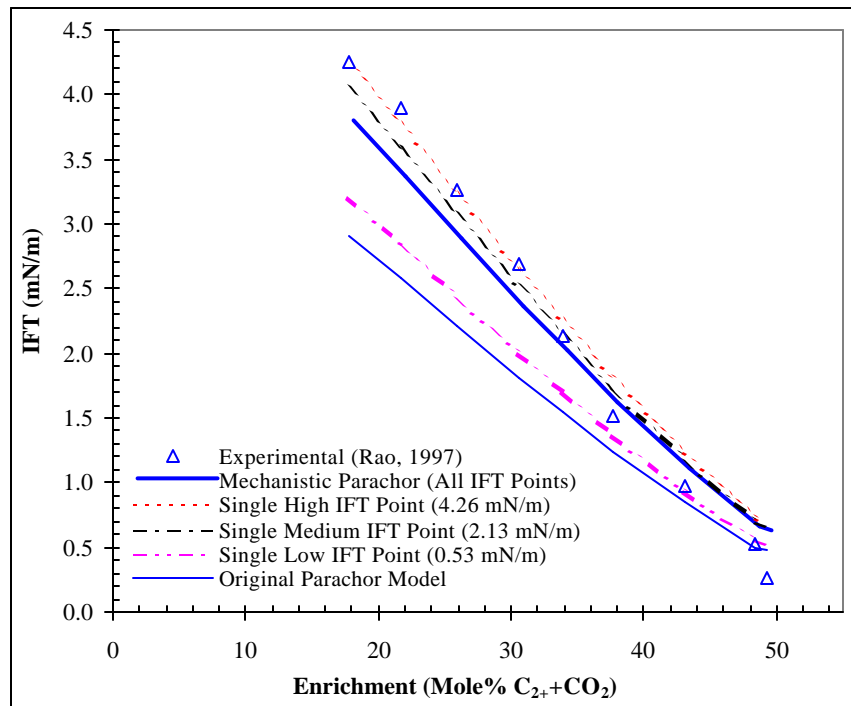


**Figure 54: Sensitivity Studies for the Effect of Number of Experimental Data Points on Mechanistic Model Results for RKR Fluids at 87° C and 14.8 MPa**

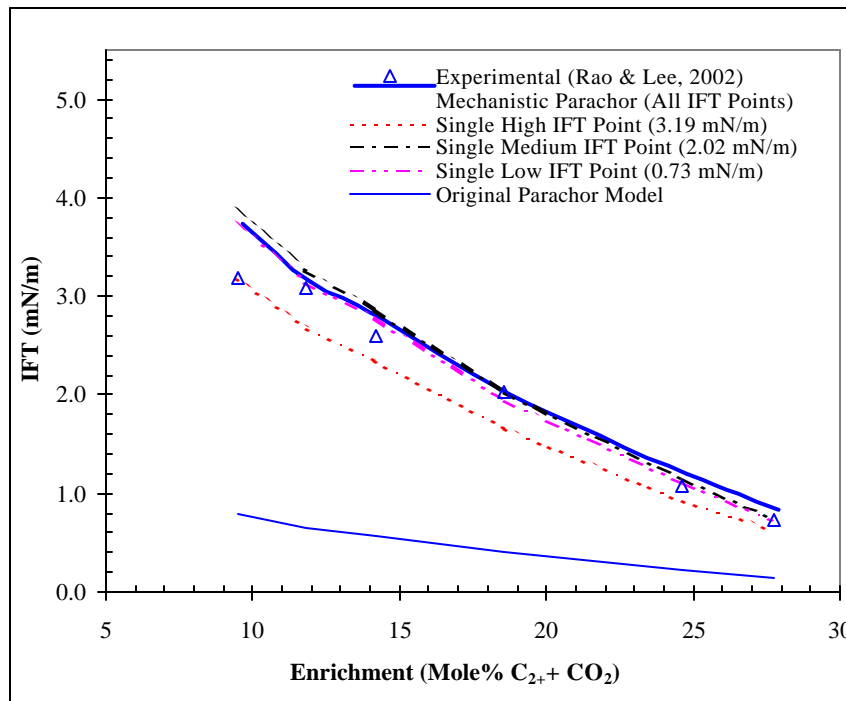


**Figure 55: Sensitivity Studies for the Effect of Number of Experimental Data Points on Mechanistic Model Results for Terra Nova Fluids at 96° C and 30.0 MPa**

From Figure 54 for RKR fluids, it can be seen that there are no significant differences among the mechanistic model IFT predictions using single high and medium IFT measurement points and all the IFT experimental data in the mechanistic model. However, the use of low single IFT measurement point in the mechanistic model resulted in significantly deviating IFT values when compared to the mechanistic model with all the experimental points. It can be further observed that even the provision of single low IFT measurement point as input to the mechanistic model yielded better IFT predictions compared to original Parachor model. Similar results can be seen even for Terra Nova fluids. From Figure 55 for Terra Nova fluids, it can be seen that the provisions of single high, medium and low IFT measurement points as well as all the experimental data in the mechanistic model resulted in almost similar IFT predictions. The IFT predictions from all these combinations matched extremely well with experiments when compared to original Parachor model. Based on these observations, it can be concluded that the provision of a single high or medium experimental IFT measurement in the proposed mechanistic model is sufficient for reasonable IFT predictions from the model. Thus, the mechanistic model IFT predictions with a single experimental IFT measurement of medium or high IFT range can be used to determine fluid-fluid miscibility conditions using the proposed mechanistic model.

#### **4.5.5 Generalized Regression Models for Mechanistic Model Exponent Prediction**

Interestingly, the exponent ( $n$ ) in the proposed mechanistic model exhibits similar characteristics as Parachor, which can be seen in the discussion on Parachor physics and thermodynamics provided in Section 2.7.3.1. The exponent is specific for a crude oil (equilibrium liquid and vapor phases) or crude oil-solvent system. It is independent of

pressure (as can be seen in Figures 51 - 53). The exponent appears to be independent of temperature, although this needs to be still verified with experiments. Based on these observations, like for the Parachor, a linear relationship between the exponent and solute composition is hypothesized. For testing this hypothesis, crude oil-solvent (Terra Nova and RKR fluids) and crude oil (crude oils A, C and D) systems have been used.

In crude oil-solvent systems such as RKR and Terra Nova fluids, simultaneous counter-directional mass transfer interactions occur from both the oil and solvent (gas) phases. These include vaporization of lighter components ( $C_1-C_3$ ) from crude oil phase to solvent (gas) phase and condensation of intermediate to heavier components ( $C_4-C_{7+}$ ) from the solvent (gas) phase to crude oil phase.  $CO_2$  has also been included in these models, as it is the active component involved in both the mechanisms of vaporization from crude oil and condensation from the injection gas. Therefore, the compositions of ( $C_1-C_3 + CO_2$ ) in crude oil and ( $C_4-C_{7+} + CO_2$ ) in gas constitute the solute composition. These compositions are normalized as a molar ratio:  $(C_1-C_3 + CO_2) / (C_4-C_{7+})$  in crude oil to represent vaporizing drive mechanism from the oil and  $(C_4-C_{7+} + CO_2) / (C_1-C_3)$  in gas phase to represent condensing drive mechanism from the gas. The mechanistic model exponents for the two crude oil-solvent systems of RKR and Terra Nova are now related to the normalized solute compositions using multiple regression analysis. The results are summarized in Figure 56.

From Figure 56, it can be seen that a good linear relationship between the exponent and the normalized solute compositions is obtained for the two crude oil-solvent systems with a multiple determination coefficient ( $R^2$ ) of 0.984. The regression model obtained for predicting the exponent ( $n$ ) values is also shown in Figure 56.

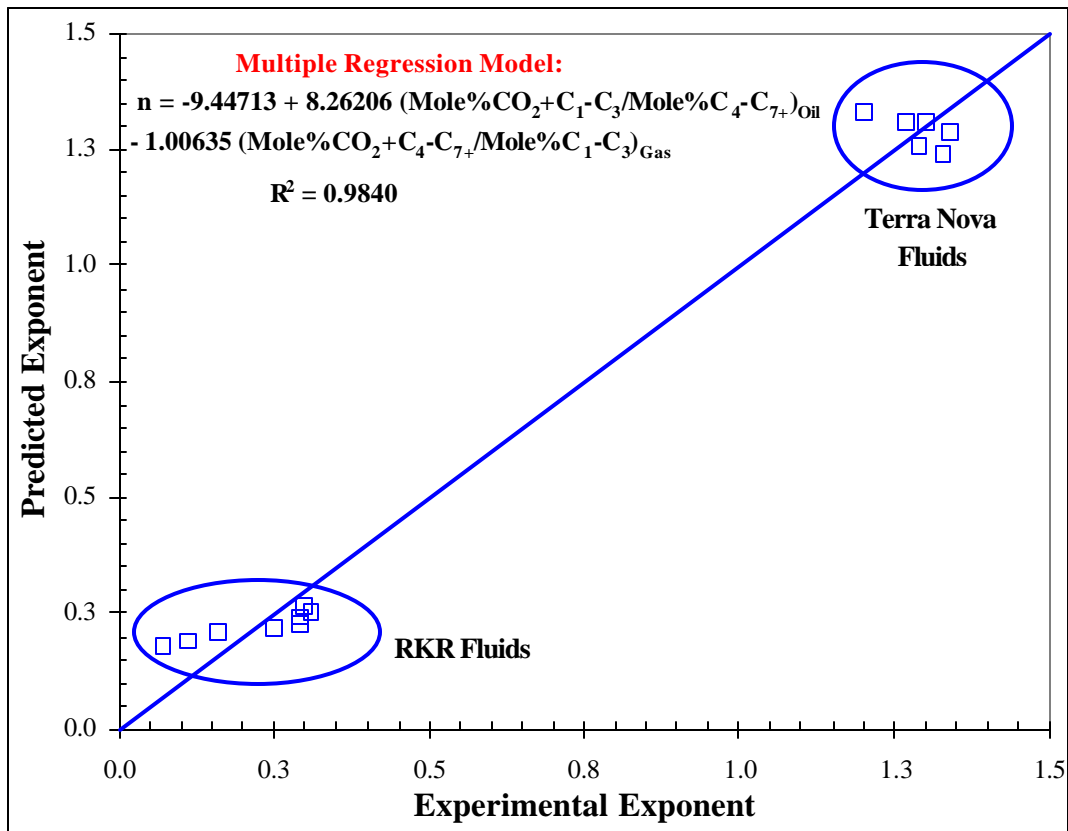


**Figure 56: Multiple Linear Regression Model for the Mechanistic Model Exponent Prediction in Crude Oil-Solvent Systems**

Higher absolute value of the slope for vaporizing drive mechanism (8.262) when compared to condensing drive mechanism (1.006) in the regression model indicates that the vaporization of lighter components from crude oil to gas phase is the governing mass transfer mechanism for the attainment of fluid phase equilibria between the vapor and liquid phases of these two crude oil-solvent systems. This regression model can be used for *a-priori* estimation of exponent (n) in the mechanistic model for crude oil-solvent systems. Thus, the exponent (n) in the mechanistic model can be simply determined by using the compositions of crude oil and solvent and thereby completely eliminating the need for even a single experimental IFT data in the proposed mechanistic model. Although this regression model incorporates both the mechanisms of vaporization and

condensation, the correlation obtained is based on the systems where vaporization mechanism is dominant and hence this model is applicable mainly to vaporizing drive crude oil-gas systems.

In crude oil systems such as crude oils A, C and D, the equilibrium vapor phase is formed primarily due to vaporization of lighter components ( $C_1-C_3$ ) from crude oil. Therefore, the composition of lighter ends ( $C_1-C_3$ ) in the crude oil constitutes the solute composition.  $CO_2$  in crude oil has also been included, as it can be considered as an active component involved in the vaporization process. Hence the mechanistic model exponents for these three crude oil systems are related to the normalized solute composition  $(C_1-C_3 + CO_2)/(C_4-C_{7+})$  in the crude oil, using regression analysis. The results are shown in Figure 57. As before for the crude oil-solvent systems, a good linear relationship between the exponent and the normalized solute composition can be seen even in this case with a determination coefficient ( $R^2$ ) of 0.965. The regression equation obtained is shown in Figure 57. This regression equation can be used for *a-priori* prediction of exponent ( $n$ ) in the mechanistic model for crude oil systems simply by knowing the composition of crude oil, without fitting any experimental data.

Therefore, it can be concluded that Parachor and the exponent ( $n$ ) in the mechanistic model have similar characteristics. Thus this interesting feature observed during the course of this study has been well utilized to develop generalized regression models for the mechanistic model exponent prediction by simply knowing the compositional data of reservoir fluids, without using any experimental IFT data. The summary of similarities observed in the characteristics between the exponent ( $n$ ) and the Parachor are shown in Table 36.

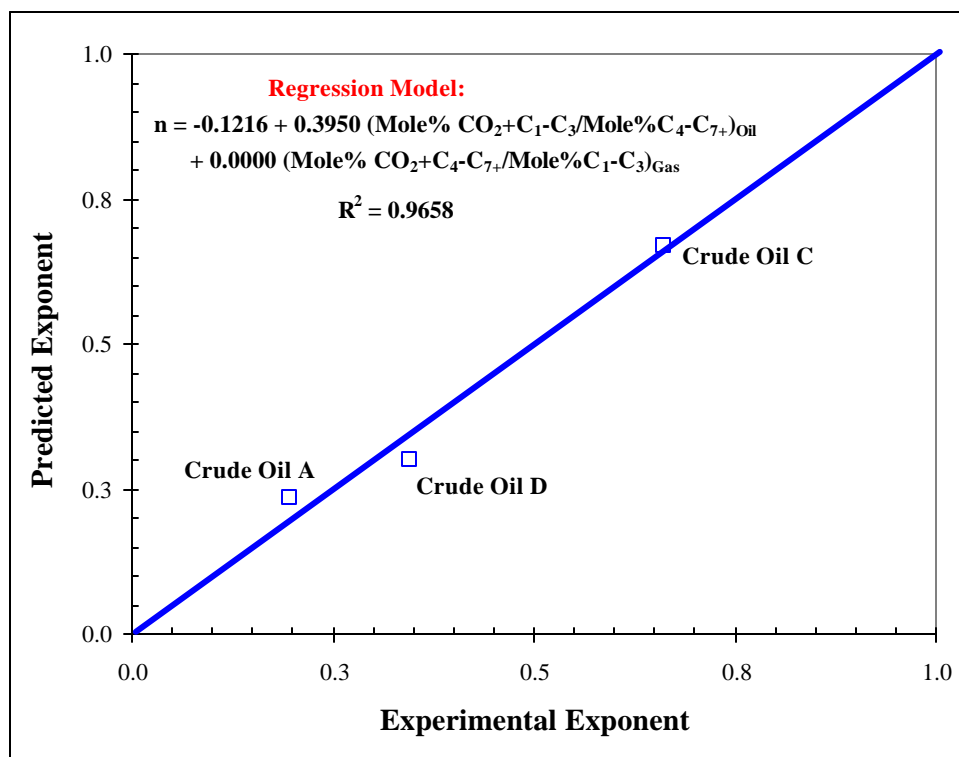


**Figure 57: Simple Linear Regression Model for the Mechanistic Model Exponent Prediction in Crude Oil Systems**

**Table 36: Summary of Similarities Observed between the Exponent in the Mechanistic Model and the Parachor**

S.No	Parachor	Exponent (n)
1	Compound specific	Specific for a crude oil (equilibrium liquid and vapor phases) or crude oil-solvent system
2	Independent of temperature	Appears to be temperature independent and still needs to be examined
3	Independent of pressure	Independent of pressure
4	Linearly related to solute concentration	Linearly related to solute composition present in either of the two fluid phases in equilibrium

#### 4.5.6 Validation of Generalized Regression Models for Exponent Prediction

The proposed generalized regression models were now utilized to predict the exponents in the mechanistic model and consequently interfacial tension for Prudhoe Bay

reservoir fluids for validation. The experimental IFT data on Prudhoe Bay fluids at 200° F from Dorshow [144] were used for comparison with the results from the proposed regression models.

**(a) Prudhoe Bay Crude Oil - Solvent System**

A feed composition of 65 mole% of crude oil and 35 mole% of solvent was used in IFT calculations to match the composition used in the experiments. A mechanistic model exponent of 0.699 is obtained for Prudhoe Bay crude oil - solvent system by using the compositional data of reservoir fluids in the proposed generalized regression model of crude oil-solvent systems. This exponent calculated using the regression model deviated by only about 9.9% from the mechanistic model exponent of 0.636 obtained by using all the available IFT experimental data.

The comparison of the IFT measurements with the predictions of Parachor model and mechanistic Parachor model with the exponent calculated using the compositional data of reservoir fluids is shown in Figure 58. The mechanistic Parachor model IFT predictions with the exponent obtained by fitting all the experimental IFT data are also shown in Figure 58 for better comparison.

From Figure 58, it can be seen that IFT under-predictions are obtained with original Parachor model. However, better match of IFT predictions with experiments can be seen with both the mechanistic Parachor models. Moreover, the IFT predictions from the mechanistic model for both the exponents used are almost similar. Therefore, this validates the proposed regression model to predict the exponent in the mechanistic model without using even a single IFT measurement in the mechanistic Parachor model.

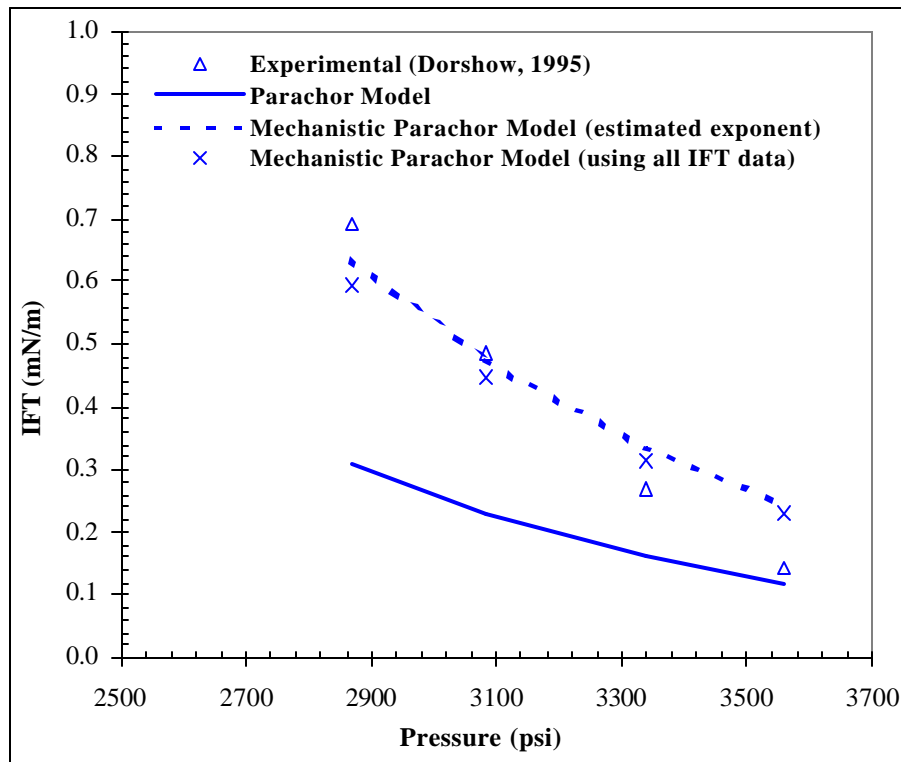


**Figure 58: Validation of the Generalized Regression Model for Exponent Prediction in Prudhoe Bay Crude Oil - Solvent System**

**(b) Prudhoe Bay Crude Oil System**

A mechanistic model exponent of 0.380 is obtained by using the compositional data of reservoir fluids in the proposed generalized regression model of crude oil systems for this case. This exponent calculated using the regression model deviated by only about 6.1% from the mechanistic model exponent of 0.405 obtained by fitting all the available IFT experimental data.

The comparison of the IFT measurements with the predictions of Parachor model and mechanistic Parachor model with both the exponents calculated using the reservoir fluids compositional data as well as all the available IFT experimental data is shown in Figure 59.

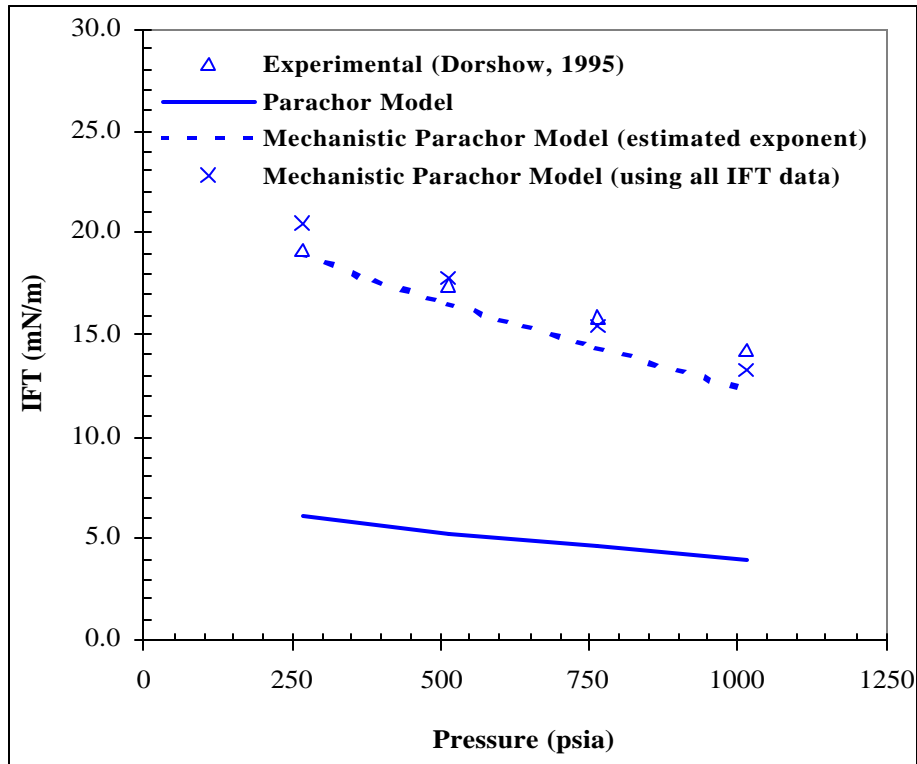


**Figure 59: Validation of the Generalized Regression Model for Exponent Prediction in Prudhoe Bay Crude Oil System**

From Figure 59, significant IFT under-predictions can be seen with Parachor model when compared to the experiments. However, an excellent match of IFT predictions with experiments is obtained with both the mechanistic Parachor models. Furthermore, almost similar IFT predictions can be seen from the mechanistic model for both the exponents used. Therefore, this validates the proposed regression model to predict the exponent in the mechanistic model without fitting any experimental IFT data.

#### **4.5.7 Prediction of Dynamic Gas-Oil Miscibility Using the Mechanistic Model**

The proposed mechanistic Parachor model can be used to predict dynamic interfacial tension in multicomponent crude oil-gas systems simply either by using the compositional data of reservoir fluids or a single gas-oil interfacial tension measurement.

The interfacial tension predictions from the proposed mechanistic model can be then plotted against solvent enrichment or pressure and the extrapolation of the plot to zero interfacial tension can be used to infer dynamic gas-oil miscibility. In addition, if the measured data are available, then the model also provides information on governing mass transfer mechanism responsible for dynamic gas-oil miscibility development. However, the proposed regression model for the exponent prediction in the mechanistic Parachor model for crude oil-gas systems is applicable mainly to vaporizing drive systems, where vaporization of lighter components from crude oil to gas are mainly responsible for gas-oil miscibility development. Such vaporizing drive mechanisms for gas-oil miscibility development are widely believed to be associated with lighter crude oils. Therefore, the proposed mechanistic model has immense application for gas-oil miscibility prediction in light oil reservoirs, where miscible gas injection applications are most widely practiced for improved oil recovery. Thus, the IFT's from the proposed mechanistic model can be used to predict the gas-oil miscibility of the most popular gas injection EOR field projects.

The IFT measurements in heavy crude oil-gas systems are rarely reported and hence development of generalized regression model for exponent prediction in condensing drive systems has not been attempted. Therefore, IFT measurements with heavy crude oil-gas systems are recommended to develop such generalized models in future. Although thermal EOR processes (steam injection) are still considered to be the most effective means of improved oil recovery in heavy oil reservoirs, the high costs associated with steam generation indicate better economic prospects for the applicability of miscible gas injection in light to medium heavy crude oil reservoirs.

#### **4.6 Modeling of Dynamic Gas-Oil Interfacial Tension and Miscibility in Standard Gas-Oil Systems at Elevated Pressures and Temperatures**

The interfacial tension measurements in standard gas-oil systems of n-decane-CO<sub>2</sub> and synthetic live oil mixture-CO<sub>2</sub> at elevated pressures and temperatures reported in Section 4.2 were now modeled using the Parachor and newly proposed mechanistic Parachor models. Since the IFT's were shown to be independent of gas-oil ratio near equilibrium, IFT measurements reported at a gas-oil ratio of 80/20 mole% gas and oil were used for modeling purpose in both the standard gas-oil systems.

The fluid phase compositions for gas-oil IFT modeling were obtained by performing flash calculations with the commercial simulator Winprop [124] using the QNSS/Newton algorithm [132] and PR-EOS [17]. The measured densities of the fluid phases and the pure component Parachor values reported in literature [81 - 84] were used for IFT calculations. The gas-oil interfacial tension modeling results obtained in both the standard gas-oil systems are summarized below.

##### **4.6.1 n-Decane -CO<sub>2</sub> System at 100° F**

The comparison between the IFT predictions from the Parachor model and the experiments at various pressures is given in Table 37. The results are also shown in Figure 60. As can be seen in Table 37 and Figure 60, a good match between the experiments and the model predictions is obtained with the Parachor model. This agrees well with the previous reports that the Parachor model predicts IFT reasonably well in binary mixtures [85, 87]. The good match of experimental IFT's with Parachor model indicates an exponent of zero in the proposed mechanistic Parachor model. The zero value for the exponent in the mechanistic model suggests equal proportions of vaporizing

and condensing drive mechanisms in the combined vaporizing and condensing drive mechanism for gas-oil miscibility development in this standard gas-oil system.

**Table 37: Comparison of IFT Measurements with Parachor Model in n-Decane-CO<sub>2</sub> System at 100° F**

Pressure (psi)	IFT (mN/m)	
	Experimental	Parachor Model
0	22.45	22.21
200	20.13	19.90
400	16.24	16.10
600	10.27	10.10
800	6.07	5.96
1000	3.34	3.21
1100	0.33	0.13

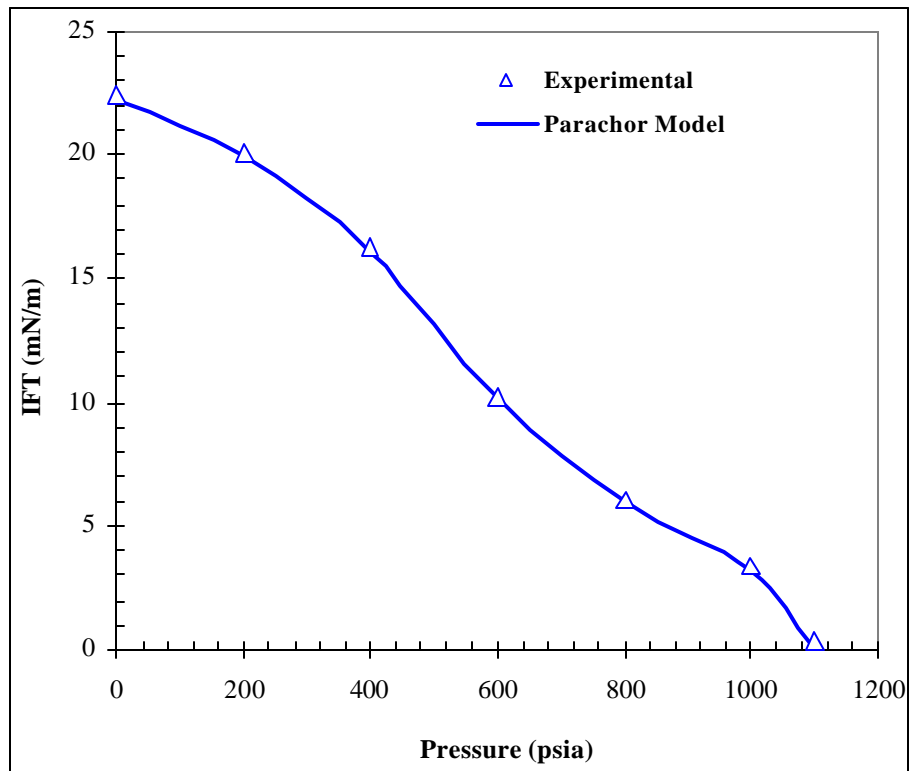


**Figure 60: Comparison of IFT Measurements with Parachor Model in n-Decane-CO<sub>2</sub> System at 100° F**

#### 4.6.2 Synthetic Live Oil-CO<sub>2</sub> System at 160° F

The dynamic nature of IFT measurements in this system has been discussed earlier in Section 4.2.5. The comparison between the IFT predictions from the Parachor model and the dynamic interfacial tension measurements at various pressures is given in Table 38 and shown in Figure 61 for this standard gas-oil system at 160° F.

**Table 38: Comparison of IFT Measurements with Parachor Model in Synthetic Live Oil – CO<sub>2</sub> System at 160° F**

Pressure (psi)	IFT (mN/m)		Weighted Square Dev.
	Experimental	Parachor Model	
1100	4.048	2.394	0.167
1150	3.458	1.936	0.194
1200	2.672	1.526	0.184
1250	2.361	1.263	0.216
1300	2.023	1.056	0.229
1350	1.823	0.776	0.330
1400	1.371	0.614	0.305
1500	1.125	0.411	0.403
1550	0.878	0.300	0.434
1600	0.606	0.185	0.482
1650	0.435	0.138	0.466
1700	0.120	0.028	0.588
1750	0.044	0.014	0.462
Objective Function ( $\Delta$ ) =			4.460

As can be seen in Table 38 and Figure 61, the match between the experiments and the Parachor model predictions is not good and IFT under-predictions are obtained with the Parachor model. This observation further substantiates the poor performance of Parachor model for IFT predictions in multicomponent hydrocarbon systems, previously reported by others [86, 87].

Therefore, correction factors are used for original Parachor model predictions in mechanistic Parachor model to minimize the objective function. The mass transfer

enhancement parameter ( $k$ ), the correction factor at which the objective function becomes the minimum is computed to be 2.19. The diffusivities between the fluid phases at various pressures in this gas-oil system are given in Table 39.

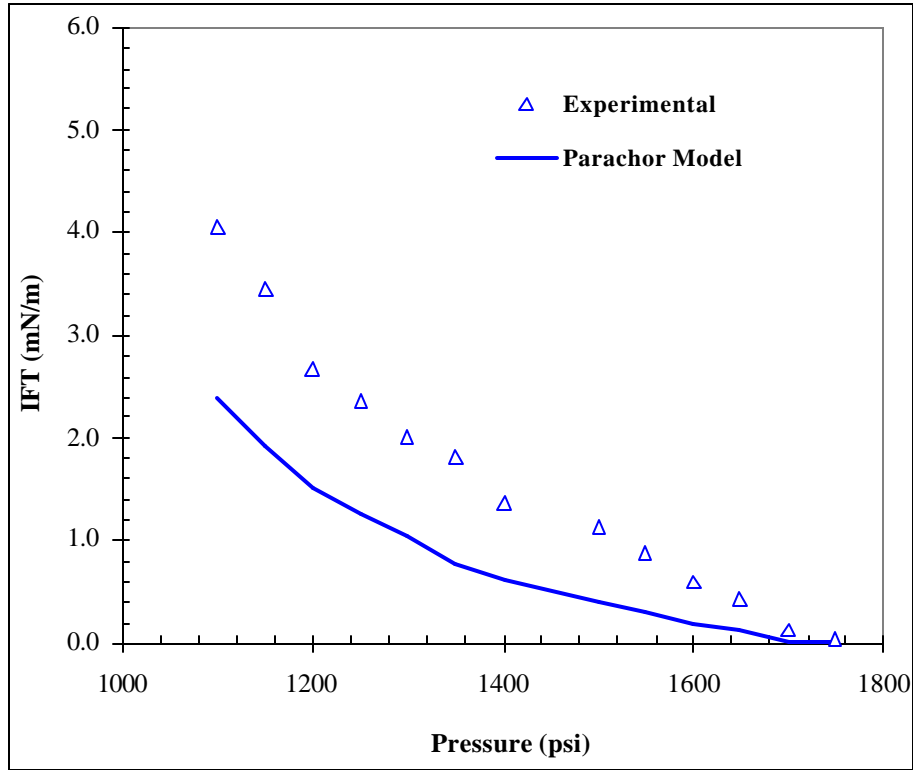


**Figure 61: Comparison of IFT Measurements with Parachor Model in Synthetic Live Oil-CO<sub>2</sub> System at 160° F**

From Table 39, it can be seen that the average ratio of diffusivities between the fluids at all pressures is 3.0. From the mass transfer enhancement parameter and the average ratios of diffusivities between the fluid phases, the exponent ( $n$ ) characterizing the governing mass transfer mechanism is found to be + 0.712. The positive sign of  $n$  indicates that vaporization of components from the oil into the gas phase is the controlling mass transfer mechanism in the combined vaporizing and condensing drive mechanism for attaining gas-oil miscibility in this standard gas-oil system. This can be

attributed to the presence of significant amounts of lighter components (55 mole% C<sub>1</sub> and C<sub>4</sub>) in the synthetic live oil.

**Table 39: Diffusivities between Oil and Gas at Various Pressures in Synthetic Live Oil – CO<sub>2</sub> System at 160° F**

Pressure (psi)	D <sub>os</sub> (m <sup>2</sup> /sec)	D <sub>so</sub> (m <sup>2</sup> /sec)	D <sub>os</sub> /D <sub>so</sub>
1100	4.178E-08	1.251E-08	3.339
1150	4.100E-08	1.244E-08	3.295
1200	4.024E-08	1.238E-08	3.251
1250	3.952E-08	1.231E-08	3.210
1300	3.881E-08	1.224E-08	3.171
1350	3.797E-08	1.217E-08	3.119
1400	3.716E-08	1.211E-08	3.068
1500	3.521E-08	1.198E-08	2.940
1550	3.438E-08	1.192E-08	2.885
1600	3.333E-08	1.185E-08	2.812
1650	3.234E-08	1.180E-08	2.742
1700	3.141E-08	1.173E-08	2.677
1750	3.043E-08	1.167E-08	2.607
Average =			3.009

The comparison between the mechanistic Parachor model IFT predictions and the experiments at various pressures is given in Table 40 and shown in Figure 62. As expected, a reasonably good match is obtained between the experiments and the mechanistic model predictions.

**Table 40: Comparison between IFT Measurements and Mechanistic Parachor Model Predictions in Synthetic Live Oil - CO<sub>2</sub> System at 160° F**

Pressure (psi)	IFT (mN/m)		Weighted Square Dev.
	Experimental	Mechanistic Parachor Model	
1100	4.048	5.243	0.087
1150	3.458	4.240	0.051
1200	2.672	3.342	0.063
1250	2.361	2.766	0.029
1300	2.023	2.313	0.020
1350	1.823	1.699	0.005
1400	1.371	1.345	0.000
1500	1.125	0.900	0.040
1550	0.878	0.657	0.064
1600	0.606	0.405	0.109
1650	0.435	0.302	0.093
1700	0.120	0.061	0.240
1750	0.044	0.031	0.090
Objective Function ( $\Delta$ ) =			0.891

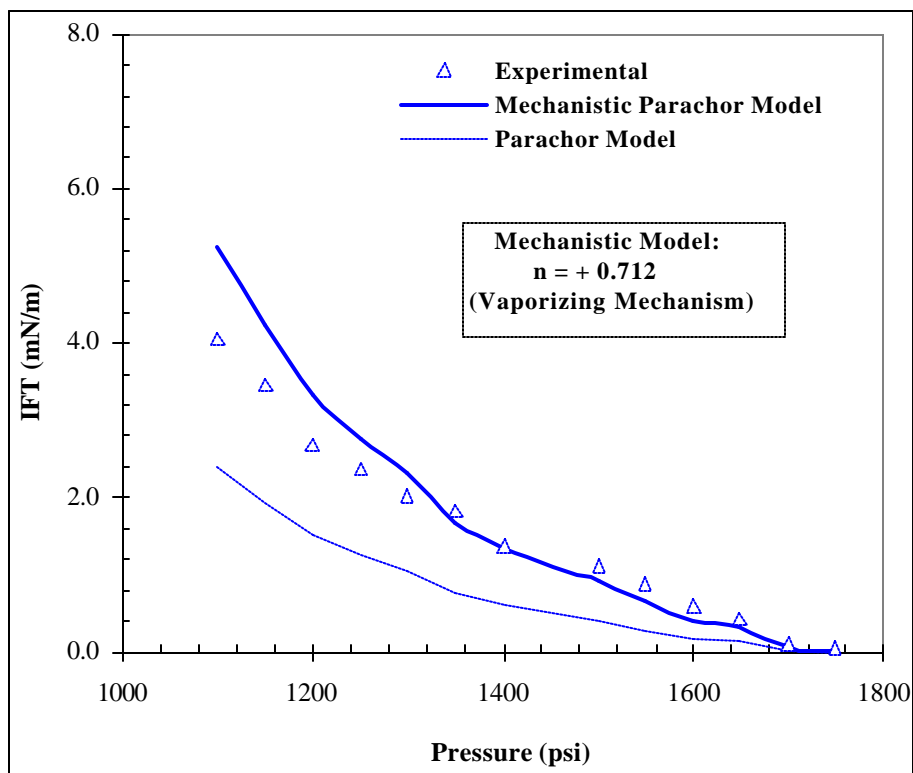


**Figure 62: Comparison of IFT Measurements with Mechanistic Parachor Model in Synthetic Live Oil - CO<sub>2</sub> System at 160° F**

Now, the generalized regression model proposed for mechanistic model exponent prediction in crude oil-solvent systems was utilized to determine the model exponent in this standard gas-oil system. This regression model was originally developed for crude oil-solvent systems where solvent is the hydrocarbon gas mixture. However, in this standard gas-oil system, the solvent is the pure CO<sub>2</sub> gas. Therefore, the term representing condensing drive mechanism of intermediate to heavy components from solvent to oil in the regression model is not applicable and hence can be ignored. But the portion of the regression model representing the vaporizing drive mechanism holds good even for this case, as the lighter components (solute) vaporizing from oil into gas are almost similar in both the gas-oil systems. Furthermore, it is reasonable to add the component n-C<sub>4</sub> to the numerator in the term representing vaporizing drive mechanism, as its tendency will be primarily towards vaporization in the standard gas-oil system. With these assumptions, a mechanistic model exponent of 0.651 is obtained using the live synthetic oil composition in the generalized regression model for this standard gas-oil system. Thus, this exponent calculated using the regression model deviated by only about 8.6% from the mechanistic model exponent of 0.712 obtained by using all the available IFT experimental data.

The comparison between experiments and the predictions obtained using both the exponents in the mechanistic Parachor model for this standard gas-oil system is shown in Figure 63. From Figure 63, almost similar IFT predictions as well as good match with IFT measurements can be seen from both the mechanistic Parachor models. This once again validates the use of generalized regression model for the mechanistic model exponent prediction in crude oil-gas systems. However, IFT measurements with more multicomponent hydrocarbon constituents in the live synthetic oil and CO<sub>2</sub> gas systems

need to be conducted in future to develop accurate generalized regression models for the mechanistic model exponent prediction in standard synthetic live oil-CO<sub>2</sub> gas systems.

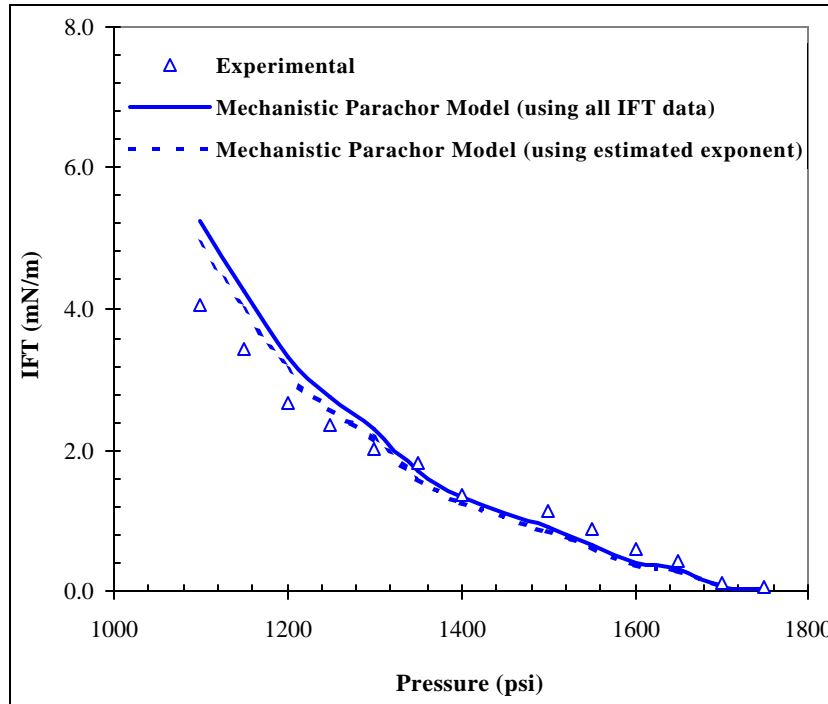


**Figure 63: Comparison between Mechanistic Parachor Model Results Using the Exponents from both Compositional as well as IFT Data**

#### **4.7 Relationship between Developed Miscibility in Gas Injection EOR Projects and Laboratory Gas-Oil Interfacial Tension Measurements**

From this study which involved both experimental and modeling work to determine fluid-fluid miscibility in multicomponent hydrocarbon systems, the following important observations can be made on the relationship between various types of developed miscibility in field gas injection EOR projects and the laboratory gas-oil interfacial tension measurements.

##### **❖ First Contact Miscibility**

In this process, the injection gas enrichment will be below its solubility saturation limit in the reservoir crude oil or at reservoir pressure both the compositions of reservoir

crude oil and the injected gas are below their respective solubility saturation limits in each other. In the existence of such a scenario between the fluids in crude oil reservoirs, the injected gas, as soon as it first sees the reservoir crude oil, immediately dissolves into reservoir crude oil to become miscible and consequently forms a single phase. Thus, both the crude oil and the injected gas become miscible instantaneously on their first contact itself without allowance for any mass transfer of components to occur between the fluid phases and hence the process is known as first contact miscible.

All the characteristics of the first contact miscible displacement process taking place in crude oil reservoirs are well reflected in the laboratory gas-oil interfacial tensions measured between the injected gas and live crude oil immediately upon their first contact at reservoir temperature without allowing for any mass transfer to take place between the oil and gas. The gas-oil interfacial tensions can then be measured in this manner at various pressures or enrichment levels of gas phase. By plotting these interfacial tensions against pressure or enrichment and then by extrapolating the plot to zero interfacial tension, a representative measure of first contact miscibility (FCM) conditions can be obtained. Rao [1] determined the first contact hydrocarbon gas enrichments needed for miscibility development in Rainbow Keg River reservoir using this approach and were successfully implemented in the field.

#### ❖ **Dynamic Miscibility**

In this process, the injection gas enrichment will be above its solubility saturation limit in the reservoir crude oil or at reservoir pressure both the compositions of reservoir crude oil and the injected gas are above their respective solubility saturation limits in each other. As a result, the simultaneous counter-directional mass transfer of components

takes place between the crude oil and the injected gas to alter the fluid phase compositions for attaining their respective saturation solubility limits due to the continuous interactions between the injected gas and the reservoir crude oil. Thus, gas-oil miscibility develops dynamically in crude oil reservoirs and hence the process is known as dynamic gas-oil miscibility development. It is generally accepted that this dynamic gas-oil miscibility involving the simultaneous counter-directional mass transfer of components between the fluid phases is the one that occurs most frequently in any miscible gas injection displacement process [16].

The dynamic gas-oil miscibility development occurring in crude oil reservoirs is well reflected in the dynamic (or time-dependent variations) in the gas-oil interfacial tension measurements when the crude oil and the injected gas are brought into contact with each other. Therefore, the dynamic behavior of gas-oil interfacial tension represents the dynamic aspects of counter-directional mass transfer effects and hence can be used to predict the dynamic gas-oil miscibility occurring in crude oil reservoirs. The dynamic interfacial tension measurements can also be used to determine the dominating mass transfer mechanism (either vaporizing or condensing) in the combined vaporizing and condensing drive mechanism responsible for dynamic gas-oil miscibility development in gas injection EOR field projects. Thus, dynamic gas-oil interfacial tension can be used to predict dynamic gas-oil miscibility as well to characterize the governing mass transfer mechanism by which dynamic gas-oil miscibility development occurs. All these utilities of dynamic interfacial tension in fluid-fluid miscibility were substantiated in Section 4.5 with the supporting modeling results in several crude oil-gas systems.

### ❖ **Multiple Contact Miscibility**

Even in this process, initially both the crude oil and the injected gas compositions will be above their respective saturation solubility limits. This initiates the simultaneous mass transfer of components in both directions between the fluid phases and alters the phase compositions by multiple contacts between the injected gas and the reservoir crude oil. Once, the fluid phases reach their saturation solubility limits, the mass transfer between the injected gas and the crude oil finally ceases. Thus, the gas-oil miscibility is attained in the crude oil reservoir after all the mass transfer of components between the fluid phases ceases due to the mutual saturation of the fluid phases by the multiple contacts and hence the process is known as multiple contact miscible.

The multiple contact miscibility development between the crude oil and the injected gas in crude oil reservoirs can be determined from the laboratory interfacial tension measurements by measuring the equilibrium value of gas-oil interfacial tension between the crude oil and the injected gas. This equilibrium value is attained after all the counter-directional mass transfer of components ceases between the oil and gas due to the saturation of fluid phase compositions and the consequent absence of the concentration gradients driving the mass transfer across the interface between the fluid phases. Thus, the equilibrium interfacial tension includes all the mass transfer effects that occur between the crude oil and the injected gas due to multiple contacts of crude oil with the injected gas. Hence, the equilibrium interfacial tensions measured in laboratory can be plotted against pressure or enrichment and then extrapolation of the plot to zero interfacial tension gives the representative multiple contact miscibility conditions between the crude oil and the injected gas. Furthermore, equilibrium interfacial tension

being an equilibrium thermodynamic property does not depend upon the quantities of fluids in the feed mixture and hence it can be considered as being independent of compositional path. Thus equilibrium value of interfacial tension might be reached by several compositional paths due to the varying gas-oil ratios in the feed mixture, but all of them must lead to a unique value of IFT at equilibrium. However, though gas-oil ratio has no effect on equilibrium interfacial tension, it affects the mass transfer rates between the fluid phases and hence determines the rate at which the thermodynamic equilibrium state is attained. Therefore, the multiple contact miscibility pressures or enrichments determined using the equilibrium interfacial tensions include all the mass transfer effects and are independent of compositional paths due to varying gas-oil ratios in the feed mixtures. All these aspects of multiple contact miscibility determination using the equilibrium interfacial tension measurements and their compositional path independence due to varying gas-oil ratios in the feed mixtures are substantiated with supporting experimental data in Sections 4.1 and 4.2.

#### ❖ **Equilibrium IFT vs. Dynamic IFT**

Interfacial tension, being a property of the interface between the two bulk fluid phases in contact, depends on compositions of both the bulk fluids as well as on the concentration gradients that exist at the interface. IFT reaches its equilibrium value when both the bulk fluids approach their equilibrium composition due to prolonged mass transfer of components across the interface as well as due to intra-phase mass transfer within the bulk fluid phases. The changing concentration profiles of a diffusing component across the interface and within bulk fluid phases due to mass transfer interactions in a gas-liquid system for both vaporizing and condensing modes of mass

transfer can be well understood from Figure 30 of Section 4.2.5. Once equilibrium IFT is attained, there is no further change in the bulk fluid compositions as the mass transfer ceases due to the absence of concentration gradient. Therefore, the equilibrium IFT is a strong function of composition alone and hence is not affected by the mass transfer. This implies that the thermodynamics of equilibrium IFT is not related to the mass transfer related transport properties. The equilibrium IFT seems to be unaffected by the mass ratio of the two bulk fluid phases in contact. The mass ratio of the phases has an impact on mass transfer rates and determines the time taken to attain the final equilibrium composition, but does not affect the final composition. The equilibrium phase composition measurements in gas-oil systems at various mass ratios of phases are being planned in future to validate this hypothesis.

On the other hand, the dynamic IFT's represent the time dependent variations in IFT due to the continuing mass transfer interactions across the interface between the two bulk fluid phases. Thus, dynamic IFT's are measured while mass transfer is still in progress and hence reflect the changes in the composition on both sides of the interface with time. Therefore, dynamic IFT's are a function of mass transfer related transport properties and hence can be modeled using the diffusivities. This is well substantiated in Section 4.5 where the dynamic IFT's reported for several crude oil-gas systems in literature are modeled using the diffusivity coefficients between the fluid phases. Unlike the equilibrium IFT discussed above, the dynamic IFT's could display dependence on mass ratio of the bulk fluid phases, which affects mass transfer rates and hence instantaneous component concentrations at the interface. The influence of mass ratio of bulk fluid

phases on mass transfer rates and hence on dynamic IFT's is evident in the experimental results discussed in Section 4.2.5 (Figure 29).

#### ❖ **Dynamic Miscibility vs. Multiple Contact Miscibility**

The terms “dynamic miscibility” and “multiple contact miscibility” have been often used interchangeably in the literature. However, they are discussed in separate subsections previously above so as to relate them in a mechanistic manner to the laboratory gas-oil interfacial tension measurements. The gas-oil interfacial tension measurements made in a manner that does not allow any mass transfer between phases, reflect first contact miscibility, while the IFT measurements made after allowing for complete mass transfer (after equilibrium) reflect multiple contact miscibility. In between these two extremes, dynamic gas-oil IFT's measured reflect the contacts or stages between first and the multiple contact miscibility. The experimental IFT data from Rao [1] is re-plotted in Figure 64 to show the multi-stages involved in gas-oil interfacial tension before attaining equilibrium and hence in the VIT miscibility.

From Figure 64, it can be seen that the gas-oil IFT measurements made without allowing for mass transfer between the fluid phases resulted in a VIT first contact miscible (FCM) condition of 60.0 mole%  $C_{2+}$  enrichment in the injection gas. However, an equilibrium (multiple contact) VIT miscibility (MCM) condition of 51.2 mole%  $C_{2+}$  enrichment in the injection gas was obtained using the gas-oil IFT's measured after complete mass transfer or at equilibrium. The dynamic gas-oil interfacial tensions in between first and multiple contacts would represent various multi-stages or contacts of injected gas with crude oil before attaining the final equilibrium condition of multiple contact miscibility and hence result in VIT dynamic miscibility conditions ranging from

51.2 – 60.0 mole% C<sub>2+</sub> enrichment in the injection gas. The mass ratio of the phases used during IFT measurements does not affect multiple contact miscibility as the multiple contact miscibility is attained at equilibrium composition. However, the mass ratio of the phases determines the number of dynamic stages or contacts in between first and multiple contacts. Therefore, the VIT technique, in which the equilibrium gas-oil interfacial tensions are used to determine multiple contact miscibility, is not a single contact technique. This technique also offers multiple contacts as the other conventional techniques, wherein the multi-stages of contact between the injected gas and crude oil are reflected in the dynamic behavior of gas-oil interfacial tension before attaining the final equilibrium composition, as can be seen in Figure 64. This is probably the reason for good match of VIT miscibilities obtained in this study with slim-tube miscibilities reported in literature.

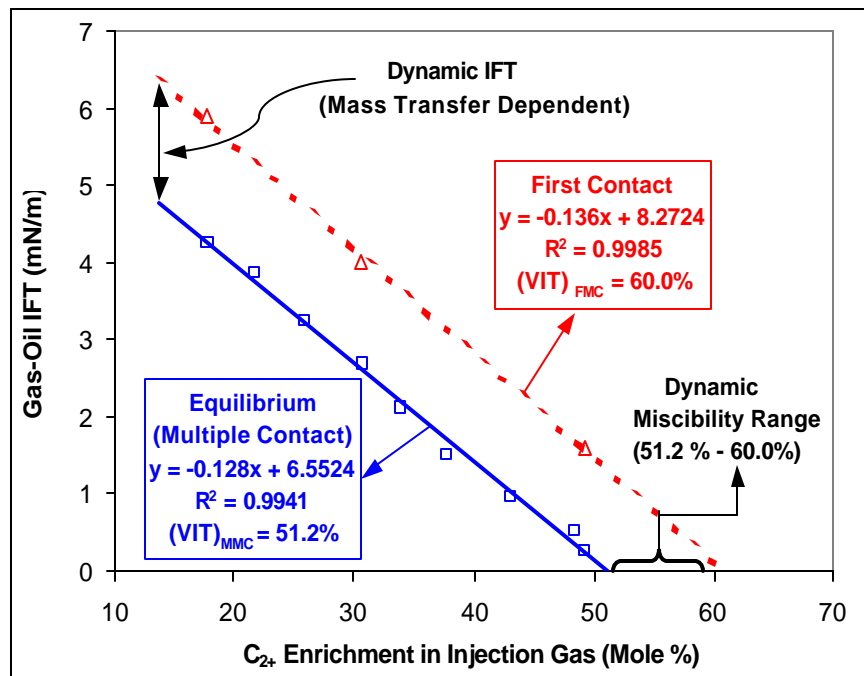


**Figure 64: Demonstration of Multi-Stages of Gas-Oil Contact in VIT Technique (Using the Data from Rao, 1997; Ref. 1)**

Thus, by careful exploitation of laboratory interfacial tension measurements to reflect the realistic reservoir phenomena occurring between the reservoir crude oil and the injected gas in crude oil reservoirs, it is possible to simulate all the different types of gas-oil miscibility development that occur in gas injection EOR field projects. This clearly indicates the indisputable interrelationship between interfacial tension and the thermodynamic aspect of fluid-fluid miscibility and hence validates the VIT technique to determine fluid-fluid miscibility in multicomponent hydrocarbon systems.

## 5. CONCLUSIONS AND RECOMMENDATIONS

### 5.1 Summary of Conclusions

The significant contributions of this study to the existing literature are:

- \* Successfully used the well-known glass tube based capillary rise technique for low interfacial tension measurements in multicomponent hydrocarbon systems at elevated pressures and temperatures.
- \* Correlated interfacial tension with solubility characteristics in multicomponent hydrocarbon systems and hence revealed the use of interfacial tension for solubility predictions.
- \* Further validated the applicability of new vanishing interfacial tension (VIT) technique to determine fluid-fluid miscibility in multicomponent hydrocarbon systems.
- \* Recognized the absence of gas-oil ratio effects on equilibrium interfacial tension and hence indicated the compositional path independence of multiple contact miscibilities determined from equilibrium interfacial tension measurements due to varying gas-oil ratios in the feed mixtures.
- \* Recognized the importance of counter-directional mass transfer effects (combined vaporizing and condensing mass transfer mechanisms) on fluid-fluid miscibility based on experimental as well as modeling results.
- \* Developed a new mechanistic Parachor model to predict dynamic gas-oil interfacial tension in multicomponent hydrocarbon systems.

- \* Identified the utility of dynamic gas-oil interfacial tension to predict dynamic gas-oil miscibility as well as to characterize the governing mass transfer mechanism (either vaporizing or condensing) responsible for dynamic gas-oil miscibility development.
- \* Substantiated the presence of all mass transfer effects in equilibrium interfacial tension and hence justified the use of equilibrium interfacial tension to determine multiple contact miscibility conditions.
- \* Correlated various types of developed miscibility in gas injection EOR field projects with laboratory gas-oil interfacial tension measurements.
- \* Identified the importance and the multitude of roles played by interfacial tension in phase equilibrium characteristics and hence emphasized the need to recognize interfacial tension as a good phase behavior indicator in fluid-fluid phase equilibria studies.

All the above-mentioned contributions resulted from this study are discussed briefly below.

- **Successful Use of Capillary Rise Technique for IFT Measurements at Elevated Pressures and Temperatures**

The well-known glass tube based capillary rise technique has been successfully used in this study for low interfacial tension measurements in standard ternary liquid system of benzene, ethanol and water as well as in the standard gas oil systems of n-decane-CO<sub>2</sub> and synthetic live oil-CO<sub>2</sub>. The capillary rise IFT measurements have been validated by calibrating against the pendent drop technique in n-decane-CO<sub>2</sub> system at 100° F. After Park and Lim [53], we are the next to use this technique for interfacial tension measurements in multicomponent hydrocarbon systems at elevated pressures and temperatures. This enabled us to measure gas-oil interfacial tensions down to 0.044

mN/m, while the lowest gas-oil IFT measured with the conventional technique of pendent drop shape analysis was about 3.0 mN/m. This in turn enabled better accuracy in miscibility determination using the VIT technique.

- **Correlation of Solubility with Interfacial Tension**

The experiments in the standard ternary liquid system of benzene, ethanol and water have clarified the long existing confusion about the distinction between the terms solubility and miscibility, in that the distinction between them lies in insoluble and partially soluble regions and that solubility in all proportions (completely soluble) is nothing but miscibility between the fluid phases. This study has also demonstrated different regions of solubility characteristics and their relation to interfacial tension. The comparison of interfacial tension measurements with solubility data showed a strong mutual correlation between solubility and reciprocal of IFT and hence revealed the use of IFT for solubility predictions in multicomponent hydrocarbon systems. Thus this study has been able to correlate all the three thermodynamic properties of solubility, miscibility and interfacial tension in multicomponent hydrocarbon systems.

- **Further Validation of Vanishing Interfacial Tension (VIT) Technique to Determine Fluid-Fluid Miscibility in Multicomponent Hydrocarbon Systems**

Interfacial tension measurements have been conducted in standard ternary liquid system of benzene, ethanol and water at ambient conditions and in the standard gas-oil systems of n-decane-CO<sub>2</sub> at 100° F and synthetic live oil-CO<sub>2</sub> at 160° F to validate the VIT technique for fluid-fluid miscibility determination.

In benzene, ethanol and water standard ternary liquid system at ambient conditions, a VIT miscibility of 80 mole% ethanol enrichment in aqueous phase has been obtained, which is in good agreement with the reported minimum miscibility enrichment from the

phase diagram (83 %) and solubility data (>78 %). For n-decane-CO<sub>2</sub> system at 100° F, the minimum miscibility pressure obtained from VIT experiments (1150 psi) matched well with the reported miscibilities from slim-tube (1250 psi) and rising bubble (1280 psi) measurement techniques. A VIT minimum miscibility pressure of 1760 psi has been obtained in live synthetic oil-CO<sub>2</sub> system at 160° F, which agreed well with the reported miscibilities of 1700 psia from phase diagram, slim-tube and analytical model predictions.

Thus, fluid-fluid miscibility has been shown to be well represented by the condition of zero interfacial tension in all the three standard fluid systems studied. This clearly exposes the sound conceptual basis of VIT technique and validates this technique for accurate, quick and cost-effective determination of fluid-fluid miscibility conditions in multicomponent hydrocarbon systems.

- **Effect of Gas-Oil Ratio on IFT and Miscibility**

As the fluid phases approached equilibrium, the interfacial tension is found to be unaffected by gas-oil ratio in all the three standard fluid systems studied. Though gas-oil ratio has no effect on near equilibrium interfacial tension, it is found to have an impact on mass transfer rates to determine the time duration needed for attaining the thermodynamic equilibrium between the two immiscible fluid phases. Thus, this study has identified the compositional path independence of miscibilities determined using the VIT technique due to varying gas-oil ratios in the feed mixture.

- **Effect of Mass Transfer on Fluid-Fluid Miscibility**

The VIT experimental results of Rainbow Keg River (RKR) and Terra Nova reservoir fluids have been compared with equations of state (EOS) calculations. The effect of EOS

tuning on miscibility calculations has been examined. Superior miscibility predictions have been obtained with untuned EOS when compared to tuned EOS for both the reservoir fluids. Gas-oil miscibility over-predictions by about 3.5 MPa (500 psi) have been obtained with untuned EOS when compared to VIT experiments for RKR fluids. The utility of conventional Parachor IFT model to determine fluid-fluid miscibility in multicomponent hydrocarbon systems has been investigated using Rainbow Keg River reservoir fluids. Miscibility over-predictions by about 4.5 MPa (650 psi) have been obtained with Parachor computational model when compared to VIT experiments. The inability of the both these computational models (EOS and Parachor) to account for counter-directional mass transfer effects (combined vaporizing and condensing drive) has been identified as the cause for these miscibility over-predictions.

- **Development of a New Mechanistic Parachor Model to Predict Dynamic IFT and to Identify Governing Mass Transfer Mechanism for Dynamic Gas-Oil Miscibility**

A new mechanistic Parachor model has been developed in this study to include simultaneous counter-directional mass transfer effects for the prediction of dynamic gas-oil interfacial tension as well as to identify the governing mass transfer mechanism for the attainment of fluid phase equilibria and miscibility in multicomponent hydrocarbon systems. The ratio of diffusivities between the fluid phases raised to an exponent is introduced into the original Parachor model to incorporate mass transfer effects. The sign and value of the exponent in the mechanistic model characterize the type and the extent of dominant mass transfer mechanism (either vaporizing or condensing) in the combined vaporizing and condensing mechanism for fluid phase equilibria and miscibility. The

exponent in the mechanistic model has been obtained by fitting the experimental IFT data to the mechanistic Parachor model IFT predictions.

The proposed mechanistic model has been used to predict interfacial tension for Rainbow Keg River and Terra Nova reservoir fluids. A good match of IFT predictions with experiments has been obtained with the proposed mechanistic model. The positive exponents obtained in the mechanistic model for both these reservoir fluids indicate the vaporization of lighter components from crude oil into the gas to be the governing mass transfer mechanism for attaining compositional equilibrium and gas-oil miscibility. The relatively higher value of exponent obtained for Terra Nova fluids when compared to RKR fluids indicate more pronounced vaporization mass transfer effects from crude oil into the gas for Terra Nova reservoir fluids, which appears to be reasonable considering the higher amount of light ends in the Terra Nova crude oil.

The negative exponent obtained for the proposed mechanistic model, implying the condensation of intermediate to heavy components from gas into the crude oil to be the governing mass transfer mechanism for fluid phase equilibria, has been validated using Schrader Bluff reservoir fluids. The proposed mechanistic model has also been applied to predict interfacial tension in three different crude oil systems. A good match of IFT predictions with experiments are obtained with the proposed model. Positive exponents obtained in the mechanistic model for all three crude oil systems indicate the vaporization of lighter components from crude oil to be the governing mass transfer mechanism for fluid phase equilibria. Sensitivity studies on proposed mechanistic model results for RKR and Terra Nova fluids indicate that the provision of a single IFT measurement to the

mechanistic model is sufficient for reasonably accurate IFT predictions from the new mechanistic model developed in this study.

Generalized regression correlations have been developed to predict the exponent in the mechanistic model by knowing simply reservoir fluids composition, without using even a single IFT measurement in the mechanistic model. These models can be used for *a-priori* prediction of the mechanistic model exponent without the need for any experimental IFT data. The proposed regression models have been validated for mechanistic model exponent prediction in both crude oil and crude oil-gas systems using Prudhoe Bay reservoir fluids.

The gas-oil interfacial tensions measured in the two standard gas-oil systems of n-decane-CO<sub>2</sub> and synthetic live oil-CO<sub>2</sub> at elevated pressures and temperatures have been modeled using the proposed mechanistic Parachor model. The zero exponent obtained in the mechanistic model for n-decane-CO<sub>2</sub> system at 100° F indicates a condition of equal mass transfer in both directions before attaining miscibility. The positive exponent obtained in the mechanistic model for synthetic live oil-CO<sub>2</sub> system at 160° F indicates vaporization of lighter components from live oil into CO<sub>2</sub> gas to be the dominant mechanism for gas-oil miscibility development in this standard gas-oil system.

Thus this study has resulted in a new mechanistic Parachor model to predict dynamic gas-oil interfacial tension as well as to characterize the governing mass transfer mechanism (either vaporizing or condensing) responsible for dynamic gas-oil miscibility development in gas injection EOR field projects.

- **Mass Transfer Effects in Equilibrium Interfacial Tension**

The ability of the proposed mechanistic model to predict IFT by the inclusion of mass transfer effects as well as the dynamic interfacial behavior observed in the synthetic live oil-CO<sub>2</sub> system at 160° F indicate the role of mass transfer effects on interfacial tension. This clearly substantiates the presence of all the mass transfer effects in equilibrium interfacial tension measurements and hence justifies the use of equilibrium interfacial tension to determine multiple contact miscibility conditions between the crude oil and the injected gas.

- **Correlated Various Types of Developed Miscibility in Gas Injection EOR Projects with Gas-Oil IFT**

This study has related various types of developed miscibility in gas injection EOR namely, first contact miscibility, dynamic miscibility and multiple contact miscibility with laboratory interfacial tension measurements. This clearly shows the indisputable interrelationship between interfacial tension and the thermodynamic aspect of fluid-fluid miscibility in multicomponent hydrocarbon systems.

- **Multitude of Roles Played by Interfacial Tension in Fluid-Fluid Phase Equilibria**

This study has delineated the multitude of roles played by interfacial tension in fluid-fluid interactions of phase equilibria. The phase equilibrium characteristics of solubility, miscibility and mass transfer between the fluid phases in contact have been shown to be well correlatable to interfacial tension. In the process of seeking such correlations, it was found that incorporating counter-current diffusivities between the fluid phases raised to an exponent to account for multicomponent mass transfer occurring across the interface between the two contacting phases enhances significantly the ability of the Parachor model to predict interfacial tension. Furthermore, the solubility in all proportions, or

miscibility of two phases in contact, has been shown to be well represented by the condition of zero interfacial tension between the two immiscible fluid phases. The solubility between the two fluid phases has been found to be mutually correlated to reciprocal of interfacial tension and hence interfacial tension can be used for solubility predictions in multicomponent hydrocarbon systems. The governing mass transfer mechanism (either vaporizing or condensing) for fluid phase equilibria and miscibility has been inferred from interfacial tension in several complex hydrocarbon fluid systems. Therefore, the fluid-fluid interfacial tension measurements at representative conditions of pressure and temperature are essential to understand the phase behavior characteristics of complex hydrocarbon fluids. Thus, this study has identified the importance of interfacial tension in phase behavior characterization and hence emphasizes the need to recognize interfacial tension as a good phase behavior indicator in fluid-fluid phase equilibria studies.

## **5.2 Recommendations for Future Work**

Gas-oil interfacial tension measurements in crude oil-gas systems of known miscibility conditions need to be conducted at reservoir temperatures to further validate the VIT technique to determine fluid-fluid miscibility conditions. The interfacial tension measurements of several pure hydrocarbon compounds against different binary, ternary and multicomponent hydrocarbon mixtures are recommended to test the effect of interaction of other components in a mixture on pure component Parachor values. The gas-oil interfacial tension measurements with heavy crude oil-gas systems need to be carried out to develop generalized regression models for mechanistic model exponent prediction in condensing drive systems. Counter-current extraction or leaching

experiments are recommended to simulate the dynamic gas-oil miscibility development due to multiple contacts of crude oil and the injected gas in crude oil reservoirs with laboratory interfacial tension and phase composition measurements.

## REFERENCES CITED

1. Rao, D.N.: "A New Technique of Vanishing interfacial Tension for Miscibility Determination," *Fluid Phase Equilibria*, **139** (1997) 311-324.
2. Rao, D.N. and Lee, J.I.: "Application of the New Vanishing Interfacial Tension Technique to Evaluate Miscibility Conditions for the Terra Nova Offshore Project," *Journal of Petroleum Science and Engineering*, **35** (2002) 247-262.
3. Rao, D.N. and Lee, J.I.: "Determination of Gas-Oil Miscibility Conditions by Interfacial Tension Measurements," *Journal of Colloid and Interface Science*, **262** (2003) 474-482.
4. Moritis, G.: "EOR Continues to Unlock Oil Resources," *Oil & Gas Journal*, **102** (2004) 45-65.
5. Stosur, G.J., Singer, M.I., Luhning, R.W. and Yurko, W.J.: "Enhanced Oil Recovery in North America: Status and Prospects," *Energy Resources*, **12** (1990) 429-437.
6. Benham, A.L., Dowden, W.E. and Kunzman, W.J.: "Miscible Fluid Displacement - Prediction of Miscibility," Petroleum Transactions Reprint Series No. 8, Society of Petroleum Engineers of AIME (1965) 123.
7. Stalkup Jr., F.I., *Miscible Displacement*, SPE Monograph, Vol.8, SPE of AIME (1983), New York.
8. Holm, L.W.: "Miscible Displacement," in H.B. Bradley (Ed.), *Petroleum Engineering Hand Book*, Society of Petroleum Engineers, Richardson, TX (1987) 1-45.
9. Lake, L.W., *Enhanced Oil Recovery*, Prentice-Hall Englewood Cliffs, NJ (1989) 234.
10. Elsharkawy, A.M., Poettmann, F.H. and Christiansen, R.L.: "Measuring CO<sub>2</sub> Minimum Miscibility Pressure: Slim-Tube or Rising-Bubble Method?," *Energy & Fuels*, **10** (1996) 443-449.
11. Klins, M.A., *Carbon Dioxide Flooding-Basic Mechanisms and Project Design*, International Human Resources Development Corporation, Boston, 1984.
12. Holm, L.W. and Josendal, V.A.: "Effect of Oil Composition on Miscible-Type Displacement by Carbon Dioxide," *Soc. Pet. Eng. J.* (Feb. 1982) 87-98.
13. Williams, C.A., Zana, E.N. and Humphrys, G.E.: "Use of Peng-Robinson Equation of State to Predict Hydrocarbon Phase Behavior and Miscibility for Fluid Displacement," paper SPE 8817 presented at the 1<sup>st</sup> Joint SPE/DOE Symposium on Enhanced Oil Recovery, Tulsa, April 20-23, 1980.

14. Perry, G.E.: "Weeks Island S Sand Reservoir B Gravity Stable Miscible CO<sub>2</sub> Displacement, Iberia Parish, Louisiana, Third Annual Report," DOE/METC-5232-4, June 1980.
15. Johnson, J.P. and Pollin, J.S.: "Measurement and Correlation of CO<sub>2</sub> Miscibility Pressures," paper SPE 9790 presented at the 2<sup>nd</sup> Joint SPE/DOE Symposium on Enhanced Oil Recovery, Tulsa, April 5-8, 1981.
16. Zick, A.A.: "A Combined Condensing/Vaporizing Mechanism in the Displacement of Oil by Enriched Gases," paper SPE 15493 presented at SPE 61<sup>st</sup> Annual Technical Conference and Exhibition, New Orleans, LA, Oct. 5-8, 1986.
17. Peng, D.Y. and Robinson, D.B.: "A New Two-Constant Equation of State," *Ind. Eng. Chem. Fundam.*, **15** (1976) 59-64.
18. Coats, K.H. and Smart, G.T.: "Application of a Regression-Based EOS PVT Program to laboratory Data," *SPE Reservoir Engineering Journal*, **1** (1986) 277-299.
19. Coats, K.H.: "Simulation of Gas Condensate Reservoir Performance," *JPT*, **40** (1988) 1870-1886.
20. Behbahania, A.R.: "A Universal Set of Weight Factors for Tuning Peng-Robinson Equation of State," paper presented at the Petroleum Society's Canadian International Petroleum Conference 2001, Calgary, Alberta, Canada, June 12-14, 2001.
21. Pederson, K.S., Thomassen, P. and Fredenslund, A.: "On the Dangers of Tuning Equation of State Parameters," *Chemical Engineering Science*, **43** (1988) 269-278.
22. Danesh, A., *PVT and Phase Behavior of Petroleum Reservoir Fluids*, Elsevier Science B.V., Amsterdam (1998).
23. Lee, J.I. and Reitzel, G.A.: "High Pressure, Dry Gas Miscible Flood - Brazeau River Nisku Oil Pools," *JPT*, **34** (1982) 2503-2509.
24. Firoozabadi, A. and Aziz, K.: "Analysis and Correlation of Nitrogen and Lean Gas Miscibility Pressure," *SPE Reservoir Engineering Journal*, **1** (1986) 575-582.
25. Hagen, S. and Kossack, C.A.: "Determination of Minimum Miscibility Pressure Using a High-Pressure Visual Sapphire Cell," paper SPE 14927 presented at the 1986 SPE/DOE Enhanced Oil Recovery Symposium, Tulsa, OK, April 20-23.
26. Ahmed, T.: "A Generalized Methodology for Minimum Miscibility Pressure," paper SPE 39034 presented at the 1997 Latin American and Caribbean Petroleum Engineering Conference and Exhibition, Rio de Janeiro, Brazil, Aug. 30-Sept.3.

27. Welge, H.J., Johnson, E.F., Ewing Jr., S.P. and Brinkman, F.H.: "The Linear Displacement of Oil from Porous Media by Enriched Gas," *JPT*, **13** (1961) 787-796.
28. Helfferich, F.G.: "Theory of Multicomponent Multiphase Displacement in Porous Media," *SPE Reservoir Engineering Journal*, **271** (1981) 51-62.
29. Dumore, J.M., Hagoort, J. and Risseeuw, A.A.: "An Analytical Model for One-Dimensional Three-Component Condensing and Vaporizing Gas Drives," *SPE Journal*, **24** (1984) 169-179.
30. Monroe, W.W., Silva, M.K., Larsen, L.L. and Orr F.M., Jr.: "Composition Paths in Four-Component Systems: Effect of Dissolved Methane on 1D CO<sub>2</sub> Flooding Performance," *SPE Reservoir Engineering Journal* (Aug. 1990) 423-432.
31. Johns, R.T., *Analytical Theory of Multicomponent Gas Drives with Two-Phase Mass Transfer*, PhD dissertation, Stanford University, 1992.
32. Dindoruk, B., *Analytical Theory of Multiphase, Multicomponent Displacement in Porous Media*, PhD dissertation, Stanford University, 1992.
33. Johns, R.T., Dindoruk, B. and Orr, F.M., Jr.: "Analytical Theory of Combined Condensing/Vaporizing Gas Drives," *SPE Adv. Tech. Series*, **2** (1993) 7-16.
34. Dindoruk, B., Johns, R.T. and Orr F.M., Jr.: "Analytical Solution for Four Component Gas Displacements with Volume Change on Mixing," paper presented at the 3<sup>rd</sup> European Conference on the Mathematics of Oil Recovery, Delft, Holland, June 1992.
35. Orr, F.M., Jr., Johns, R.T. and Dindoruk, B.: "Development of Miscibility in Four Component CO<sub>2</sub> Floods," *SPE Reservoir Engineering Journal* (May 1993) 135-142.
36. Wang, Y. and Orr, F.M., Jr.: "Calculation of Minimum Miscibility Pressure," paper SPE 39683 presented at the 1998 SPE/DOE Improved Oil Recovery Symposium, Tulsa, OK, April 19-22.
37. Jessen, K., Michelsen, M.L. and Stenby, E.H.: "Effective Algorithm for Calculation of Minimum Miscibility Pressure," paper SPE 50632 presented at the 1998 European Petroleum Conference, Hague, Netherlands, Oct. 20-22.
38. Wang, Y. and Peck, D.G.: "Analytical Calculation of Minimum Miscibility Pressure: Comprehensive Testing and Its Application in a Quantitative Analysis of the Effect of Numerical Dispersion for Different Miscibility Development Mechanisms," paper SPE 59378 presented at the 2000 SPE/DOE Improved Oil Recovery Symposium, Tulsa, OK, April 3-5.

39. Jessen, K., Michelson, M.L. and Stenby, E.H.: "Global Approach for Calculation of Minimum Miscibility Pressure," *Fluid Phase Equilibria*, **153** (1998) 251-263.
40. Wang, Y. and Orr, F.M., Jr.: "Analytical Calculation of Minimum Miscibility Pressure," *Fluid Phase Equilibria*, **139** (1997) 101-124.
41. Wang, Y. and Orr, F.M., Jr.: "Calculation of Minimum Miscibility Pressure," *Journal of Petroleum Science and Engineering*, **27** (2000) 151-164.
42. Rao, D.N. and Ayirala, S.C.: "The Multiple Roles of Interfacial Tension in Fluid Phase Equilibria and Fluid-Solid Interactions," Invited paper presented at Fourth International Symposium on Contact Angle, Wettability and Adhesion, Philadelphia, PA, June 14-16, 2004.
43. Blanco, A.M. and Ortega, J.: "Experimental Study of Miscibility, Density and Isobaric Vapor-Liquid Equilibrium Values for Mixtures of Methanol in Hydrocarbons (C<sub>5</sub>, C<sub>6</sub>)," *Fluid Phase Equilibria*, **122** (1996) 207-222.
44. Lee, L.H.: "Relevance of Film Pressures to Interfacial Tension, Miscibility of Liquids, and Lewis Acid – Base Approach," *Journal of Colloid and Interface Science*, **214** (1999) 64-78.
45. van Oss, C.J., Chaudhury, M.K. and Good, R.J.: "Monopolar Surfaces," *Adv. Colloid Interface Sci.*, **28** (1987) 35.
46. Simon, R., Rosman, A. and Zana, E.: "Phase-Behavior Properties of CO<sub>2</sub>-Reservoir Oil Systems," *SPEJ* (Feb. 1978) 20-26.
47. Rusanov, A.I., Prokhorov, V.A., *Interfacial Tensiometry*, Elsevier, Amsterdam (1996).
48. Drelich, J., Fang, ch. And White, C.L.: "Measurement of Interfacial Tension in Fluid-Fluid Systems," *Encyclopedia of Surface and Colloid Science*, Marcel Dekker, Inc., 2002, pp. 3152-3166.
49. Adamson, A.W., *Physical Chemistry of Surfaces*, John Wiley and Sons, Inc., New York (1990).
50. Manning, C.D., Pesheck, C.V., Puig, J.E., Seeto, Y., Davis, H.T. and Scriven, L.E.: "Measurement of Interfacial Tension, Topical Report," U.S. Dept. of Energy, DOE/BC/10116-12 (1983).
51. Richards, T.W. and Carver, E.K., A Critical Study of the Capillary Rise Method of Determining Surface Tension, with Data for Water, Benzene, Toluene, Chloroform, Carbon Tetrachloride, Ether and Dimethyl Aniline, *J. Am. Chem. Soc.*, **43** (1921) 827-847.

52. Harkins, W.D. and Brown, F.E.: "The Determination of Surface Tension (Free Surface Energy) and the Weight of Falling Drops: the Surface Tension of Water and Benzene by the Capillary Height Method," *J. Am. Chem. Soc.*, **41** (1919) 499-525.
53. Park, J.Y. and Lim, J.S.: "Effect of F-AOT Surfactant on the Interface between Supercritical CO<sub>2</sub> and Nickel Plating Solution," Power Point Presentation, Department of Chemical Engineering, Sogang University, Korea.
54. Sonntag, H., *Koloidy*, PWN, Warszawa, 1982.
55. du Nuoy, P.L.: "A New Apparatus for Measuring Surface Tension," *J. Gen. Physiol.*, **1** (1919) 521-524.
56. Harkins, W.D. and Jordan, H.F.: "A Method for Determination of Surface and Interfacial Tension from the Maximum Pull on a Ring," *J. Am. Chem. Soc.*, **52** (1930) 1751-1772.
57. Zuidema, H.H. and Waters, G.W.: "Ring Method for the Determination of Interfacial Tension," *Ind. Eng. Chem. Anal. Ed.*, **13** (1941) 312-313.
58. Neiderhauser, D.O. and Bartell, F.E., *Report of Progress - Fundamental Research on the Occurrence and Recovery of Petroleum*, Publication of the American Petroleum Institute, The Lord Baltimore Press, Baltimore, 1950, p. 114.
59. Stauffer, C.E.: "The Measurement of the Surface Tension by the Pendent Drop Technique," *J. Phys. Chem.*, **69** (1965) 1933-1938.
60. Bashforth, F. and Adams, J.C., *An Attempt to Test the Theory of Capillary Action*, Cambridge University Press and Deighton Bell & Co., Cambridge (1883).
61. Hartland, S. and Hartley, R.W., *Axisymmetric Fluid-Fluid Interfaces*, Elsevier, Amsterdam (1976).
62. Maze, C. and Burnet, G.: "A Non-Linear Regression Method for Calculating Surface Tension and Contact Angle from the Shape of a Sessile Drop," *Surface Sci.*, **13** (1969) 451-470.
63. Maze, C. and Burnet, G.: "Modification of a Non-Linear Regression Technique used to Calculate Surface Tension from Sessile Drops," *Surface Sci.*, **24** (1971) 335-342.
64. Rotenberg, Y., Boruvka, L. and Neumann, A.W.: "Determination of Surface Tension and Contact Angle from the shapes of Axisymmetric Fluid Interfaces," *J. Colloid Interface Sci.*, **93** (1983) 169-183.

65. Lahooti, S., del Rio, O.I., Cheng, O. and Neumann, A.W., in "Applied Surface Thermodynamics," Chap. 10, pp. 509-556, Marcel Dekker, New York, 1996.
66. Jennings, J.W., Jr. and Pallar, N.R.: "An Efficient Method for the Determination of Interfacial Tensions from Drop Profiles," *Langmuir*, **4** (1988) 959-967.
67. del Rio, O.I. and Neumann, A.W.: "Axisymmetric Drop Shape Analysis: Computational Methods for the Measurement of Interfacial Properties from the Shape and Dimensions of Pendent and Sessile Drops," *Journal of Colloid Interface Sci.*, **196** (1997) 136-147.
68. Gasem, K.A.M., Dickson, K.B., Shaver, R.D. and Robinson, R.L., Jr.: "Experimental Phase Densities and Interfacial Tensions for Two Multicomponent Systems Involving CO<sub>2</sub> Plus a Synthetic Oil and CO<sub>2</sub> Plus a Reservoir Oil," *SPE Reservoir Engineering Journal* (Aug. 1993) 170-174.
69. Firoozabadi, A., Katz, D.L., Saroosh, H. and Sajjadian, V.A.: "Surface Tension of Reservoir Crude Oil/Gas Systems Recognizing the Asphalt in the Heavy Fraction," *SPE Reservoir Engineering Journal* (Feb. 1988) 265-272.
70. Vonnegut, B.: "Rotating Bubble Method for the Determination of Surface and Interfacial Tensions," *Review of Scientific Instruments*, **13** (1967) 6-9.
71. Princen, H.M., Zia, I.Y.Z. and Mason, S.G.: "Measurement of Interfacial Tension from the Shape of a Rotating Drop," *J. Colloid Int. Sci.*, **13** (1967) 99.
72. Cayias, Y.L., Schechter, R.S. and Wade, W.H.: "The Measurement of Interfacial Tension via the Spinning Drop Technique," in *Adsorption at Interfaces*, Edited by K.L. Mittal, ACS Symposium Series 8, 1975, p. 234.
73. Couper, A., Newton, R. and Nunn, C.: "A Simple Derivation of Vonnegut's Equation for the Determination of Interfacial Tension by the Spinning Drop Technique," *Colloid Polym. Sci.*, **261** (1983) 371-372.
74. *Manual of the Spinning Drop Tensiometer Site 04*, Kruss GmbH, Hamburg, Germany, 1995.
75. Mannhardt, K., *The Measurement of Interfacial Tension by the Spinning Drop Apparatus*, Technical Report Submitted to Petroleum Recovery Institute, Calgary, Canada, Mar. 13 (1987).
76. Macleod, D.B.: "On a Relation between Surface Tension and Density," *Trans. Faraday Soc.*, **19** (1923) 38-42.

77. Sudgen, S.: "The Variation of Surface Tension with Temperature and Some Related Functions," *Journal of Chemical Society*, **125** (1924) 32-41.
78. Brock, H.L. and Bird, R.B.: "Surface Tension and Principle of Corresponding States," *AIChE J.*, **1** (1955) 174-177.
79. Clever, H.L. and Chase, W.E., Jr.: "Thermodynamics of Liquid Surfaces, Surface Tension of n-hexane-cyclohexane mixtures at 25, 30 and 35° C," *J. Chem. Eng. Data*, **8** (1963) 291-292.
80. Carey, B.S., *The Gradient Theory of Fluid Interfaces, PhD Dissertation* (1979), University of Minnesota, Minneapolis.
81. Quale, O.R.: "The Parachors of Organic Compounds," *Chem. Review*, **53** (1953) 439-586.
82. Fanchi, J.R.: "Calculation of Parachors for Compositional Simulation: An Update," *SPE Reservoir Engineering Journal*, **5** (1990) 433-436.
83. Ali, J.K.: "Predictions of Parachors and Petroleum Cuts and Pseudo Components," *Fluid Phase Equilibria*, **95** (1994) 383-398.
84. Schechter, D.S. and Guo, B.: "Parachors Based on Modern Physics and Their Uses in IFT Prediction of Reservoir Fluids," *SPE Reservoir Evaluation & Engineering Journal*, **1** (1998) 207-217.
85. Weinaug, C.F. and Katz, D.L.: "Surface Tensions of Methane-Propane Mixtures," *Industrial Engineering Chemistry*, **35** (1943) 239-246.
86. Danesh, A.S., Dandekar, A.Y., Todd, A.C. and Sarkar, R.: "A Modified Scaling Law and Parachor Method Approach for Improved Prediction of Interfacial Tension of Gas-Condensate Systems," paper SPE 22710 presented at the 66<sup>th</sup> SPE Annual Technical Conference and Exhibition, Dallas, TX, October 6-9, 1991.
87. Fawcett, M.J.: "Evaluation of Correlations and Parachors to Predict Low Interfacial Tension in Condensate Systems," paper SPE 28611 presented at the 69<sup>th</sup> SPE Annual Technical Conference and Exhibition, New Orleans, LA, September 25-28, 1994.
88. Hough, E.W. and Stegemeier, G.L.: "Correlation of Surface and Interfacial Tension of Light Hydrocarbons in the Critical Region," *SPE Journal*, **1** (1961) 259-263.
89. Hugill, J.A. and Van Welsenes, A.J.: "Surface Tension: A Simple Correlation for Natural Gas and Condensate Systems," *Fluid Phase Equilibria*, **29** (1986) 383.

90. Lee, S.T. and Chien, M.C.H.: "A New Multicomponent Surface Tension Correlation Based on Scaling Theory," paper SPE 12643 presented at the SPE/DOE Fourth Symposium on Enhanced Oil Recovery, Tulsa, OK, April 15-18, 1984.
91. Exner, O.: "Additive Physical Properties. III. Re-Examination of the Additive Character of Parachor," *Collect. Czech. Chem. Commun.*, **32** (1967) 24-54.
92. Katz, D.L., Monroe, R.R. and Trainer, R.P.: "Surface Tension of Crude Oils Containing Dissolved Gases," *JPT* (Sept. 1943) 1-10.
93. Rossini, F.D., *Selected Values of Physical and Thermodynamic Properties of Hydrocarbons and Related Compounds*, Carnegie Press, Pittsburgh (1953).
94. Bowden, S.T. and Butler, E.T.: "Intermolecular Forces in Liquid Systems. Part II. Viscosity, Surface Tension, and Parachor Relationships in Binary Systems," *J. Chem. Soc.*, **140** (1939) 79- 83.
95. Hammick, D.L. and Andrew, L.W.: "The Determination of the Parachors of Substances in Solution," *J. Chem. Soc.*, **130** (1929) 754-759.
96. van Der Waals, J.D., *Z. Phys. Chem.*, **13** (1894) 716.
97. Ferguson, A., *Phil. Mag. (vi)*, **31** (1916) 37.
98. Guggenheim, E.A.: "The Principle of Corresponding States," *J. Chem. Phys.*, **13** (1945) 253-261.
99. Wright, F.J., *J. Appl. Chem.*, **11** (1961) 193.
100. Eckert, C.A., Prausnitz, J.M.: "Statistical Surface Thermodynamics of Simple Liquid Mixtures," *AIChE J.*, **10** (1964) 677-683.
101. Cahn, J.W. and Hillard, J.E.: "Free Energy of a Nonuniform System. 1. Interfacial Free Energy," *J. Chem. Phys.*, **28** (1958) 258-267.
102. van Der Waals, J.D., *Z. Phys. Chem.*, **13** (1894) 657.
103. Urlic, L.E., Florusse, L.J., Straver, E.J.M., Degrange, S. and Peters, C.J.: "Phase and Interfacial Tension Behavior of Certain Model Gas Condensates: Measurements and Modeling," *Transport in Porous Media*, **52** (2003) 141-157.
104. Yang, A.J.M, Flemming, P.D. and Gibbs, J.H. "Molecular Theory of Surface Tension," *J. Chem. Phys.*, **64** (1976) 3732-3747.

105. Yang, A.J.M, Flemming, P.D. and Gibbs, J.H.: "Theory for the Influence of Gravity on Liquid-Vapor Interfaces," *J. Chem. Phys.*, **67** (1977) 74-80.
106. Bongiorno, V., Scriven, L.E. and Davis, H.T.: "Molecular Theory of Fluid Interfaces," *J. Colloid Interface Sci.*, **57** (1976) 462-475.
107. Carey, B.S., Scriven, L.E., Davis, H.T.: "On Gradient Theory of Fluid Interfacial Stress and Structure," *J. Chem. Phys.*, **69** (1978) 5040-5049.
108. Carey, B.S., Scriven, L.E., Davis, H.T.: "Semiempirical Theory of Surface Tensions of Pure Normal Alkanes and Alcohols," *AIChE J.*, **24** (1978) 1076-1080.
109. Cornelisse, P.M.W., *The Squared Gradient Theory Applied. Simultaneous Modeling of Interfacial Tension and Phase Behaviour*, Ph.D. Thesis, TU Delft, The Netherlands, 1997.
110. Zuo, Y.X, Stenby, Y.H.: "Calculation of Interfacial Tensions with Gradient Theory," *Fluid Phase Equilibria*, **132** (1997) 139-158.
111. Miqueu, C., Mendiboure, B., Graciaa, A. and Lachaise, J.: "Modelling of the Surface Tension of Pure Components with the Gradient Theory of Fluid Surfaces: a Simple and Accurate Expression for the Influence Parameters," *Fluid Phase Equilibria*, **207** (2003) 225-246.
112. Carey, B.S., Scriven, L.E., Davis, H.T.: "Semiempirical Theory of Surface Tension of Binary Systems," *AIChE J.*, **26** (1980) 705-711.
113. Sahimi, M., Davis, H.T. and Scriven, L.E.: "Thermodynamic Modeling of Phase and Tension behavior of CO<sub>2</sub>/Hydrocarbon Systems," *SPE J.* (Apr. 1985) 235-254.
114. Gupta, M.K. and Robinson, R.L.: "Application of Gradient Theory of Inhomogeneous Fluid to Prediction of Low Interfacial Tensions in CO<sub>2</sub>/Hydrocarbon Systems," *SPE J.* (Nov. 1987) 528-530.
115. Sahimi, M. and Taylor, B.N.: "Surface Tension of Binary Liquid-Vapor Mixtures: A Comparison of Mean Field and Scaling Theories," *J. Chem. Phys.*, **95** (1991) 6749-6761.
116. Cornelisse, P.M.W., Peters, C.J. and de Swaan Arons, J.: "Application of the Peng-Robinson Equation of State to Calculate Interfacial Tensions and Profiles at Vapor-Liquid Interfaces," *Fluid Phase Equilibria*, **82** (1993) 119-129.

117. Perez-Lopez, J.H., Gonzalez-Ortiz, L.J., Leiva, M.A. and Puig, J.E.: "Estimation of Surface Tension of Pure Liquids using the Gradient Theory," *AICHE J.*, **38** (1992) 753-760.
118. Mohanty, K.K. and Davis, H.T.: "An Equation of State for Polyatomic Fluids," *AICHE J.*, **25** (1979) 701-708.
119. Kruss User's Manual, *Drop Shape analysis*, Kruss GmbH, Hamburg 2000.
120. Vijapurapu, C.S. and Rao, D.N.: "The Effect of Rock Surface Characteristics on Reservoir Wettability," in K.L. Mittal (Ed.), *Contact Angle, Wettability and Adhesion*, Vol.3, VSP International Science Publishers, 2003, pp. 407-426.
121. Chang, Y.C. and Moulton, R.W.: "Quaternary Liquid Systems with Two Immiscible Liquid Pairs," *Industrial Engineering Chemistry*, **45** (1953) 2350-2361.
122. Sidgwick, N.V. and Spurrel, W.J.: "The System Benzene-Ethyl Alcohol-Water between +25° and -5°," *Journal of Chemical Society*, **117** (1920) 1397-1404.
123. Jennings, Jr., H.Y.: "The Effect of Temperature and Pressure on the Interfacial Tension of Benzene-Water and Normal Decane-Water," *Journal of Colloid and Interface Science*, **24** (1967) 323-329.
124. Computer Modeling Group Ltd., *Winprop Phase Property Program*, Calgary, Canada, 2001.
125. Metcalfe, R.S. and Yarborough, L.: "The Effect of Phase Equilibria on the CO<sub>2</sub> Displacement Mechanism," *SPE J.* (Aug. 1979) 242-252.
126. Sternling, C.V. and Scriven, L.E.: "Interfacial Turbulence: Hydrodynamic Instability and Marangoni Effect," *AICHE J.*, **5** (1959) 514-523.
127. Zuideweg, F.J. and Harmens, A.: "The Influence of Surface Phenomena on the Performance of Distillation Columns," *Chem. Eng. Sci.*, **9** (1958) 89-103.
128. McCain, W.D., Jr., *The Properties of Petroleum Fluids*, PennWell Publishing Company, Tulsa, Oklahoma, 1990.
129. Glaso, O.: "Miscible Displacement: Recovery Tests with Nitrogen," *SPE Reservoir Engineering Journal*, **5** (1990) 61-68.
130. Whitson, C.H. and Brule, M.R., *Phase Behavior*, SPE Henry L. Doherty series, Richardson, TX (2000) 72-73.

131. Green, D.W. and Willhite, G.P., *Enhanced Oil Recovery*, Society of Petroleum Engineers of AIME, **6** (1998) 186-238.
132. Nghiem, L.X. and Heidemann, R.A.: "General Acceleration Procedure for Multiphase Flash Calculations with Application to Oil-Gas-Water Systems," paper presented at the 2<sup>nd</sup> European Symposium on Enhanced Oil Recovery, Paris, France, November 8-10, 1982.
133. Grassmann, P. and Anderes, G.: "Abhängigkeit des Stoffaustausches von der Austauschrichtung," *Chem. Eng. Tech.*, **31** (1959) 154-155.
134. Rosen, M.J. and Gao, T.: "Dynamic Surface Tension of Aqueous Surfactant Solutions 5. Mixtures of Different Charge Type Surfactants," *J. Colloid and Interface Sci.*, **173** (1995) 42- 48.
135. Taylor, K.C. and Nasr-El-Din, H.A.: "The Effect of Synthetic Surfactants on the Interfacial Behavior of Crude Oil/Alkali/Polymer Systems," *Colloids and Surfaces A: Physicochemical and Eng. Aspects*, **108** (1996) 49-72.
136. Campanelli, J.R. and Wang, X.: "Dynamic Interfacial Tension of Surfactant Mixtures at Liquid - Liquid Interfaces," *J. Colloid and Interface Sci.*, **213** (1999) 340-351.
137. Diamant, H., Ariel, G. and Andelman, D.: "Kinetics of Surfactant Adsorption: the Free Energy Approach," *Colloids and Surfaces A: Physicochemical and Eng. Aspects*, **183-185** (2001) 259-276.
138. Sigmund, P.M.: "Prediction of Molecular Diffusion at Reservoir Conditions. Part II – Estimating the Effects of Molecular Diffusion and Convective Mixing in Multicomponent Systems," *JCPT* (July-September 1976) 53-62.
139. Wilke, C.R.: "Diffusional Properties of Multicomponent Gases," *Chem. Eng. Progress*, **46** (1950) 95-104.
140. Fayers, F.J.: "Crossflow Mechanisms by Gas Drive in Heterogeneous Reservoirs," paper SPE 24934 presented at the 67<sup>th</sup> SPE Annual Technical Conference and Exhibition, Washington, DC, October 4-7, 1992.
141. Wilke, C.R. and Chang, P.: "Correlation of Diffusion Coefficients in Dilute Solutions," *AIChE J.*, **1** (1955) 264-270.
142. Wilke, C.R.: "Estimation of Liquid Diffusion Coefficients," *Chem. Eng. Progress*, **45** (1949) 218-224.

143. Sharma, G.D., Kamath, V.A., Khataniar, S. and Patil, S.L., *Study of Hydrocarbon Miscible Solvent Slug Injection Process for Improved Recovery of Heavy oil from Schrader Bluff Pool, Milne Point Unit, Alaska*, Final Report under Contract No. DE-FG22-93BC14864, USDOE (November 1995).
144. Dorshow, R.B.: "The Simultaneous Measurement of Interfacial Tension and Oil Viscosity at Reservoir Conditions for Prudhoe Bay Fluids by Surface Laser Light Scattering Spectroscopy," *SPE Advanced Technology Series*, **3** (1995) 120-128.

## VITA

Subhash C. Ayirala was born in Chittoor, India, on April 1, 1975, the son of Adinarayana Reddy and Devatha Reddy. After completing his high school studies at P.C. Reddy Government Junior College, Chittoor, India, he entered College of Engineering of Sri Venkateswara University, Tirupati, India, and obtained a bachelor's degree with distinction in chemical engineering in 1996. In August 1996, he joined the graduate program at Indian Institute of Technology, Kharagpur, India, and received the degree of Master of Technology in Chemical Engineering in 1998. He worked as a Process Engineer at Amar Raja Batteries Limited, Tirupati, India from 1998 to 2000. In August 2000, he joined the Craft and Hawkins Department of Petroleum Engineering at Louisiana State University and received the degree of Master of Science in Petroleum Engineering in December 2002. He is currently pursuing graduate study at Louisiana State University for a doctoral degree in the same discipline. The doctoral degree in Petroleum Engineering will be conferred in August 2005.

\*\*\*\*\*